L-Università ta' Malta
Faculty of Science
Department
of Geosciences

A study on the dynamics of particulate matter infiltration in buildings

Ryan Vella

August 2019

Supervisor: Dr Noel Aquilina

A dissertation presented to the Faculty of Science in part fulfillment of the requirements for the degree of Masters of Science in Geosciences at the University of Malta

The research work disclosed in this publication is partially funded by the Endeavour Scholarship Scheme (Malta). Scholarships are part-financed by the European Union - European Social Fund (ESF) - Operational Programme II – Cohesion Policy 2014-2020 "*Investing in human capital to create more opportunities and promote the well-being of society*".

European Union – European Structural and Investment Funds
Operational Programme II – Cohesion Policy 2014-2020
"Investing in human capital to create more opportunities and promote the well-being of society"
Scholarships are part-financed by the European Union - European Social Funds (ESF)
Co-financing rate: 80% EU Funds;20% National Funds

L-Università ta' Malta

FACULTY/INSTITUTE/CENTRE/SCHOOL_____

DECLARATIONS BY POSTGRADUATE STUDENTS

Student's I.D. /Code _____

Student's Name & Surname _____

Course _____

Title of Dissertation

_____

_____

_____

(a) Authenticity of Dissertation

I hereby declare that I am the legitimate author of this Dissertation and that it is my original work.

No portion of this work has been submitted in support of an application for another degree or qualification of this or any other university or institution of higher education.

I hold the University of Malta harmless against any third party claims with regard to copyright violation, breach of confidentiality, defamation and any other third party right infringement.

(b) Research Code of Practice and Ethics Review Procedures

I declare that I have abided by the University's Research Ethics Review Procedures.

As a Master's student, as per Regulation 58 of the General Regulations for University Postgraduate Awards, I accept that should my dissertation be awarded a Grade A, it will be made publicly available on the University of Malta Institutional Repository.

_____ _____

Signature of Student Name of Student (in Caps)

_____

Date

Dedication

To my parents,
Rita & Raymond
who thought me to believe that great things can be achieved with hard work and perseverance.

Contents

List of Figures

List of Tables

Acknowledgements

First, and most of all, I would like to thank my supervisor Dr Noel Aquilina, for his assistance and guidance throughout the project and the writing of this dissertation. I am grateful for his immediate feedback to all of my queries and rigorous examination of my work. From the Department of Geosciences, I would like to thank Dr Sara Fenech, not only for her support in setting up the experimental campaign but also for her assistance and helpful discussions. I thank Mr Renato Camilleri who made the sampling campaign at the University of Malta Junior College possible and run smoothly. I also thank Mr Camilleri for providing a very useful dataset from a sampling campaign he was running at a residential home in Birżebbuġa for his PhD and for providing technical assistance. Finally, my deepest gratitude goes to my family for their never-ending support, especially my parents.

Abstract

The increased health risks related to the exposure of particulate matter (PM) pollution are evident. Given that people spend around 90% of their time indoors, indoor exposure to particles of outdoor origin has become an important focus in recent years. Several studies have attempted to estimate the relative contribution of outdoor particulates in indoor environments. In this study, an unoccupied room was used to conduct indoor and outdoor continuous PM measurements. The air exchange rate (AER) of the room was also measured and was varied by opening the windows at different amounts. A simple modification in the experimental procedure was also implemented to determine the indoor deposition rates (k) at different PM size fractions. Different models were considered and their ability to estimate the indoor PM concentration from outdoor PM data was investigated. This study provides estimates of the Infiltration Factor and also indicates the best-performing model, for different PM size fractions given no indoor sources and under natural ventilation conditions in a local setting. All models considered performed better for finer fractions (PM_1) and models assuming steady-state conditions performed better than more complex models employing a dynamic solution of the mass balance equation (MBE) however, such models have problems in low AER conditions. BC was not found to be a reliable infiltration surrogate of PM and the high variability of the AER both with regards to the wind speed and its direction was exposed.

Acronyms

AER air exchange rate.

BBG Birżebbuġa.

BC black carbon.

CEN European Committee of Standardisation.

CHD coronary heart disease.

CMA centrifugal mass analyser.

COMEAP Committee on the Medical Effects of Air Pollutants.

COPD chronic obstructive pulmonary disease.

CVD cardiovascular disease.

DMA differential mobility analyser.

EC elemental carbon.

EEA European Environment Agency.

IAQ indoor air quality.

IR infrared.

JC Junior College.

MAQL mobile air quality laboratory.

MBE mass balance equation.

NDIR non-dispersive infrared.

OC organic carbon.

PHE Public Health England.

PM particulate matter.

RM recursive model.

SEM scanning electron microscope.

TEM transmission electron microscope.

VOCs volatile organic compounds.

Chapter 1

Introduction

Air quality has been linked with health complications as far back as Hippocrates [2]. Common ambient air pollutants that impair the air quality are carbon dioxide, carbon monoxide, formaldehyde, nitrogen dioxide, sulfur dioxide, volatile organic compounds (VOCs), and particulate matter (PM). PM in particular is considered to be the largest contributor to urban air pollution and has a wide range of detrimental health effects attributed to it [3]. In fact, given the established studies and documented exposure, both for short-term and long-term effects of PM, it can be said that adverse effect on health due to PM exposure occurs with certainty [4].

1.1 Particulate matter

PM, refers to a condensed phase suspended in the air that can be made up of molecules, radicals and atoms with diameters ranging from 10 nm to and 50 μm [5]. PM is usually classified into two primary groups; coarse particles and fine particles, depending upon the particle size. Coarse particulates include the fraction of particles with a larger size ranging from 2.5 μm to 10 μm, the fine fraction contains particles of size up to 2.5 μm in aerodynamic diameter ($PM_{2.5}$). The finer particle fraction is mostly composed of secondary formed aerosols (e.g. particles formed from gas-

to-particle conversion), combustion particles, and particles condensed from organic and metal vapours. On the other hand, coarser particles are typically made up of earth crust material and fugitive dust i.e. suspended dust primarily sourced from Earth's soil.

Most of the mass of PM is attributed to the fine mode particles (particles between 100 nm and 2.5 μm) however, the bulk of particles is found in the ultrafine regime, less than 0.1 μm. In fact, ultrafine particles contribute to just a fraction of the mass but contribute to over 90% to the number of particles [6].

The classification of particulates by their aerodynamic diameter is of paramount importance as this property governs three fundamental characteristics in PM dynamics namely; transport and deposition of particles in the atmosphere, penetration within the respiratory system and the association of the chemical composition and source of the particle [6].

PM is perhaps the most relevant pollutant as it is a crucial atmospheric constituent affecting a range of atmospheric processes. In a study it has been shown that aerosols impact the Earth's radiation budget [7]. The number of aerosols in the atmosphere impact climate systems both directly and indirectly. The direct effect comes about the scattering and absorption of the incoming solar radiation from the aerosols themselves. Additionally, aerosols are also responsible for the formation and the lifetime of clouds as they act as a 'seed', providing a nucleus where condensation can take place. This is an indirect effect of aerosols on the radiation budget as the number of clouds in the atmosphere influence the absorption and reflection of incoming and outgoing solar radiation (i.e. Earth's Albedo) [7]. PM can also affect vegetation in various ways. Particulate deposition can physically cover plants and thus interfering with photosynthetic processes that are vital for plants and also clog stomatal openings. Such phenomena can lead to growth stunting and even mortality in some plant species. A more noticeable effect of PM is visibility impairment caused by the absorption and scattering of light due to suspended particles. $PM_{2.5}$ is often

responsible for such visibility impairment and even though $PM_{2.5}$ is composed of numerous chemical species the main contributors to visibility impairment in $PM_{2.5}$ are: sulfates, nitrates, organic carbon, elemental carbon, and crustal material [8]. In indoor environments, besides dust settling on furniture that would require frequent cleaning, most issues of indoor PM are related to health problems.

The adverse health effects of PM not only depend on the composition and toxicity of the constituents of the suspension but also its size as this determines the ability of the PM to penetrate the human body. Coarse particulates (PM_{10}) can penetrate the human body but in general, such particles are deposited in the upper airway passages i.e. nose, nasal cavity and throat. Fine ($PM_{2.5}$, PM_1) and ultrafine ($PM_{0.1}$) particles, however, can penetrate deep into the lungs and easily reaching the bloodstream through the alveoli. The European Committee of Standardisation (CEN) defines PM fractions according to their ability to penetrate the human respiratory system as follows [9]:

- Inhalable fraction - the mass fraction of total airborne particles which is inhaled through the nose and mouth.
- Extrathoracic fraction - the mass fraction of inhaled particles failing to penetrate beyond the larynx.
- Thoracic fraction - the mass fraction of inhaled particles penetrating beyond the larynx.
- Respirable fraction - the mass fraction of inhaled particles penetrating to the unciliated airways.

Relative to the total suspended airborne particulates, particle sizes with a 50% penetration of the thoracic and respirable fractions are 10 μm and 4 μm respectively [9, 10]. Both fine and ultrafine particles can be extremely toxic as they become coated with heavy metals and other chemicals [11].

Public Health England (PHE) highlights short-term effects of PM exposure such as exacerbation of asthma, and longer-term effects including respiratory and cardiovascular diseases (CVDs), lung cancer, and strokes [12]. The Committee on the Medical Effects of Air Pollutants (COMEAP) reported that PM has the strongest association to both short-term and long-term CVD morbidity through various complex biological mechanisms all triggered by the exposure to fine particulate air pollution [13]. A PHE report states that in 2017 63,430 ($\pm$ 2,154) incidence cases of disease were attributed to $PM_{2.5}$ exposure with most of the cases being coronary heart disease (CHD), diabetes and chronic obstructive pulmonary disease (COPD) [12].

Several other adverse health effects have been attributed to a wide range of components typically found in PM. Sulfates have been found to facilitate the toxicity of PM in various mechanisms such as decreasing the pH of fluids within the lungs and mobilising metals in the lungs. Since nitrates are only weakly acidic, they are less likely to have the health effects mentioned, however, ambient particulate nitrate has been less studied, and thus the effects of nitrate exposure may not yet be completely understood [14]. Toxicological data also suggest that black carbon (BC)/elemental carbon (EC) may not be toxic in itself but acts as a carrier of various toxic chemicals from combustion. Sulfates and nitrates could also act as carriers of chemical species arising from combustion. The available evidence suggests that many toxic components can be attributed to several health effects but since many pollutants within PM are highly correlated it is still not clear to distinguish specific effects from specific chemicals in epidemiological studies [14].

According to the European Environment Agency (EEA) people spend about 90 % of their time indoors, being at home, at work or school [15]. The investigation of the indoor air quality (IAQ) is thus important to determine the exposure of hazardous pollutants that might have negative effects on the health of the occupants. The state of the IAQ not only depends on indoor sources such as cooking, cleaning, heating and smoking but also on ambient pollutants that penetrate the indoor environment.

Indoor air pollution is being given more attention as its threats to human health are becoming more apparent and relevant [15].

1.2 PM sources

PM is usually produced from the mechanical break-up of larger particles starting from large solid particles, such as wind-blown dust from agricultural and industrial processes, and dust from natural weathering of rock. Such mechanisms produce the coarse fraction of PM. Near coasts, hydrosols, a stable suspension made from water molecules, are produced from the evaporation of sea-spray. Living vegetation also emits a range of coarse particles such as mould spores and pollen grains [6].

The mechanical break-up of large particulates establishes a threshold in the production of these coarse particles of approximately 1 μm. Most of the fine fraction particles are formed from gases through mechanisms such as nucleation, condensation or chemical reactions. The low equilibrium pressure of heavy metals, EC, organic carbon (OC), sulfates and nitrates in the atmosphere make them the major sources that yield nuclei mode particulates. Particles in the nucleation mode tend to grow in size by coagulation and condensation mechanisms. Coagulation and condensation are more efficient for a large number of particles and large surface area respectively and thus the efficiency in producing PM through both processes decreases as the particles get larger. This sets an upper limit where particles do not grow more than 1 μm through coagulation and condensation. This is the reason why the abundance of particles tends to accumulate in the range between 0.1 and 1 μm. This is indeed referred to as the accumulation range [6]. Metals and organic compounds are vaporised in high-temperature reactions such as combustion. The condensation of such gases yields ultrafine particles. Ultrafine particles are also formed by condensation of other gases produced in atmospheric reactions yielding low-vapour-pressure substances.

Combustion of fossil fuels is perhaps the largest source of anthropogenic PM. Fossil fuels are extensively used worldwide to generate electricity, power vehicles and machinery, and heating. Burning fossil fuels releases coarse particulates form non-combustible materials in the fuel such as ash and soot, but also releases sulfur and nitrogen oxides that result in the formation of secondary particles through the above-mentioned mechanisms [6].

1.3 PM infiltration models

There are different approaches to model the indoor particle concentration of outdoor origin. The different approaches are grouped into four categories according to the formulation of their methodology: (1) steady-state assumption using the steady-state form of the mass balance equation (MBE); (2) dynamic solution of the MBE; (3) experimental studies using conditions that simplify model calculations; (4) infiltration surrogates using PM constituents with no indoor sources to act as surrogate of indoor PM of outdoor origin [16].

1.3.1 Mass balance equation

The indoor PM concentration depends on a balance between sources and sinks of PM within the indoor environment. Figure 1.1 presents a schematic of an indoor environment with the various mechanisms influencing the indoor PM concentration.

This area has been left intentionally blank.

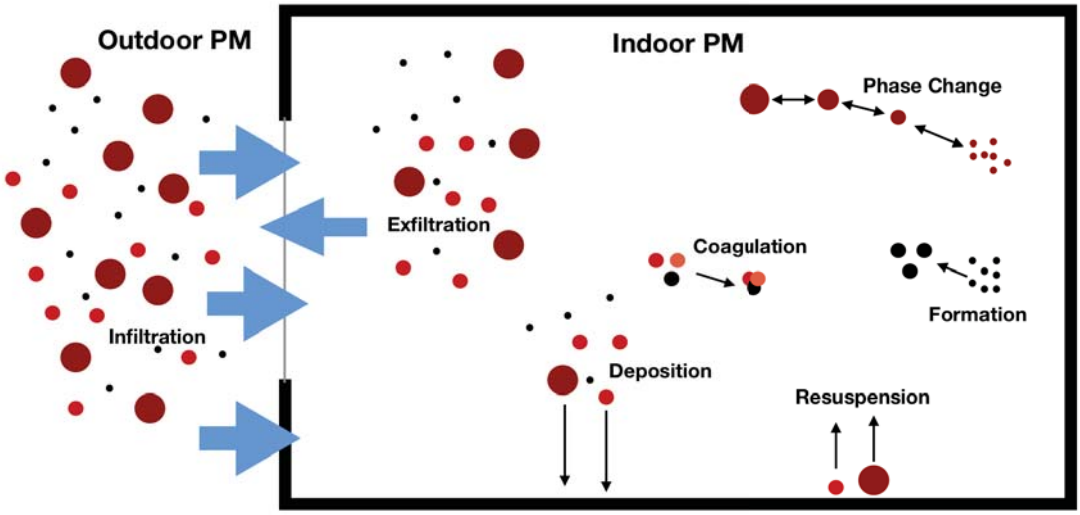

Figure 1.1: A schematic illustrating the various sources and sinks in an indoor environment.

The indoor PM concentration can thus be described by a function of all these mechanisms through the following equation known as the MBE [17]:

$$\frac{\mathrm{d}C_{in}}{\mathrm{d}t} = PaC_{out} - (a+k)C_{in} + S + G + F + V + H \tag{1.1}$$

where C_{in}, C_{out} are the indoor and outdoor concentrations respectively (μg m^{-3})

a is the air exchange rate (AER) (hr^{-1})

P is the penetration efficiency (unit less)

k is the deposition rate of particles (hr^{-1})

S is the indoor generation rate (μg m^{-3})

G is the particle formation through gas-particle conversions (μg m^{-3})

F is the particle formation from chemical reactions (μg m^{-3})

V is the particle size change due to coagulation processes (μg m^{-3})

H is the particle size change through hygroscopic growth (μg m^{-3}).

The AER, a, is the number of times the air enters and leaves the building envelope

on an hourly basis, P is defined as the fraction of outdoor dust that penetrates the building and makes it indoors while k refers to the rate at which PM is deposited on the indoor surfaces through several mechanisms such as gravitational settling and Brownian diffusion [18]. In most cases, particle mass losses or gains due to condensation of gas-phase species, chemical reactions, coagulation processes and hygroscopic growth are ignored [19] allowing Equation 1.1 to be written as

$$\frac{\mathrm{d}C_{in}}{\mathrm{d}t} = PaC_{out} - (a+k)C_{in} + S \tag{1.2}$$

Equation 1.2 is the most basic form of the MBE and all models that study the infiltration of PM into a building are based on one form or another of this equation.

1.3.2 Steady-state assumption

A steady-state assumption is a popular approach in deriving infiltration models as it drastically simplifies the MBE. Besides its simplicity, since steady-state conditions are required, such methodology does not require continuous concentration data but rather averaged data that is often obtained more easily [16].

In 1981 an infiltration model was derived from the MBE under steady-state conditions i.e. assuming a, P, and k remain constant over a given time period Δt [20].

Defining average values over the sampling period as:

$$\overline{C_{in}} = \frac{1}{t_s}\int_0^{t_s} C_{in}\mathrm{d}t = \text{indoor average concentration} \tag{1.3}$$

$$\overline{C_{out}} = \frac{1}{t_s}\int_0^{t_s} C_{out}\mathrm{d}t = \text{outdoor average concentration} \tag{1.4}$$

Integrating Equation 1.2 over the sampling period t_s, assuming P, k and a remain constant

$$\frac{C_{in}(t_s) - C_{in}(0)}{t_s} = Pa\overline{C_{out}} - (a+k)\overline{C_{in}} \tag{1.5}$$

Bringing the average indoor/outdoor ratio subject of the formula we get:

$$\frac{\overline{C_{in}}}{\overline{C_{out}}} = \frac{Pa}{(a+k)} + \frac{C_{in}(0) - C_{in}(t_s)}{\overline{C_{out}} t_s (a+k)} \tag{1.6}$$

The first term on the RHS of Equation 1.6 represents the average behaviour of the system for the time period considered. The second term on the RHS is referred to as the 'dynamic term' and describes how the average indoor concentration behaves when there are fluctuations in the outdoor concentration. The dynamic term is highly dependant on the averaging time period as the magnitude of $\frac{C_{in}(0)-C_{in}(t_s)}{\overline{C_{out}} t_s}$ diminishes at longer averaging times [21]. In fact, for long enough averaging time periods - more than 3 hours [21]- the dynamic term becomes negligible and Equation 1.6 becomes:

$$\overline{C_{in}} = \frac{a.P}{a+k}.\overline{C_{out}} \tag{1.7}$$

where a, P and k are as previously defined.

Regressing $\overline{C_{in}}$ on $\overline{C_{out}}$ yields estimates of $\frac{a.P}{a+k}$ from the gradient of the regression line. The term $\frac{a.P}{a+k}$ is genrally referred to as the infiltration factor (F_{INF}) where, by definition, it differs from P as it considers k of the infiltrated particles. For high ventilation rates - < 0.5 hr^{-1} for $PM_{2.5}$ and < 0.05 hr^{-1} for PM_1) - k becomes negligible and the F_{INF} can be approximated as P [20].

$$F_{\text{INF}} = \frac{a.P}{a+k} = \frac{a.P}{a} = P \tag{1.8}$$

Thus, Equation 1.7 becomes

$$\overline{C_{in}} = P.\overline{C_{out}} \tag{1.9}$$

The approach assuming steady-state conditions (Equation 1.7), was used and modified in several other studies (e.g. [22],[23], [24], [25]) investigating scenarios involving indoor sources. A physical-statistical model has been used to estimate penetration efficiencies and deposition rates of different particulate sizes in homes [26]. This particular study attempted to determine the infiltration factor by estimating P and k separately rather than estimating the infiltration factor directly from regression analysis as done in the previously mentioned studies.

Starting from the MBE and ignoring both indoor particle generation and resuspension, the steady-state indoor concentration of particles is expressed as

$$C_{in} = \frac{Pa}{a+k} C_{out} \tag{1.10}$$

Equation 1.10 can be rearranged such that

$$\frac{C_{out}}{C_{in}} = \frac{k}{P}\left(\frac{1}{a}\right) + \frac{1}{P} \tag{1.11}$$

Applying linear regression on a plot of $\frac{C_{out}}{C_{in}}$ versus $\frac{1}{a}$ yields estimates of P and k using the slope and intercept values of the regression line. From the values of P and k, F_{INF} can be then calculated [26].

In this study, the authors considered nine homes with different building and ambi-

ent characteristics. The extreme variability in the infiltration factor with different building dynamics was evident [26]. The study also remarked the significant time lags between indoor and outdoor concentration peaks even if the air exchange rate was high. Such data exposes problems in estimating the infiltration factor using short-term (e.g. 20-minute average) indoor/outdoor data [26]. The deposition rate was found to be a highly variable process depending on particle size as well as air turbulence and mixing, near-surface flow, temperature, surface materials, and room volume [26]. The use of continuous data from different homes may have allowed P and k to be estimated more accurately compared to other studies that used averaged data.

P and k are mostly related to the building characteristics (such as surface roughness indoors) and the indoor/outdoor concentrations, however, such parameters depend on the particle dimensions, composition and electrical charge as well. This makes it somewhat difficult to determine P and k and, in the last two decades, various methodologies were developed to give a better estimate to such parameters.

1.3.3 Dynamic solution of the MBE

In most real-world circumstances, steady-state conditions are rarely attained due to natural fluctuation in the outdoor PM concentration and infiltration rate - making the steady-state solution of the MBE invalid. The availability of continuous indoor and outdoor PM concentration data allow the evaluation of dynamic models based on the non-linear solution of the MBE.

Recalling the MBE (Equation 1.2) but assuming no indoor sources we get:

$$\frac{\mathrm{d}C_{in}}{\mathrm{d}t} = PaC_{out} - (a+k)C_{in} \tag{1.12}$$

A commonly-used approach to obtain an analytical solution of Equation 1.12 is by employing a basic "forward-marching" scheme with time step, Δt (e.g. [19], [27], [28]). Equation 1.12 is re-written below changing the derivative term with a discrete time step term $\frac{\Delta C_{in}}{\Delta t}$ where $\Delta C_{in} = C_{in_{i+1}} - C_{in_i}$.

$$C_{in_{i+1}} - C_{in_i} = PaC_{out}\Delta t - (a+k)C_{in}\Delta t \tag{1.13}$$

Which can be rearranged to:

$$C_{in_{i+1}} = Pa\Delta tC_{out_{i+1}} + (1-(a+k)\Delta t)C_{in_i} \tag{1.14}$$

Equation 1.14 shows the finite time step form of the solution, where $C_{in_{i+1}}$ is the concentration determined from the outdoor concentration at the same time step ($C_{out_{i+1}}$) and the indoor concentration of the previous time step ($C_{out_{i+1}}$).

A similar approach was evaluated by using an integrated form of the iterative solution of the MBE [29]. Equation 1.15, which involves k, a and P, shows the finite time step proposed by the model.

$$C_{in(i)} = C_{in(i-1)}e^{-(k+a)\Delta t} + C_{out(i-1)}\frac{Pa}{a+k}(1-e^{-(k+a)\Delta t}) \tag{1.15}$$

This model assumes no indoor sources, incompressible flow into and out of the building, instantaneous mixing and that all parameters remain constant within each time step considered. The model also assumes constant AER over the entire sampling period even though variations in the AER are typically expected for long time frames. The model predicts the indoor concentration from the values of C_{in} and C_{out} of the previous time step [29].

Another method that model the infiltration of PM into buildings involves a linear

solution to the recursive mass balance model. The recursive model (RM) is derived from the differential MBE assuming indoor and outdoor constant concentrations, AER and a well-mixed air during each discrete time step [30]. When applied to hourly concentrations, the model states that the average indoor particulate concentration (C_t^{in}) is equal to the sum of a fraction of the average outdoor concentration (C_t^{out}) and a fraction of the average indoor concentration from the previous hour (C_{t-1}^{in}), and the concentration from indoor sources (S_t^{in}): [17]

$$C_t^{\text{in}} = \beta_1 C_t^{\text{out}} + \beta_2 C_{t-1}^{\text{in}} + S_t^{\text{in}} \tag{1.16}$$

where

$$\beta_1 = F_{\text{INF}}\{1 - \exp[-\lambda \Delta t]\} \tag{1.17}$$

and

$$\beta_2 = \exp[-\lambda \Delta t]\} \tag{1.18}$$

and

$$F_{\text{INF}} = \frac{\beta_1}{1 - \beta_2} \tag{1.19}$$

β_1 is associated with the outdoor particulates once they penetrate indoor while β_2 describes the decay of indoor particles. λ in Equation 1.17 is the total particle loss rate (h^{-1}). The use of hourly average data implies that $\Delta t = 1$ h and values of a and k are in units of h^{-1}. Taking $\Delta t = 1$ h is somewhat counter-intuitive as the original derivation of the RM assumes constant concentrations during the discrete time steps, however, the outdoor concentration is typically slow-varying and thus this departure can be expected to have minimal effects on the model's performance.

A similar methodology involving a dynamic solution of the MBE was adopted later in 2001 [31]. The study revealed that the AER play an important role in the transmission of pollutants from outdoor to indoor environments. The theoretical approach proposed relates the integrated average of the indoor/outdoor ratio with the AER through:

$$y = \frac{< C_{in} >}{< C_{out} >} = 1 - Ae^{-\eta a} \tag{1.20}$$

where $\frac{<C_{in}>}{<C_{out}>}$ is the indoor/outdoor integrated concentration average, A and η are two parameters related to the contaminant transport process and a is the AER.

This model assumes that there are no indoor sources of PM and that the infiltration of contaminants is only due to natural ventilation, excluding air conditioners and any artificial ventilation. The authors conducted sampling campaigns to test the model in areas where the ambient air quality is poor and so the outdoor PM concentration is very high compared to that indoors. The proposed model was found to be reliable for AERs ranging from 0.5 to 4.3 h^{-1}. At AERs lower than 0.5 h^{-1}, particle deposition cannot be assumed to be negligible while at air exchange rates above 4.3 h^{-1} resuspension becomes significant. However, according to the authors, this range falls into the typical AERs of residential buildings [31] .

1.3.4 Experimental approaches

Sometimes it can be challenging to obtain dynamic solutions of the MBE and thus specific experimental protocols are employed such that one of the parameters within the MBE is determined from specific experimental procedures. A common approach is the experimental determination of k from indoor PM concentration decay curves.

One method used to determine k experimentally involves the elevation of the indoor

PM concentration by opening the windows of the building shell under investigation [32]. After some time the indoor particle concentration reaches equilibrium with the outdoor concentration and becomes steady. At this sage, all windows and doors of the room investigated are closed and the room is left undisturbed [32]. The decay of the indoor particle concentration is then modelled using the MBE through the equation:

$$C_{in} = \frac{a.P}{a+k}.C_{out} + \left(C_{int} - \frac{a.P}{a+k}.C_{out}\right)e^{-(a+k).t} \tag{1.21}$$

where the first term, $\frac{a.P}{a+k}.C_{out}$, corresponds to the steady-state particle concentration (C_{SS}), transforming the above equation as follows:

$$C_{in} = C_{\mathrm{SS}} + (C_{\mathrm{int}} - C_{\mathrm{SS}})\mathrm{e}^{-(\lambda)t} \tag{1.22}$$

where:

C_{in} is the instantaneous indoor concentration (μg m^{-3})

C_{SS} is the steady-state (final) indoor particle concentration (μg m^{-3})

C_{int} is the initial indoor particle concentration (μg m^{-3})

t is the time (h)

$\lambda = a + k$ is the total particle loss rate (h^{-1})

a is the AER (h^{-1})

k is deposition rate (h^{-1}) .

The deposition rate (k) can then be estimated from the logarithmic regression of Equation 1.23, using experimental data of the AER (a).

$$\ln\left[\frac{C_{\mathrm{in}} - C_{\mathrm{SS}}}{C_{\mathrm{int}} - C_{\mathrm{SS}}}\right] = -(\lambda)t \tag{1.23}$$

The penetration coefficient (P) can then be calculated from the steady state indoor concentration:

$$P = \left(1 + \frac{k}{a}\right).\frac{C_{SS}}{C_{out}} \tag{1.24}$$

In this particular study, the penetration coefficient and deposition rates were estimated for six different residences. The highest value of penetration coefficient was found to be 0.79 at the size range of 0.8-1.4 μm while the minimum penetration (0.48) was in the size range between 4.70 - 9.65 μm. The deposition rate ranged between 1.00 and 0.27 hr^{-1}. The model proposed was later refined by including simultaneous data of the indoor and outdoor concentration [16].

1.3.5 Infiltration Surrogates

The final approach used for particle infiltration models makes use of distinct chemical species that are used as surrogates of particulate matter of outdoor origin [16]. Chemical species used as surrogates must have specific properties, namely: do not have indoor sources, can be measured continuously, are abundant to allow accurate measurements, and are chemically stable [33].

Literature suggests sulfate (or sulfur) as a good surrogate for $PM_{2.5}$ of ambient origin infiltrating indoors [16]. Sulfates have been used as surrogates of indoor $PM_{2.5}$ of outdoor origin in numerous studies [16]. In a particular investigation, the effective penetration efficiency was estimated using a steady-state solution of the MBE (equation 1.10) as already discussed.

EC and BC are tpically associated with outdoor traffic-related sources and thus make a great infiltration surrogate for homes without significant indoor combustion [34]. A study estimated the infiltration factor using different surrogates including BC

[16]. Seven primary schools in the Athens area were investigated using continuous indoor and outdoor data. The mean $PM_{2.5}$ was calculated from the slope of the regression line of the indoor versus outdoor data. The values of the F_{INF} estimated through different methodologies are shown in Table 1.1. [16, 1]

Methodology	F_{INF}
BC as surrogate	0.77
SO_4^{2-} as surrogate	0.84
SO_4^{2-} as surrogate with a correction factor	0.75
Dynamic model	0.75

Table 1.1: F_{INF} values estimated from different methodologies [1].

From the three alternative scenarios (using BC, SO_4^{2-} , and SO_4^{2-} with a correction factor for different size distributions) investigated in the area of Athens, BC seems to be a better surrogate of indoor $PM_{2.5}$ of outdoor origin [16, 1].

1.3.6 Comparing different infiltration models

A comprehensive understanding of the dynamics of outdoor particulate infiltration in building envelopes is still lacking. The different methodologies discussed give useful insight into the various approaches in estimating the penetration efficiency (P) and deposition rate (k). However, these parameters differ extensively in the literature and thus increase the ambiguity in the parameter values suggested [16]. In a review paper, different methodologies and approaches in determining the k, P and F_{INF} were compared [16]. k not only varied broadly between size fractions but also between different studies [16]. Some authors suggest that k is highly influenced by the building characteristics as well as the indoor and ambient conditions, which may partly explain the variability of in the deposition rate suggested in literature [35, 24]. In the case of ultrafine particles, k can be easily overestimated as the

indoor particulate concentration can decrease through aggregation processes [36]. Other experimental and theoretical studies suggest that the k may also increase with increasing aerosol charge [37].

Variations in k at different size fractions can be explained through various physical phenomena. Coarse particle deposition mostly occurs due to gravitational settling, which is possibly influenced by internal compaction. Ultrafine particles are often deposited through Brownian diffusion which makes deposition particularly higher onto vertical surfaces. Accumulation mode particles do not seem to be affected by the mentioned mechanisms and retain the lowest deposition on indoor surfaces [38, 39].

P also varied considerably. P estimated through the steady-state model ([26]) ranged from 0.54 to 1.00. Such a high value of P was obtained during warm periods where windows were kept open more often. The estimation of the penetration efficiencies using different dynamic solutions of the MBE agreed with each other and were also consistent with theoretical approaches, indicating that the largest penetration occurs for accumulation mode particles. The accumulation mode size fraction tends to stay in the air stream as it is hardly affected by diffusion or gravitational settling [40].

The estimation of F_{INF} through different methodologies reported in various literature comes in better agreement compared to the independent estimation of P and k. The reported values of F_{INF} for $PM_{2.5}$ were found to be in good agreement with a mean value of 0.70. Only a few values exhibited large deviation and this may be associated with ambient conditions, building characteristics, and PM chemical compositions and particle distribution. The good agreement of the estimation of F_{INF} by the use of dynamic models and infiltration surrogates (which is usually simple) suggest that the latter method can be employed given that chemical speciation data is available [16].

Chapter 2

Methodology

This chapter presents details of the instrumentation typically used to measure PM concentrations. The physical parameters employed in the infiltration models discussed in Chapter 1 were identified to set up a sampling campaign for their validation. The campaign aimed to obtain continuous indoor and outdoor PM concentration data as well as daily estimates of the AER. In this chapter, the methodology employed in the 13-day campaign carried out at the University of Malta Junior College (JC) in Msida is discussed thoroughly. Details including the calculations used to estimate the AER are also presented.

2.1 Measurement of PM

Several instruments employ different techniques for measuring various characteristics of PM. The most important characteristics of particles are the particle size and particle concentration. The main measuring principles used to determine the concentration of PM are: gravimetric, optical and microbalance methods, while the methods used to measure size distribution are: microscopical, impaction, diffusion and charging [41].

2.1.1 Concentration methods

The gravimetric method is widely used to quantify the concentration of PM. Filter-based sampling starts by weighing blank filters on a balance in the laboratory. The filters are then loaded into filter cartridges and preconditioned. At the testing site, the sampled air is passed through the filter at a known flow rate for a specific duration. Any PM in the sampled air is retained on the filter which is then re-weighed in the laboratory. The weight of PM is determined by subtracting the weight of the blank filter and the concentration is computed using the flow rate of the air sample [42]. Such procedure would give the total PM present in the air sample however, $PM_{2.5}$ and PM_{10} fractions can be determined by adding $PM_{2.5}$ and PM_{10} cyclone sampling heads respectively [43].

This sampling method cannot provide real-time measurements, however, particles are physically collected and thus can be further analysed using techniques such as scanning electron microscope (SEM) and transmission electron microscope (TEM) [41]. Besides filter-based sampling, impactors are also used for determining particle gravimetric mass size distribution.

PM concentration is often determined using optical detection methods as well. Such methods are all based on the principle of projecting a light beam into the air sample and measuring the absorbed and scattered light. The main advantage of optical instruments is that they can measure particle concentration in real-time. The detection is based on the principles of scattering, absorption, and light extinction [41].

The microbalance is an instrument capable of executing very precise measurements of weight of objects having a very small mass and is also used to determine PM concentration. The instrument consists of an oscillatory microbalance element oscillating at its resonance frequency. As PM deposits on the surface of the oscillatory element, the resonant frequency is altered slightly. These small alterations of the frequency are used to determine the mass of the deposited particles.

2.1.2 Size distribution methods

Size distribution methods measure the aerosol size, typically represented by diameter and the aerosol concentration. The particle size is determined through several particle properties including geometric size, inertia, mobility, electric mobility, and optical properties. Particle size distribution usually involves a combination of different measuring instruments involving the loading of particles in corona charger, particle size classification, and detection [41].

One method of determining particle size is to collect particles from the filters used in sampling and inspect the collected PM using a microscope. This method allows rigorous analysis of the morphology of particles however, ample time is required to analyse a statistically significant number of particles [44]. Impactors are sometimes used for measuring mass distribution. The most common impactors are of the cascade type and their operation is based on the internal classification of particles [41].

Particles in the ultrafine regime are hardly effected by gravitational and inertial forces. At this size fraction, particle movement is typically governed by diffusion processes. For such particles, it is more appropriate to use the equivalent diameter in volume from diffusion coefficients of the particles obtained in diffusion battery. In a diffusion battery, the air is moved in streamline flow through long, narrow, parallel channels. The diffusion constant and particle size is determined from the measurement of the fractional penetration of the ultrafine particles through the battery [45].

Electrostatic classification of particles is an alternative to other techniques such as optical sizing. Optical techniques are not able to measure particles smaller than 50 nm - 100 nm due to errors resulting from variations in particle shape and refractive index. Differential mobility analyser (DMA) is an instrument measuring particles down to 2.5nm by classifying charged particles according to their mobility in an

electric field. Particles are accelerated along field lines and this acceleration is opposed by viscous forces within the fluid and the inertia of the particles. When the electrical and viscous forces are balanced, terminal velocity is reached and the size of the particles is determined [46].

Modern instruments usually incorporate different techniques to determine both the concentration and the size distribution of particles. For instance, the centrifugal mass analyser (CMA) uses opposing electrostatic and centrifugal forces to examine the penetration ability of particles according to their mass-to-charge ratio [44]. In spectrometers, particles are charged and accelerated towards electrometers. Particles with greater electric mobility are immediately collected, whilst particles with inferior electrical mobility are collected further downstream [41].

2.2 Instrumentation used

2.2.1 PM measurements

The setup used to analyse ambient and indoor air quality was Fidas® 200 by PALAS®. The system provides continuous and simultaneous measurements of PM_1, $PM_{2.5}$, PM_4, PM_{10}, TSP (PM_{tot}) and particle number concentration [47].

This area has been left intentionally blank.

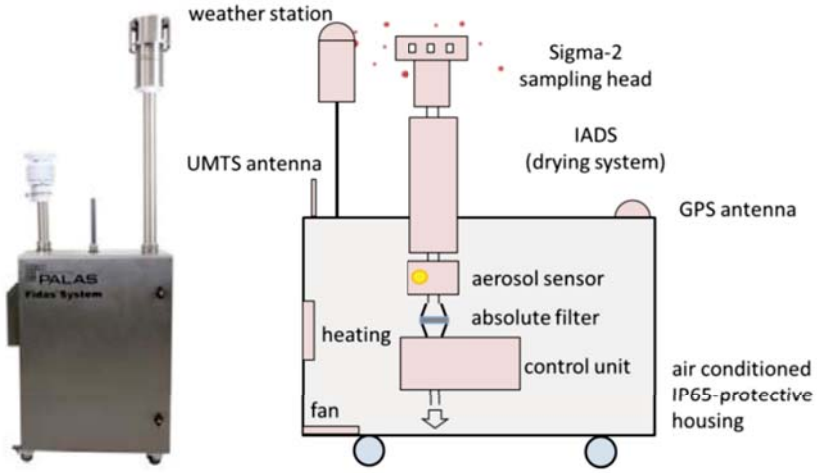

Figure 2.1: Setup of Fidas® fine dust measuring system.

Figure 2.1 illustrates the Fidas® monitoring system. The aerosol sensor is an optical spectrometer, which determines the number and size of the particles in the sampled air through the principles of Mie scattering. The particles are moved separately through an optically differentiated measurement volume and are homogeneously illuminated with white light. The number concentration is determined from the number of scattered light impulses while the particle size is deduced from the intensity of the scattered light. The measured functions are converted to mass or mass fraction by multiplying each value of the high-resolution particle size distribution with a correlation factor [47].

2.2.2 CO_2 measurements

The instrument used to monitor indoor CO_2 levels was Extech® SD800 Datalogger. The meter measures, displays and stores CO_2, temperature and relative humidity readings [48]. The CO_2 sensor is a dual-wavelength non-dispersive infrared (NDIR) sensor. Infrared (IR) lamp projects light through a tube filled with a sample air towards an IR detector. The 4.2-micron band of IR radiation is very close to the

4.26-micron absorption band of CO_2 and so as the IR light passes through the air sample the CO_2 molecules absorb the specific band of IR light while letting other wavelengths of light pass through. The difference between the amount of light radiated by the IR lamp and the light received by the detector is used to determine the number of CO_2 molecules in the sample tube [49].

2.3 Measuring the flow rate

The flow rate of an indoor environment is a measure of the volume of air (m^3) entering and leaving the building shell every hour. It is a cardinal parameter in infiltration models and indoor air quality in general. The flow rate is usually calculated by measuring the concentration of a tracer gas with time. The calculation of the flow rate using a tracer gas can be evaluated using three principal methodologies. Namely the decay rate method, the equilibrium concentration method and the constant concentration method [50]. In all three methods, Equation 2.1 is manipulated in different ways by applying distinct constraints.

$$\frac{\partial(VC_i(t))}{\partial t} = qC_0 - qC_i(t) + S \tag{2.1}$$

where
V is the volume of air inside the building (m^3)
$C_i(t)$ is the indoor tracer gas concentration at a given time t ($\mu g\ m^{-3}$)
C_0 is the outdoor background concentration of the tracer gas ($\mu g\ m^{-3}$)
q is the flow rate ($m^3\ h^{-1}$)
S is the indoor tracer gas emission rate ($\mu g\ h^{-1}$) [49].

Rearranging Equation 2.1 and solving it by integrating over the initial and final tracer gas concentrations and time gives the following expression which describes

the indoor tracer gas concentration as a function of time t.

$$C_i(t) = \left(C_0 + \frac{S}{q}\right) - \left(C_0 + \frac{S}{q} - C_{i0}\right) e^{-\frac{q}{V}(t-t_0)} \tag{2.2}$$

To determine the flow rate of a particular indoor environment, a tracer gas is generated or released indoors so that its concentration is elevated. After some time the tracer gas concentration stabilises as it reaches equilibrium within the indoor environment. As the gas emission is halted completely the indoor concentration begins to decay. These three instances (i.e. generation, equilibrium and decay) can all be used to determine the flow rate (q) from the above expression.

Although several tracer gases can be used, CO_2 is often the tracer gas of choice nowadays. The only drawback of CO_2 is that it is an existing constituent in the background air, however, this can be easily accounted for since the background CO_2 concentration is very stable if there is no human activity or other indoor sources. Nonetheless, it is important to make sure that the CO_2 concentration is elevated to levels that are high enough such that small fluctuations in the background CO_2 concentration become negligible. When an investigation needs to take place in an unoccupied building CO_2 is generated artificially either by burning a controlled flame for some time, subliming some dry ice or else by releasing lab-grade CO_2 from a gas cylinder.

2.4 Methodology employed in this study

The study made use of the mobile air quality laboratory (MAQL) to take indoor and outdoor air pollutant measurements. The MAQL consists of two sets of each equipment. One set of the equipment is installed in a van and is used to measure outdoor pollutants while the other set is mounted on portable racks and is used to investigate air quality in indoor environments.

The MAQL was essential in the investigation of this study. A sampling campaign took place at the University of Malta Junior College (hereinafter referred to as JC) between the 28th of March and 15th of April 2019. This campaign aimed to obtain simultaneous indoor and outdoor PM measurements against a varied spectrum of AERs. This data would be essential to validate different PM infiltration models. The validation of other models required simple experimental modifications that were also carried out during the same campaign.

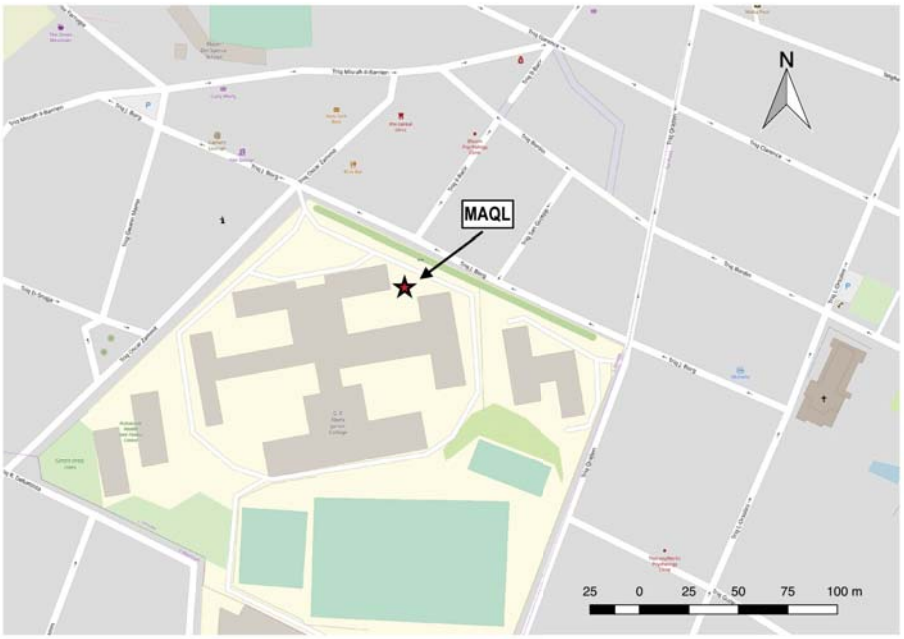

Figure 2.2: The location of the MAQL within the JC campus.

This area has been left intentionally blank.

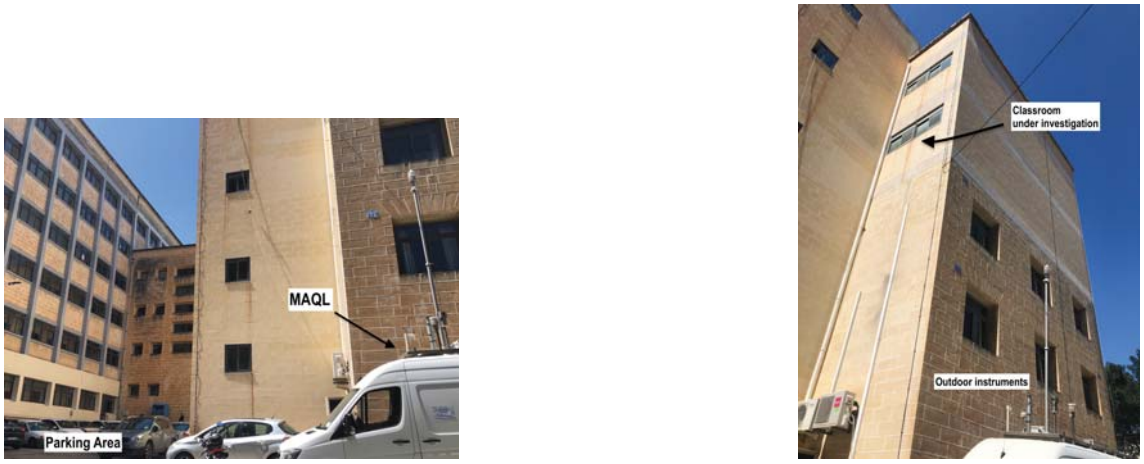

Figure 2.3: MAQL at the JC campus.

Figure 2.2 shows the position of the MAQL within the JC campus while Figure 2.3 gives an insight of the outdoor setup highlighting the parking area close by and the windows of the room investigated relative to the outdoor instruments. The indoor environment considered was a classroom located on the third floor of the building, facing a small parking area and the ring road. The classroom was not in use at the time the campaign was carried out.

Figure 2.4: Indoor equipment including the PM and BC monitors as well as CO_2 meters.

The van was parked directly beneath the windows of the classroom being investigated (Figure 2.3). Simultaneous indoor and outdoor PM and BC measurements were executed continuously throughout the whole campaign. Figure 2.4 illustrates the indoor setup including the PM and BC monitors. Along with the PM and BC monitors the indoor setup included two CO_2 meters. The room's dimensions, as well as the position of the instruments used, are presented in Figure 2.5.

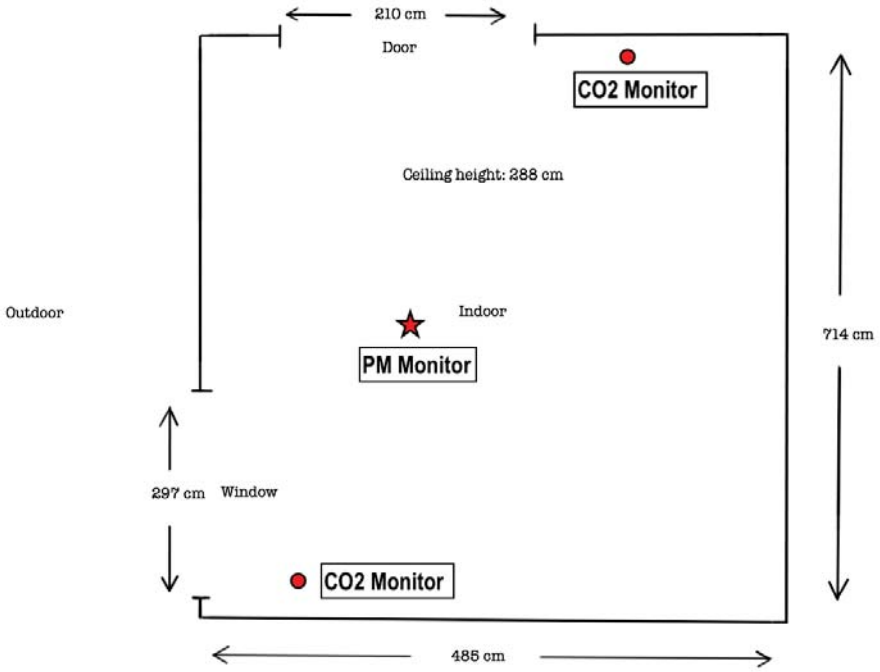

Figure 2.5: JC indoor environment schematic.

2.4.1 The sampling procedure

One day before the campaign commenced, both indoor and outdoor instruments were switched on, calibrated, and tested. All instruments used register measurements continuously (every minute) and were kept on for the whole campaign. The main task during the campaign was to vary the classroom's ventilation rate by opening the windows in different proportions to obtain a wide spectrum of AER values.

The indoor CO_2 concentration had to be elevated every day to estimate the AER. CO_2 was released from a gas cylinder for about five minutes until the indoor concentration was increased to around 5,000 ppm. A small mechanical fan was switched on during the release and left on for some minutes to ensure a good mixing of the tracer gas released.

Three days from the whole campaign were dedicated to estimating k of the indoor particulates at different size fractions. To calculate k, the indoor PM concentration needs to be increased significantly. This was done by fully opening the windows and allowing outdoor pollution to enter indoors. Additionally, the fan was switched on to generate some resuspension of the particulates already settled on the ground. The indoor PM concentration was noted until it reached a maximum. The windows were then fully closed and the room was left undisturbed for at least 17 hours. Table 2.1 illustrates the 13 days of the campaign indicating the window characteristics for the particular day and also highlight when 'decay tests' to estimate k were carried out.

This area has been left intentionally blank.

Table 2.1: Campaign information and window characteristics for each day.

Day	Date	Window Characteristics	Test Information
1	28/03/19	closed	
2	29/03/19	closed	Decay test 1
3	01/04/19	20 cm	
4	02/04/19	40 cm	
5	03/04/19	80 cm	
6	04/04/19	20 cm	
7	06/04/19	closed	
8	08/04/19	40 cm	
9	09/04/19	closed	Decay test 2
10	10/04/19	30 cm	
11	11/04/19	40 cm	
12	12/04/19	closed	Decay test 3
13	15/04/19	20 cm	

This area has been left intentionally blank.

Chapter 3

Results and discussion

Controlled experiments were conducted in an unoccupied classroom located on the third floor of the JC campus in Msida. The campaign was conducted over 13 days between March and April 2019 and involved continuous indoor and outdoor PM_1, $PM_{2.5}$ and PM_{10} measurement, indoor and outdoor BC measurements as well as daily AER estimates. The room was accessed only for some minutes every day to perform CO_2 releases and collect data from the instruments, otherwise the room was unoccupied all the time and locked to ensure no indoor sources were present at the time of sampling.

Infiltration parameters were determined from the data available and were then used to estimate the indoor PM concentration of ambient origin. The models presented in Chapter 1 were investigated and validated against the data collected and finally compared to determine the best-performing model given the data collected from this campaign. A separate campaign in a residential home in Birżebbuġa (BBG) was also carried out over 8 days between June and July 2019. This new dataset was then used to revalidate some models initially considered.

3.1 Measured quantities

3.1.1 Particulate matter

The instruments used (Palas Fidas-200) in the campaign provided continuous (1-minute) PM_1, $PM_{2.5}$ and PM_{10} indoor and outdoor data. The data were then averaged accordingly as required by the particular model investigated. In order to have distinct fractions of particulates, all analysis was carried out on PM_1, $PM_{1\text{ - }2.5}$, and $PM_{2.5\text{ - }10}$, where $PM_{1\text{ - }2.5}$ and $PM_{2.5\text{ - }10}$ refer to the fraction of particulates ranging from 1 μm to 2.5 μm and 2.5 μm to 10 μm respectively. This was done so that all analysis could be performed on discrete particle size fractions and thus yield more realistic results when quantifying the infiltration abilities of particulates.

Time series analysis was important to conceptualise and understand the typical outdoor and indoor PM concentrations and also typical trends of ambient PM peaks in relation with time of day and traffic flow around the area under investigation. Also, since the room had to be accessed for around 30 minutes on a daily basis in order to perform CO_2 releases, the indoor activity generated some indoor peaks due to resuspension of the indoor particulates. Time series plots were thus utilised to identify and exclude such indoor concentration peaks when carrying out the analyses. For this analysis it was decided to eliminate the first seven hours of data immediately after the room was closed to make sure the indoor measurements were not affected by resuspension mechanisms. One particular day from the campaign was eliminated completely as resuspesion peaks were so significant that only 12 hours of data were suitable for analysis.

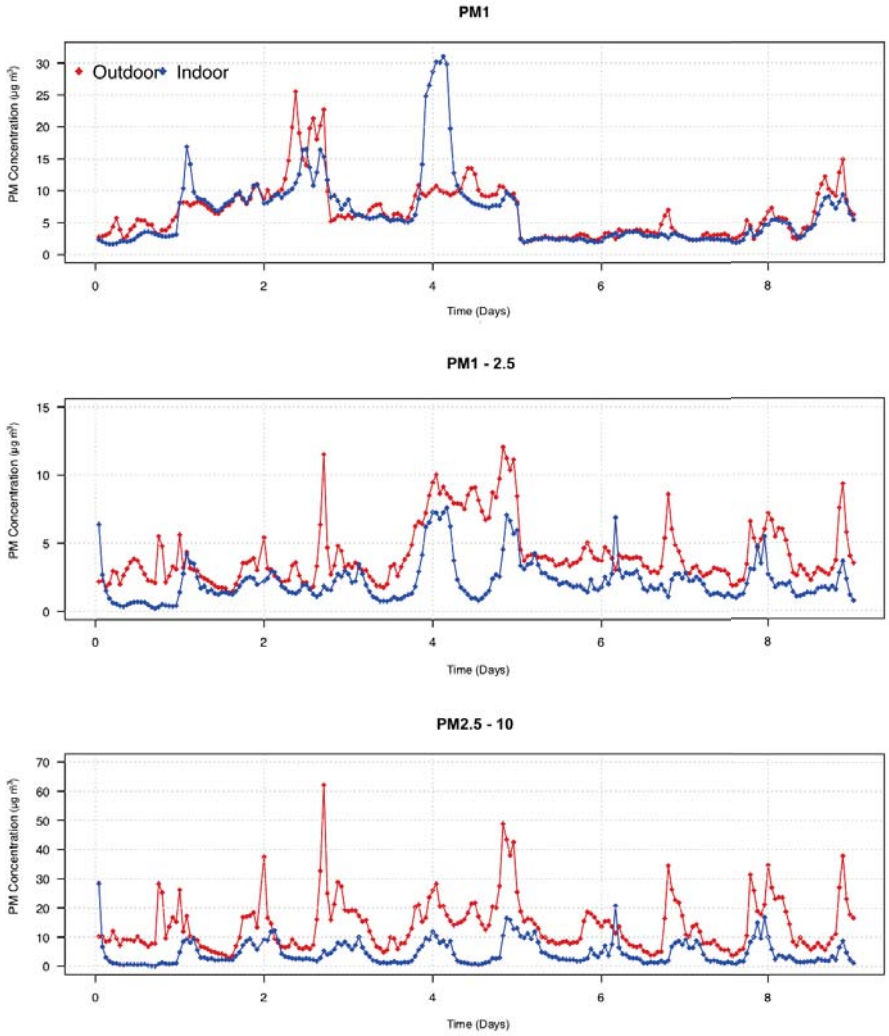

Figure 3.1: Time series plots of the indoor and outdoor concentrations for different size fractions using hourly data.

Figure 3.1 illustrates time series plots of ambient and indoor PM_1, $PM_{1\text{ - }2.5}$ and $PM_{2.5\text{ - }10}$ for nine days during the campaign. Over nine days the average indoor and outdoor PM_1 were recorded at 6.5 µg m^{-3} and 6.7 µg m^{-3} respectively, while for $PM_{1\text{ - }2.5}$, 2.2 µg m^{-3} and 4.3 µg m^{-3}, and for $PM_{2.5\text{ - }10}$, 4.5 µg m^{-3} and 14.0 µg m^{-3} respectively.

3.1.2 Air exchange rate

The AER of a building depends on many parameters including the air-tightness of the building, temperature and pressure difference across the building, and weather conditions. In practice, the AER is not a constant but varies continuously with time, at quasi-equilibrium conditions (i.e. during periods when there are little variations in the outdoor and indoor environments), however, the AER can be assumed to be a quasi-constant for that particular time frame [31].

During the campaign, the indoor environment was left undisturbed and thus the air-tightness properties of the buildings were not altered by human activities taking place indoors. This means that variations in the AER were mainly attributed to atmospheric conditions at the time of sampling.

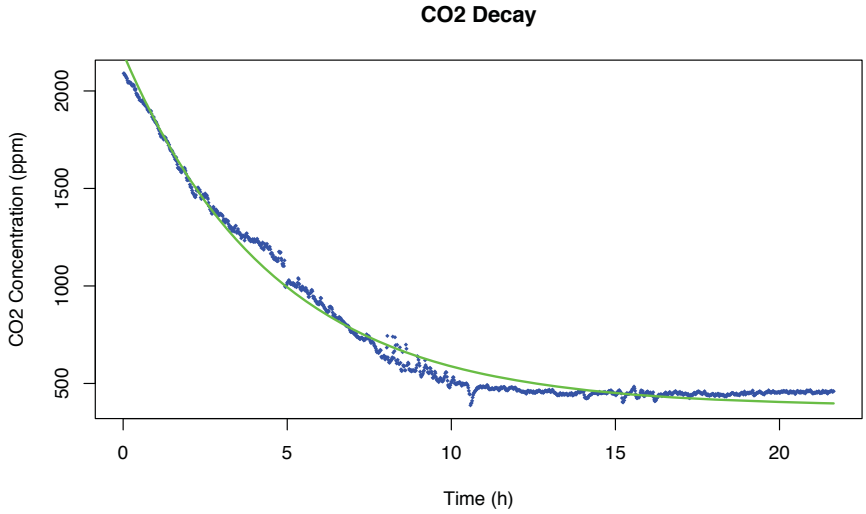

Figure 3.2: Time series plot illustrating the decay in CO_2 concentration (ppm) of the indoor environment as well as curve fitting in order to estimate the AER.

The AER was calculated by plotting a time series of the decaying indoor CO_2 concentration. During decay, the emission rate of the tracer gas in Equation 2.2 becomes zero and thus the indoor concentration during this instance can be modelled

through the equation:

$$C_i(t) = C_0 - (C_0 - C_{i_0})e^{-\frac{q}{V}(t-t_0)} \tag{3.1}$$

where $a = \frac{q}{V}$ is the AER.

An R script was used to determine the parameters by fitting Equation 3.1 to the CO_2 data (Figure 3.2) using the maximum and minimum CO_2 concentrations as the initial parameter values for $(C_0 - C_{i_0})$ and C_0 respectively. The curve fitting analysis yields estimates of the AER attributed to the given CO_2 decay curve.

The estimated AER varied from 0.21 h^{-1} to 5.10 h^{-1} with a mean of 2.80 h^{-1}. The AER data is presented together with PM data in Table 3.3. The room investigated included double-pane sliding windows, a hollow 38 mm thick door and ceiling tiles including a cassette AC system that was not operative. The door included two air vent grilles that were completely sealed off using paper and masking tape. When the windows were completely closed the estimated AERs were found to be very consistent at a mean of 0.23 $\pm$ 0.01 h^{-1} meaning that in one hour only 23% of the indoor air was being replaced.

3.2 Indoor particle removal rate k

An important parameter in the understanding of PM infiltration dynamics is the indoor particle removal rate k. This term accounts for loss mechanisms mostly taking place through deposition and diffusion of particulates. Some models ignore this parameter altogether by assuming certain conditions while other models estimate this term analytically either independently or else coupled with other parameters such as the infiltration efficiency P. However, k can be determined experimentally through the exponential decay of the indoor PM concentration. The indoor PM

levels can be increased either through indoor activities that cause significant resuspension (e.g. cleaning) or else by opening the windows to allow the free entrance of outdoor particulates. The latter methodology was employed on three days during the JC campaign to raise the indoor particulate concentration.

Figure 3.3 shows 24-hour time series of the indoor and outdoor PM_1, $PM_{1\text{ - }2.5}$, and $PM_{2.5\text{ - }10}$ fractions. The indoor concentration can be observed increasing and reaching an equilibrium with the outdoor concentration at around the 12^{th} hour. The vertical solid line in the plots represents the event when the windows were opened while the dashed line represents the time at which the windows were completely closed and the room was left undisturbed. The decay curve produced were used to determine the indoor particle removal rate.

This area has been left intentionally blank.

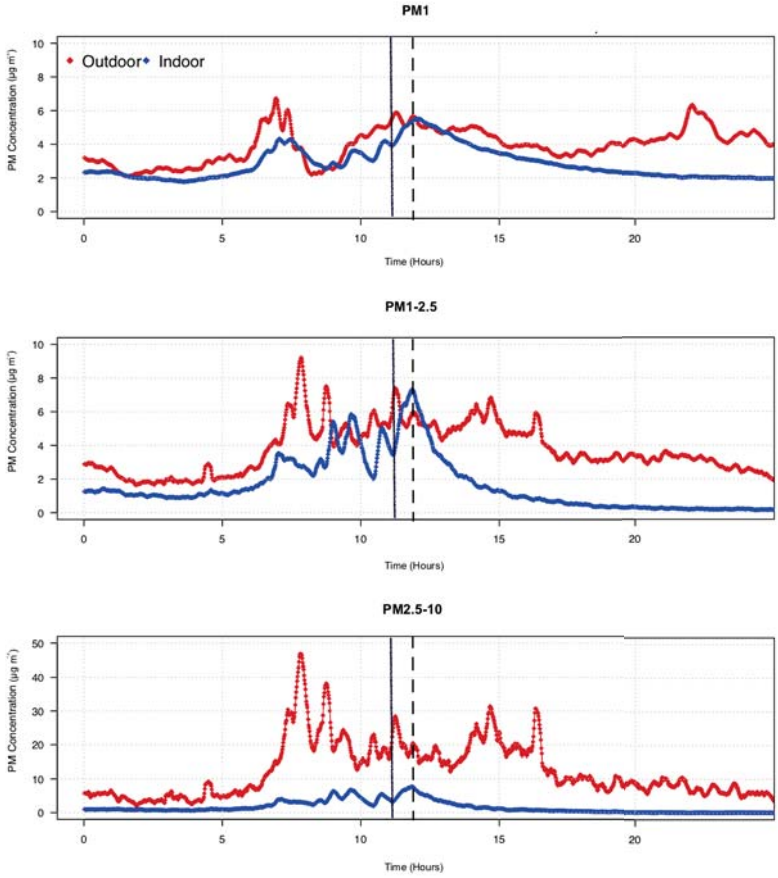

Figure 3.3: Time series plots illustrating the elevation and decay of indoor PM concentrations for different size fractions.

Figure 3.4 represents one of the decay curves of indoor particulate concentration. The plot includes values of the initial concentration (C_{int}) and the concentration at steady-state (C_{SS}). C_{int} and C_{SS} were determined by fitting Equation 1.21 (green line) to the measured data (blue points). These values were then used in Equation 1.21 to estimate λ. λ was determined for PM_1, $PM_{1\text{ - }2.5}$, and $PM_{2.5\text{ - }10}$ and the analysis was repeated three times (Test 1, Test 2 and, Test 3) as described in Table 2.1.

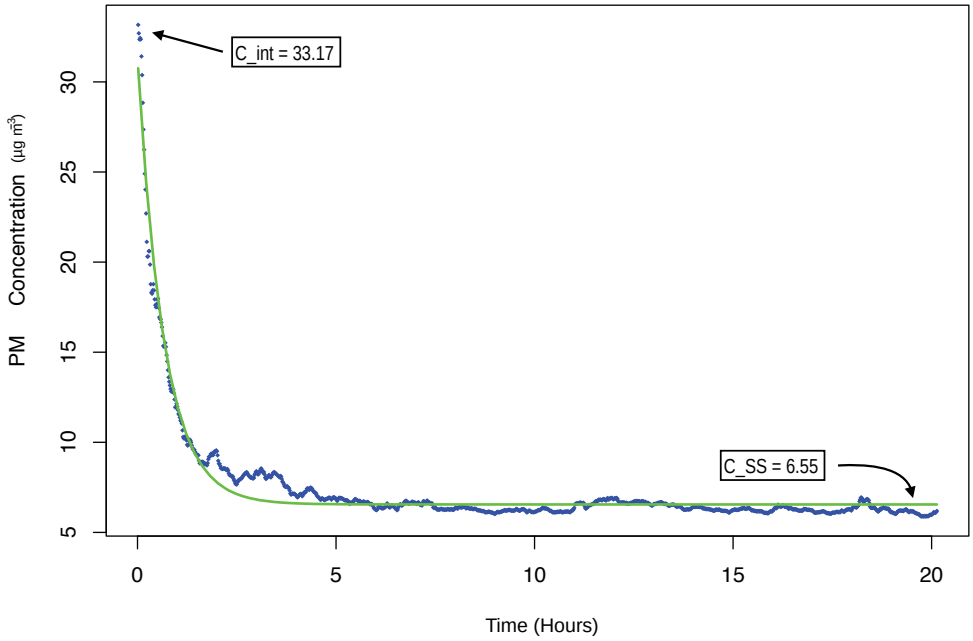

Figure 3.4: Curve fitting of the decaying indoor PM concentration.

Regression of $\ln\left[\frac{C_{\text{in}}-C_{\text{SS}}}{C_{\text{int}}-C_{\text{SS}}}\right]$ on t (Equation 1.22) yields estimates of λ. k is equivalent to the difference between the observed particle decay rate constant λ and the AER.

$$k = \lambda - a \tag{3.2}$$

The AER was calculated through the CO_2 decay method and was found to be 0.26 h^{-1}, 0.25 h^{-1} and 0.18 h^{-1} for Test 1, 2 and 3 respectively. From Equation 3.1 immediately comes clear that the k becomes negligible for high AER. Table 3.1 presents values of C_{int}, C_{SS}, and λ with the corresponding AER and calculated k. Average values of λ and k from the three tests carry out at different size fractions are presented in Table 3.2. Under conditions that the AER is greater than these values, k becomes negative which physically implies that the term is negligible in such situations. The experimentally-determined λ was used as a cut-off value determining when k becomes significant for a particular size fraction.

Table 3.1: Determination of λ through decay curves of indoor PM concentration.

Fraction	AER (h^{-1})	C_{int} (μgm^{-3})	C_{SS} (μgm^{-3})	λ (SD) (h^{-1})	R^2	k (h^{-1})
Test 1						
PM_1	0.26	7.37	5.71	0.89 (0.01)	0.97	0.63
$PM_{1 - 2.5}$	0.26	4.29	0.30	0.55 (0.01)	0.97	0.29
$PM_{2.5 - 10}$	0.26	21.62	0.72	1.24 (0.02)	0.94	0.98
Test 2						
PM_1	0.25	2.65	1.12	0.22 (0.001)	0.96	-
$PM_{1 - 2.5}$	0.25	3.99	0.39	0.39 (0.01)	0.86	0.14
$PM_{2.5 - 10}$	0.25	19.02	0.55	1.37 (0.02)	0.97	1.12
Test 3						
PM_1	0.18	5.51	1.75	0.24 (0.001)	0.99	0.06
$PM_{1 - 2.5}$	0.18	7.32	0.20	0.55 (0.002)	0.99	0.37
$PM_{2.5 - 10}$	0.18	24.31	0.28	0.82 (0.01)	0.97	0.64

Table 3.2: Average λ from Test 1, Test 2 and Test 3 for different size fractions as well as the corresponding AER.

PM Size Fraction	AER (h^{-1})	λ (h^{-1})	k (h^{-1})
PM_1	0.26	0.45	0.35
$PM_{1 -2.5}$	0.25	0.50	0.26
$PM_{2.5 - 10}$	0.18	1.19	0.91

3.2.1 Models' validation

In this section different techniques were used to estimate the infiltration parameters F_{INF}, P, and k. These parameters were subsequently used to model the indoor PM concentration of ambient origin from outdoor PM data. The following models are based on one form or another of the MBE previously derived an presented in Equation 1.1.

3.2.2 Steady-state assumption

The first set of models investigated and validated were derived from the MBE assuming steady-state conditions. Steady-state conditions imply that indoor and outdoor particulate concentrations, as well as the AER, are constant over the sampling period considered. Such assumptions were maintained by ensuring no sources and/or resuspension occurred in the indoor environment and by considering long time periods so that any abnormal peaks in the outdoor concentration are flattened out over the time-frame considered. Typically such models are validated against datasets of nightly-averaged concentration in occupied buildings (in order to avoid indoor activities) or against 24-hour averaged indoor and outdoor data. Models utilising the steady-state assumption were the earliest developed, not only because they simplify the calculations drastically, but also since they do not rely on continuous data, which was often difficult to collect in the past.

This area has been left intentionally blank.

Table 3.3: 17-hour averaged indoor and outdoor data with the corresponding AER from the JC campaign.

Day	Window	AER (h^{-1})	Indoor PM_1 (SD) (μgm^{-3})	Outdoor PM_1 (SD) (μgm^{-3})	Indoor $PM_{1\text{ - }2.5}$ (SD) (μgm^{-3})	Outdoor $PM_{1\text{ - }2.5}$ (SD) (μgm^{-3})	Indoor $PM_{2.5\text{ - }10}$ (SD) (μgm^{-3})	Outdoor $PM_{2.5\text{ - }10}$ (SD) (μgm^{-3})
1	closed	0.21	2.80 (0.55)	4.30 (1.04)	0.49 (0.15)	3.09 (1.12)	0.59 (0.23)	11.57 (7.00)
2	20 cm	0.91	8.46 (1.05)	8.05 (1.11)	1.76 (0.50)	2.45 (0.85)	4.16 (2.64)	8.43 (5.71)
3	40 cm	2.69	11.70 (3.10)	14.46 (7.11)	1.81 (0.56)	3.79 (2.47)	4.11 (2.21)	18.16 (15.30)
4	80 cm	5.10	5.69 (0.36)	6.47 (0.93)	1.38 (0.78)	3.01 (0.99)	2.81 (2.67)	10.36 (4.69)
5	40 cm	5.16	2.34 (0.24)	2.67 (0.31)	2.01 (0.41)	3.85 (0.57)	3.03 (1.20)	11.16 (4.34)
6	30 cm	1.99	3.14 (0.33)	3.97 (1.14)	2.17 (0.59)	4.19 (1.69)	3.39 (2.05)	12.06 (11.04)
7	40 cm	4.11	2.68 (0.76)	3.38 (1.03)	2.00 (1.40)	3.45 (1.54)	4.58 (5.28)	11.07 (8.93)
8	20 cm	2.21	6.19 (2.31)	7.94 (3.69)	1.65 (0.74)	3.82 (2.05)	2.82 (2.17)	12.60 (9.71)

Table 3.3 presents 17-hour averaged PM_1, $PM_{1\text{ - }2.5}$, and $PM_{2.5\text{ - }10}$ concentrations with the corresponding AER for 8 days. The second column of the table presents the status of the (sliding) window for every day of the campaign. The window was fully closed on Day 1 and opened at different amounts (in cm) on the remaining days.

The first method used was proposed and investigated by Dockery et al. in 1980, hereinafter referred to as Model 1. In Model 1 the authors assumed that k is negligible by considering data with a corresponding AER of above 1.5 h^{-1}. Under such ventilation rates, the air within the indoor environment is replaced often not allowing deposition losses to take place. As remarked in Chapter 1, under this assumption the F_{INF} becomes equivalent to the P which simplifies the model to Equation 1.9 which is recalled below for reference.

$$C_{in} = P.C_{out}$$

Values of the total particulate loss rate (λ), estimated in Section 3.2 (Table 3.2), were used to determine k associated with each sampling day. Days in which the ventilation rate was low enough such that k becomes significant were discarded to conform with the assumption of Model 1. Estimates of P were obtained through linear regression of C_{in} on C_{out} by forcing the intercept to zero (Figure 3.5). Table 3.4 presents the estimates of P for each fraction considered. N is the number of data point utilised for the regression analysis.

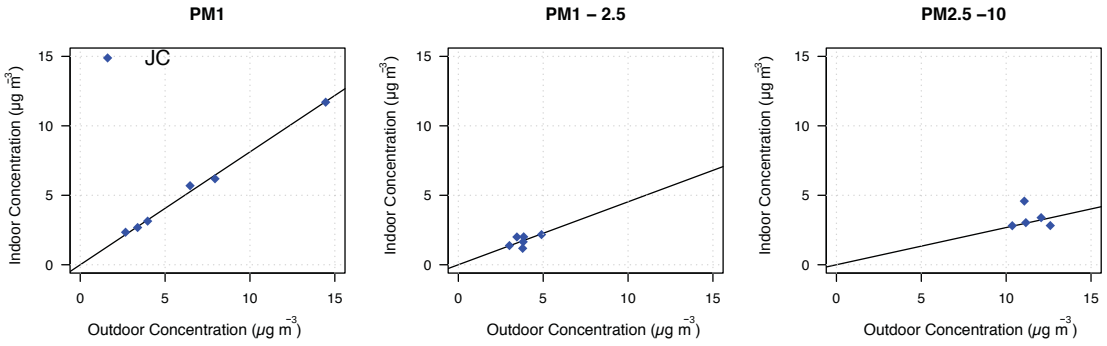

Figure 3.5: Regression plots when Model 1 was applied.

Table 3.4: Regression analysis when Model 1 was applied considering only data with negligible k.

Model 1	N	Gradient (SD)	R^2
PM_1	6	0.81 (0.01)	0.99
$PM_{1 - 2.5}$	6	0.50 (0.04)	0.99
$PM_{2.5 - 10}$	6	0.28 (0.03)	0.95

The estimated values of P for smaller particulates was found to be much higher

than that for coarser PM, suggesting that finer particles penetrate indoors much more effectively. The determined P values were then used to predict the indoor PM concentration from outdoor data through Equation 1.9.

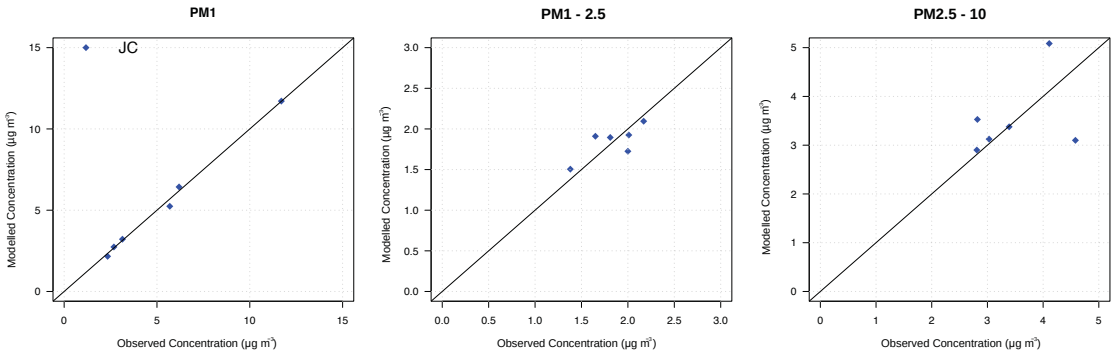

Figure 3.6: Comparison of modelled and observed values for different size fractions, when Model 1 was applied.

The performance of Model 1 is displayed graphically in Figure 3.6. Plots of the observed versus modelled PM concentration values are presented. An $x = y$ reference line was also added to each plot so that over or under predicted data points can be easily recognised. The performance of the model was also assessed by calculating root-mean-square error (RMSE) as well as the mean absolute percentage error (MAPE) between the measured and modelled indoor concentration values.

The RMSE and MAPE are commonly used statistical techniques that provide a general measure of how close the modelled values are to the actual observed values. They are defined as follows:

$$\text{RMSE} = \left(\frac{\sum_{i=1}^{n} (M_i - O_i)}{n} \right)^{1/2} \tag{3.3}$$

$$\text{MAPE} = \left(\frac{|O_i - M_i|}{O_i} \right) \times 100 \tag{3.4}$$

where n is the sample size, M_i and O_i represents the ith modelled and observed values.

Table 3.5: Statistical evaluation when Model 1 was applied.

Model 1	N	RMSE (μg m^{-3})	MAPE (%)	R^2
PM_1	6	0.23	4.01	0.99
$PM_{1\text{ - }2.5}$	6	0.17	8.49	0.57
$PM_{2.5\text{ - }10}$	6	0.78	14.65	0.15

Table 3.5 presents the RMSE and MAPE for different size fractions when Model 1 was applied. The model performs appreciably well especially for the PM_1 fraction. The MAPE was found to increase for coarser fractions however the RMSE was found to be 0.17 μg m^{-3} (lowest) for $PM_{1\text{ - }2.5}$ and 0.78 μg m^{-3} (highest) for $PM_{2.5\text{ - }10}$.

The second model considered that assumes steady-state conditions was proposed by Long et al. in 2001, hereinafter referred to as Model 2. Model 2 modified Equation 1.1 in order to separate the coupled influences of P and k, defining the F_{INF} term. Model 2 was discussed in Chapter 1 and presented through Equation 1.11 which is recalled below for reference.

$$\frac{C_{out}}{C_{in}} = \frac{k}{P}\left(\frac{1}{a}\right) + \frac{1}{P}$$

Equation 1.11 is also a linear function and the regression of $\frac{C_{out}}{C_{in}}$ on $\frac{1}{a}$ gives estimates for P and k from the y-intercept $(1/P)$ and the slope (k/P) (Figure 3.7). Table 3.6 presents the results of the estimated P and k from the regression analysis. P can be observed to be highest for PM_1 and gradually decreases at coarser fractions of PM. The value of k gets larger for coarser size fractions indicating that larger particulates are more effectively deposited due to gravitational settling. The values

of P estimated in Model 2 are in general higher than those estimated through Model 1 possibly due to the analytical estimation of k in the calculations.

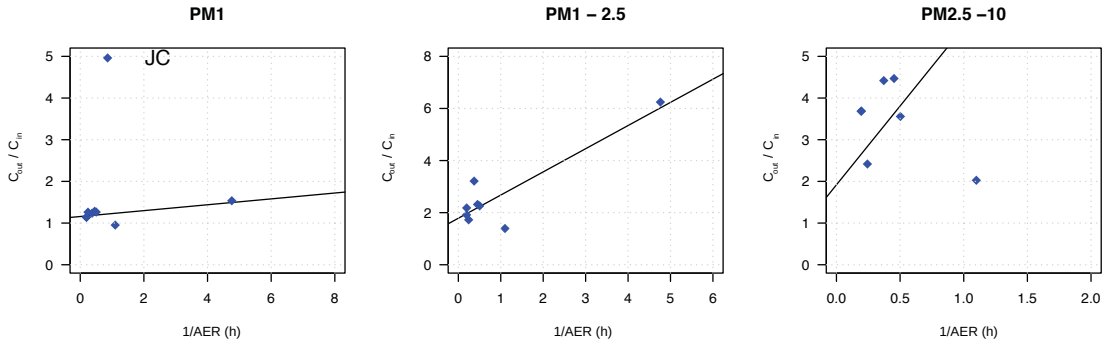

Figure 3.7: Regression plots when Model 2 was applied.

Table 3.6: Regression analysis when Model 2 was applied.

Model 2	N	Gradient (SD)	y-intercept (SD)	R^2	P	k (h^{-1})
PM_1	8	0.07 (0.03)	1.16 (0.06)	0.45	0.86	0.06
$PM_{1\ -\ 2.5}$	8	0.95 (0.13)	1.55 (0.24)	0.89	0.65	0.61
$PM_{2.5\ -\ 10}$	8	3.55 (0.44)	2.02 (0.77)	0.92	0.50	1.76

The estimated values of P and k were then used to calculate F_{INF} for every sampling event using the corresponding measured AER. Plots of the measured versus modelled data are presented in Figure 3.8 and the corresponding statistical analysis is shown in Table 3.7.

Estimates of P and k were consistent with building shielding and particle deposition theories and the estimates were also similar to values obtained in other studies [16]. P tends to be the highest for finer fractions of particulates and decrease for course particulate fractions since larger particulates are better shielded by the building

envelope. k increases for courser particulate fractions as larger particles are more effectively deposited due to gravitational settling mechanisms.

The study deriving this model (Model 2) estimated that P values varied between 0.70 - 0.90 h^{-1} for PM_1, 0.50 - 0.70 h^{-1} for $PM_{1\ -\ 2.5}$, and 0.30 - 0.60 h^{-1} for $PM_{2.5\ -\ 10}$ making all P values in Table 3.2 in range. In the same study, k varied between 0.10 - 0.35 h^{-1} for PM_1, 0.20 - 0.40 h^{-1} for $PM_{1\ -\ 2.5}$ and 0.20 - 0.60 h^{-1} for $PM_{2.5\ -\ 10}$. In this case, the estimated k was found to be underestimated for PM_1 and overestimated for $PM_{1\ -\ 2.5}$ and $PM_{2.5\ -\ 10}$ when compared to this study [26]. The discrepancies between the estimated k in this study may be attributed to the differences in building dynamics with different surface roughness which is responsible for deposition mechanisms.

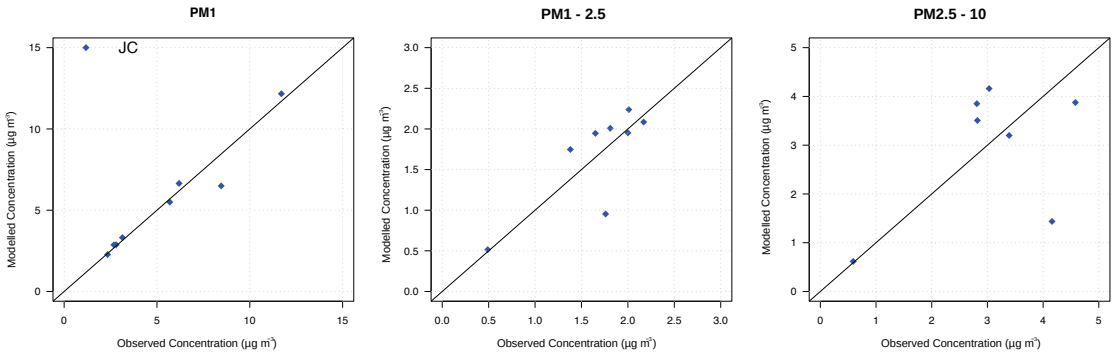

Figure 3.8: Comparison of modelled and observed values for different size fractions, when Model 2 was applied.

Table 3.7: Statistical evaluation when Model 2 was applied using the analytical estimation of k.

Model 2	N	RMSE (μgm^{-3})	MAPE (%)	R^2
PM_1	8	0.74	7.01	0.95
$PM_{1\ -\ 2.5}$	8	0.35	15.49	0.63
$PM_{2.5\ -\ 10}$	8	1.26	27.91	0.31

Model 2 was further investigated by estimating the F_{INF} using P from the regression analysis but replacing k with the one determined experimentally. The modelled concentration values using the new F_{INF} are presented in Figure 3.9 and the corresponding MAPE values are given in Table 3.8. The new F_{INF} produced less accurate predictions of the indoor concentration from outdoor particulate data.

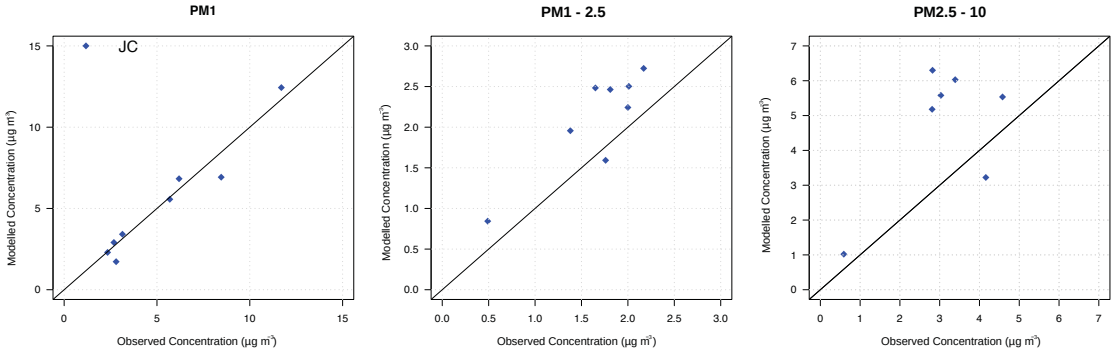

Figure 3.9: Comparison of modelled and observed values for different size fractions, when Model 2 was applied using the experimental value of k.

Table 3.8: Statistical evaluation when Model 2 was applied using the experimental value of k.

Model 2	N	RMSE (μgm^{-3})	MAPE (%)	R^2
PM_1	8	0.76	11.80	0.95
$PM_{1\text{ - }2.5}$	8	0.53	34.02	0.76
$PM_{2.5\text{ - }10}$	8	2.69	75.89	0.39

Table 3.8 confirms that Model 2 with experimental values of k did not perform as well as when the analytically-determined k was employed. This may be attributed to the fact that P and k are not determined independently through this method and in fact, both values depend on each other to provide reasonable estimates of F_{INF}.

3.2.3 Dynamic solution of MBE

In this section, continuous data were used to evaluate dynamic models based on the non-linear solution of the MBE. The first model considered that employed a dynamic solution of the MBE involved a basic "forward-marching" scheme with time step, Δt [19]. This approach, hereinafter referred to as Model 3, was previously discussed and presented through Equation 1.14, recalled below.

$$C_{in_{i+1}} = Pa\Delta tC_{out_{i+1}} + (1 - (a + k)\Delta t)C_{in_i}$$

Equation 1.14 shows the finite time step form of the solution, where $C_{in_{i+1}}$ is the concentration determined from the outdoor concentration at the same time step ($C_{out_{i+1}}$) and the indoor concentration of the previous time step ($C_{out_{i+1}}$). The indoor and outdoor concentration values, together with values of the AER (a) attributed to the day of sampling, were used to estimate P and k using the Microsoft Excel Solver Add-In Tool without employing constraints on the two unknown parameters. Values of P and k were estimated by minimising the sum of the absolute difference between the observed and predicted indoor concentrations. Initial parameter values were selected randomly between 0 and 1 [28]. Since minute data was used, Δt was set as $\frac{1}{60}$ h. The AER, determined using the tracer gas method, was assumed to be constant for the entire 17-hour sampling period.

Table 3.9: Values of P and k, at different size fractions of PM determined from the non-linear solution of Equation 1.14.

		PM_1		$PM_{1\text{ - }2.5}$		$PM_{2.5\text{ - }10}$	
Day	AER	P	k	P	k	P	k
1	0.21	0.84	0.03	0.32	0.26	0.17	0.45
2	0.91	2.32	1.09	0.82	0.16	0.57	0.16
3	2.69	0.68	0	0.40	0	0.17	0
4	5.10	0.89	0	0.36	0	0.22	0
5	5.16	0.89	0	0.53	0	0.25	0
6	1.99	0.85	0	0.53	0	0.23	0
7	4.11	0.78	0	0.50	0	0.32	0
8	2.21	0.78	0	0.42	0	0.19	0

Table 3.9 presents values of P and k determined from the non-linear solution of the MBE. Using this method k estimates were only found to be significant for Day 1 and Day 2 of the campaign where the AER was 0.21 h^{-1} and 0.91 h^{-1} respectively. Physically, k is associated with deposition losses and several literature (e.g. [20]) suggest that k is indeed negligible under certain conditions where the ventilation rate is not low enough. From the experimentally determined values of λ, it was concluded that k only becomes significant when the AER is higher than 0.45 h^{-1}, 0.50 h^{-1} and 1.19 h^{-1} for PM_1, $PM_{1\text{ - }2.5}$ and $PM_{2.5\text{ - }10}$ respectively, meaning that the estimates of k from this method fall within range of the experimental values of k.

Figure 3.10 (on page 51) illustrates time series plots showing the outdoor PM concentration as well as the measured and modelled indoor particle concentration for PM_1, $PM_{1\text{ - }2.5}$, and $PM_{2.5\text{ - }10}$. The y-axis on the left-hand side demonstrates the concentration of the outdoor data while that on the right-hand side demonstrates indoor (both measured and modelled) concentration. While all plots are presented

in the Appendix section, the plots for Day 3 are presented here. The modelled indoor concentration can be seen to follow closely the measured indoor concentration, nonetheless, during certain instances, the modelled concentration slightly departs from the measured concentration when there are sudden fluctuations in the outdoor concentration. This can be mainly attributed to the fact that the indoor concentration is directly modelled from the outdoor concentration and the infiltration parameters. As already mentioned, the AER was assumed to be constants throughout the whole sampling period, even though this was highly unlikely. The estimates of k and P were also determined from the whole 17-hour sampling data and once determined, they were kept fixed when used to model the indoor contraction from outdoor data. It is also most likely that these infiltration parameters vary marginally throughout the 17-hour time frame considered.

This area has been left intentionally blank.

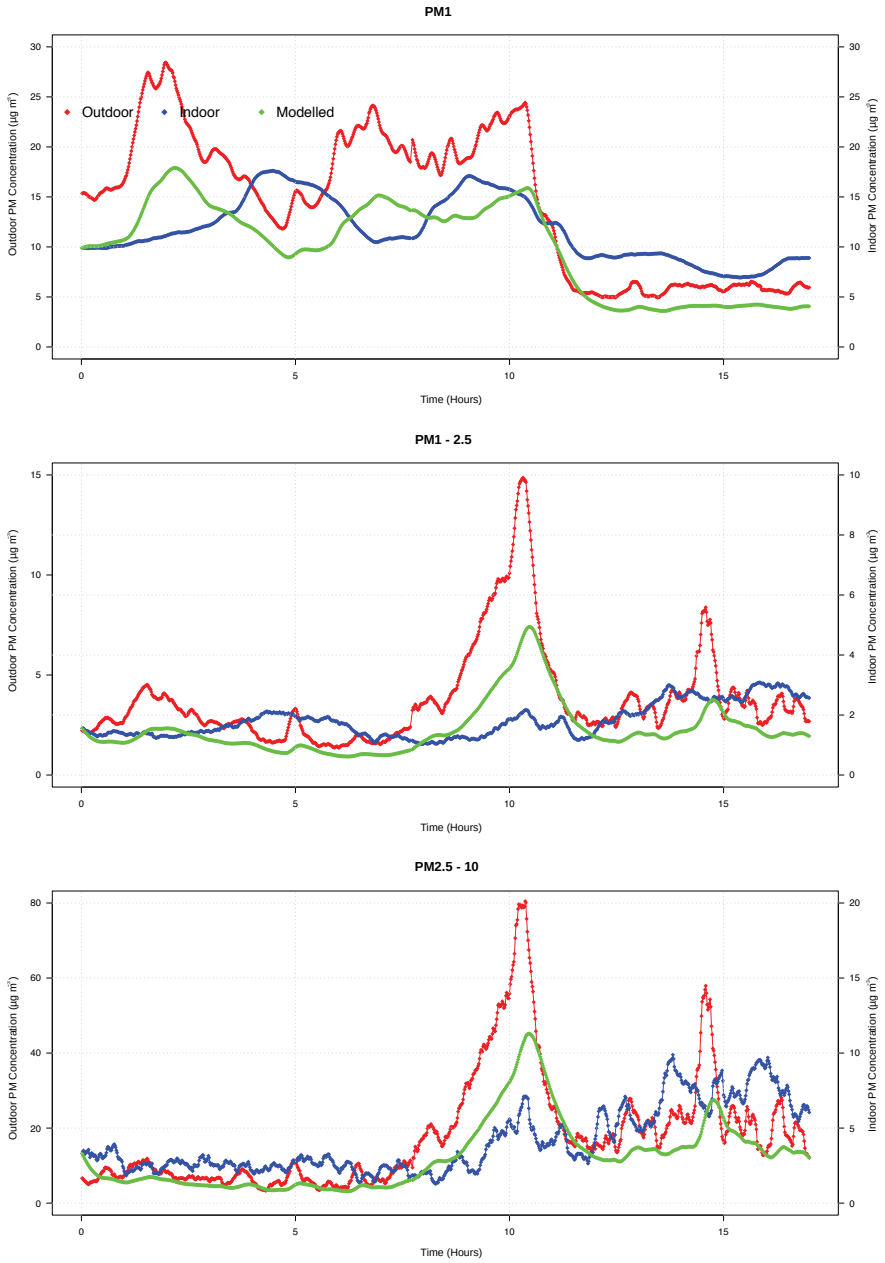

Figure 3.10: Measured indoor and outdoor concentrations together with the modelled indoor concentration using Equation 1.14, at different size fractions of PM.

Table 3.10 presents the RMSE and MAPE between the modelled and observed indoor PM concentration using the value of k and P determined from the non-linear solution of the MBE for different size fractions. The AER estimated for that

Table 3.10: Statistical evaluation when Model 3 was applied.

		RMSE (μgm^{-3})			MAPE (%)		
Day	AER	PM_1	$PM_{1 - 2.5}$	$PM_{2.5 - 10}$	PM_1	$PM_{1 - 2.5}$	$PM_{2.5 - 10}$
1	0.21	0.17	0.13	0.21	4.38	22.01	54.97
2	0.91	0.35	0.27	1.23	2.74	13.16	25.55
3	2.69	4.03	1.04	3.33	31.87	43.97	57.54
4	5.10	0.670	0.80	1.95	9.82	27.35	37.23
5	5.16	0.24	0.78	1.10	8.15	32.96	28.05
6	1.99	0.97	0.91	1.89	17.65	34.11	47.06
7	4.11	0.35	1.00	3.82	9.16	54.97	37.64
8	2.21	0.67	0.47	1.40	9.31	27.59	41.35

particular day, and that was used in the computation of the indoor concentration from outdoor data is also included in the table. Model 3 performs best for PM_1 with MAPE ranging from 3% to 32%, however the MAPE gets larger for coarser fractions with a range of 13% - 55% and 26% - 58% for $PM_{1 - 2.5}$ and $PM_{2.5 - 10}$ respectively. The mean MAPE over the eight days turned out to be 12%, 32%, and 41% for PM_1, $PM_{1 - 2.5}$, and $PM_{2.5 - 10}$ respectively.

The second regressive model considered involved an integral solution of the MBE. The model, hereinafter referred to as Model 4, was presented in Equation 1.15 and is recalled below for reference [29].

$$C_{in(i)} = C_{in(i-1)}e^{-(k+a)\Delta t} + C_{out(i-1)}\frac{Pa}{a+k}(1 - e^{-(k+a)\Delta t})$$

As done in the previous model, the value for a was taken from the tracer gas method that was measured daily while k and P were determined using the Microsoft Excel Solver Add-In Tool without employing constraints on the two unknown parameters as per the previous analysis.

Table 3.11: Values of P and k, at different size fractions of PM when Model 4 was applied.

	PM_1		$PM_{1 - 2.5}$		$PM_{2.5 - 10}$	
Day	P	k	P	k	P	k
1	0.22	0	0.29	0	0.07	0
2	0.12	0	0.33	0	0.07	0
3	0.06	0	0.24	0	0.03	0
4	0.16	0	0.30	0	0.06	0
5	0.38	0	0.26	0	0.08	0
6	0.27	0	0.24	0	0.05	0
7	0.30	0	0.22	0	0.05	0
8	0.10	0	0.17	0	0.03	0

Table 3.12: Statistical evaluation when Model 4 was applied.

		RMSE (μgm^{-3})			MAPE (%)		
Day	AER	PM_1	$PM_{1 - 2.5}$	$PM_{2.5 - 10}$	PM_1	$PM_{1 - 2.5}$	$PM_{2.5 - 10}$
1	0.21	1.40	0.18	0.38	42.73	29.41	53.28
2	0.91	2.63	1.40	4.54	24.88	64.47	78.59
3	2.69	13.7	1.79	-	86.82	89.85	-
4	5.10	-	1.04	2.62	-	85.48	89.79
5	5.16	7.86	-	3.07	118.91	-	95.63
6	1.99	-	0.98	4.19	-	44.12	94.49
7	4.11	2.31	2.43	6.99	81.09	95.83	97.48
8	2.21	6.56	1.78	3.53	96.08	94.64	95.15

Table 3.11 presents estimates of P and k for different size fractions while Table 3.12 presents RMSE and MAPE values using the observed and modelled indoor particulate concentration at the respective fractions. In some cases the model failed and when a MAPE of above 200% was registered it was not included. Table 3.12 reveals

that the model performs poorly in most cases across different fractions. Figure 3.11 illustrates the time series plots for Day 3 of the campaign using this method. It is evident that the model is unable to pick up sudden peaks in the concentration or else once a peak is picked up, the model is unable to settle back to do accurate predictions. This can be seen for the fraction $PM_{2.5\text{ - }10}$ below. All time series plots for the remaining days are presented in the Appendix section. It can be concluded that infiltration parameter determined from this approach using the JC dataset were not reliable at all and does not produce any relevant prediction when used to approximate the indoor particulate concentration from outdoor measurements.

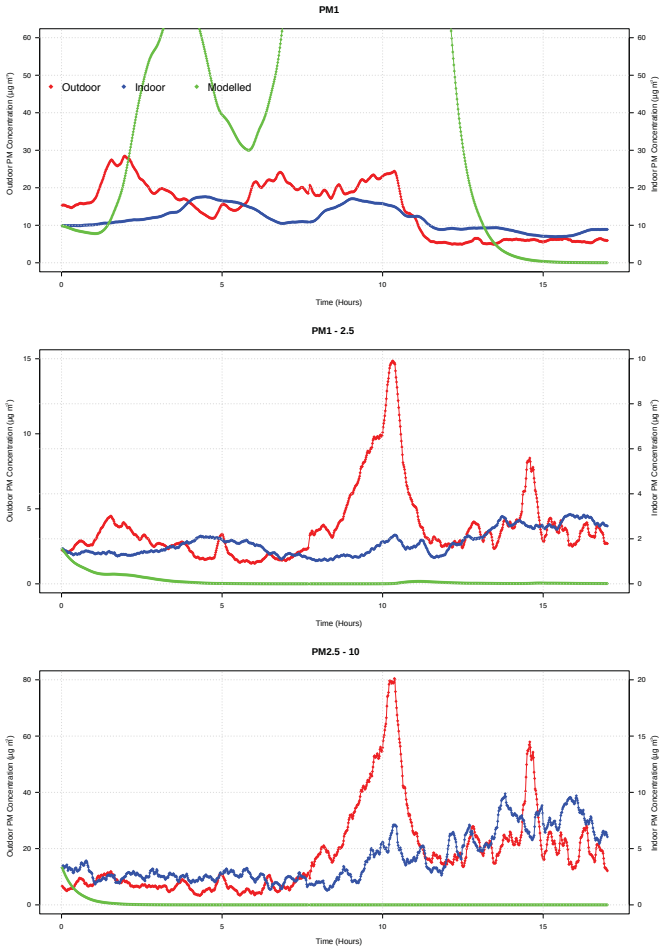

Figure 3.11: Measured indoor and outdoor concentrations together with the modelled indoor concentration using Equation 1.15, at different size fractions of PM.

Another method employing a dynamic solution of the MBE involves a linear solution to the recursive mass balance model, hereinafter referred to as Model 5. Assuming no indoor sources, Model 5 can be expressed as follows from Equation 1.16 [17].

$$C_t^{\text{in}} = \beta_1 C_t^{\text{out}} + \beta_2 C_{t-1}^{\text{in}} \tag{3.5}$$

where

$$F_{\text{INF}} = \frac{\beta_1}{1 - \beta_2} \tag{3.6}$$

The parameters β_1 and β_2 were obtained through multiple linear regression of Equation 3.4 forcing the intercept to zero and were used in Equation 3.5 to quantify the F_{INF} for each case.

Table 3.13: Regression analysis when Model 5 was applied.

		F_{INF}		
Day	AER	PM_1	$PM_{1\text{ - }2.5}$	$PM_{2.5\text{ - }10}$
1	2.21	0.72	0.16	0.05
2	0.91	1.05	0.70	0.48
3	2.69	0.74	8.80	0.33
4	5.10	0.85	0.36	0.18
5	5.16	0.85	0.48	0.25
6	1.99	0.44	0.40	0.36
7	4.11	0.83	0.72	0.61
8	2.21	0.78	0.42	-

β_1 and β_2 were estimated from multiple linear regression using an R script. The F_{INF} estimates were then determined using Equation 3.5 from hourly data and are presented in Table 3.13. The F_{INF} estimates for Day 2 PM_1 (1.05) and Day 3

$PM_{1\text{ - }2.5}$ (8.80) exceeded unity and were thus ignored. The F_{INF} for Day 8 $PM_{2.5\text{ - }10}$ was not presented as β_1 and β_2 yielded negative values of F_{INF}.

Table 3.14: Statistical evaluation when Model 5 was applied.

		RMSE (μgm^{-3})			MAPE (%)		
Day	AER	PM_1	$PM_{1\text{ - }2.5}$	$PM_{2.5\text{ - }10}$	PM_1	$PM_{1\text{ - }2.5}$	$PM_{2.5\text{ - }10}$
1	0.21	0.62	0.17	0.22	17.91	30.73	53.80
2	0.91	-	0.18	0.57	-	8.97	11.29
3	2.69	4.26	-	4.65	34.15	-	69.47
4	5.10	0.69	0.69	1.62	10.96	27.10	27.01
5	5.16	0.24	0.47	0.97	8.24	20.07	24.51
6	1.99	1.47	0.99	3.16	43.50	43.98	71.27
7	4.11	0.41	0.87	3.80	12.13	45.00	113.01
8	2.21	1.00	0.38	-	13.16	25.03	-

Table 3.14 presents RMSE and MAPE values from the measured and modelled data using the F_{INF} in Table 3.16. For the PM_1 size fraction the model performed appreciably well with MAPE values ranging from 8% to 44%. The MAPE increased for the fractions $PM_{1\text{ - }2.5}$ and $PM_{2.5\text{ - }10}$.

To evaluate the effects on the model using hourly data, which assumes constant concentrations during each hour increment, the F_{INF} was estimated once again using 1-minute averaged data. The parameters β_1 and β_2 were found to be the same (within three decimal places) as those calculated using hourly data, meaning that the same F_{INF} were yielded from the analysis. This supports the claim that hourly data would not greatly influence the estimated F_{INF}.

The final theoretical approach considered was proposed by Chao et al. in 2001, hereinafter referred to as Model 6. The authors assumed non-steady-stated conditions to derive the model presented in Chapter 1 through Equation 1.20 [32]. The

Equation is recalled below for reference.

$$y = \frac{C_{in}}{C_{out}} = 1 - Ae^{-\eta a}$$

The parameter A is related to the influence of the outdoor containment level and the prevailing indoor particulate level. A can be said to be an analogy of the filtration efficiency and represents the maximum shielding ability of the building envelope. η (h) represents the ability of the air stream to transmit the pollutant and is also associated with the particle residence time indoors. η mostly depends on the pollutant properties and building dynamics. $Ae^{-\eta a}$ in Equation 1.20 is the parameter responsible for the extent to which the outdoor contaminant was blocked by the building shell.

Taking the natural logarithm of Equation 1.20, we get:

$$\ln|1 - y| = -\eta a + \ln(A) \tag{3.7}$$

Linear regression on 17-hour averaged data produced estimates of η from the slope and values of A from the intercept of the regression line. Table 3.13 presents estimates of η and A from linear regression when the full range of 17-hour averaged data was used.

Table 3.15: Regression analysis when Model 6 was applied using the full dataset.

Chao	N	Grad (SD)	y-int (SD)	R^2	η	A
PM_1	8	−0.05 (0.13)	−1.68 (0.41)	0.03	0.05	0.19
$PM_{2.5} - PM_1$	8	−0.02 (0.06)	−0.65 (0.22)	0.01	0.02	0.52
$PM_{10} - PM_{2.5}$	8	−0.01 (0.04)	−0.31 (0.14)	0.02	0.01	0.73

Equation 1.20 can be rearranged in order to predict the indoor PM concentration from C_{out} and the newly-estimated values of η and A as follows:

$$C_{in} = C_{out}(1 - Ae^{-\eta a}) \tag{3.8}$$

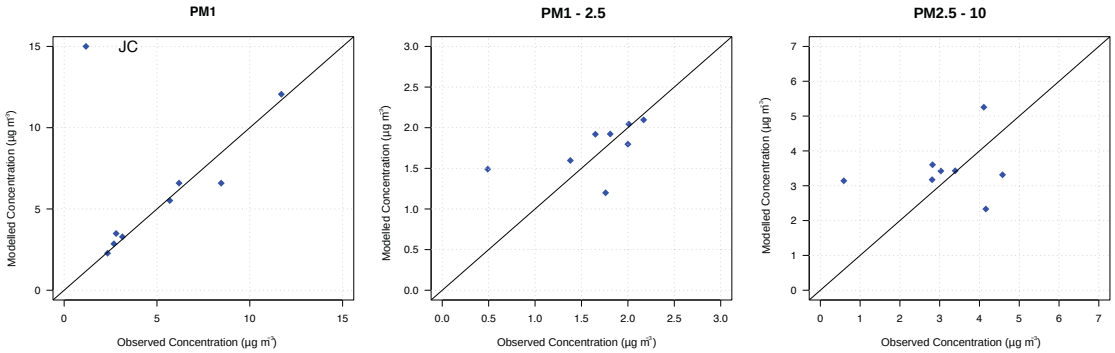

Figure 3.12: Comparison of modelled and observed values for different size fractions, when Model 6 was applied.

Table 3.16: Statistical evaluation results when Model 6 was applied.

Chao	N	RMSE (μgm^{-3})	MAPE (%)	R^2
PM_1	8	0.77	9.16	0.95
$PM_{1\text{ - }2.5}$	8	0.45	36.17	0.29
$PM_{2.5\text{ - }10}$	8	1.37	73.34	0.003

The authors deriving Model 6 suggest that the model works best for AER ranging from 0.5 h^{-1} to 4.3 h^{-1} as at lower AER the deposition effects become very much significant whilst at higher AERs resuspension cannot be neglected. The analysis was thus repeated without Day 1, Day 4 and Day 5, however, with the new subset, regression analysis resulted in negative values of A and η because the data was skewed by the data point corresponding to Day 2 with associated AER of 0.21 h^{-1}.

This data point was neglected leaving only 4 valid data points. The regression analysis results are presented in Table 3.17.

Table 3.17: Regression analysis when Model 6 was applied using the suggested range of the AER.

Chao	N	Gradient (SD)	y-intercept (SD)	R^2	η	A
PM_1	4	−0.01 (0.04)	−1.54 (0.)	0.04	0.01	0.21
$PM_{1\text{ - }2.5}$	4	−0.10 (0.06)	−0.42 (0.18)	0.58	0.10	0.66
$PM_{2.5\text{ - }10}$	4	−0.12 (0.05)	−0.02 (0.14)	0.74	0.12	0.98

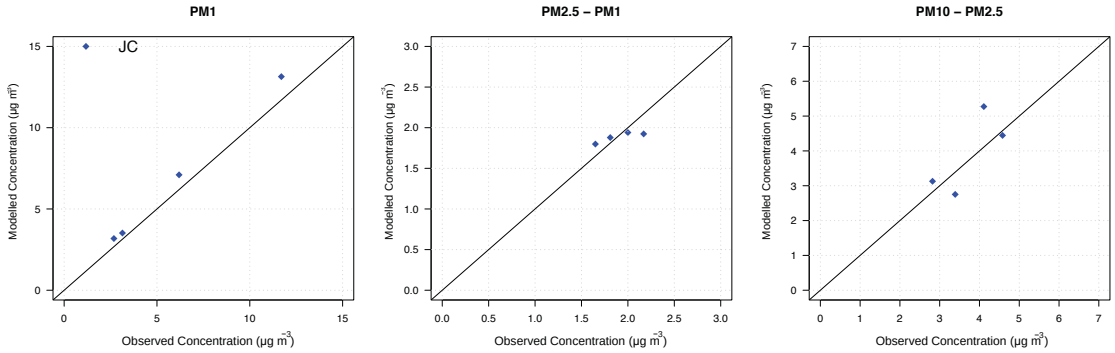

Figure 3.13: Comparison of modelled and observed values for different size fractions, when Model 6 was applied using data with corresponding AER that are within the suggested range.

Figure 3.13 presents observed versus modelled concentration plots whilst Table 3.18 gives the RMSE and MAPE for the three fractions considered. Both the RMSE and MAPR values suggest that restricting the data to the suggested AER range improved significantly for $PM_{1\text{ - }2.5}$ and $PM_{2.5\text{ - }10}$ but not for the PM_1 fraction.

Table 3.18: Statistical evaluation when Model 6 was applied using data with corresponding AER that are within the suggested range.

Chao	N	RMSE (μgm^{-3})	MAPE (%)	R^2
PM_1	4	0.91	14.45	0.99
$PM_{1\ -\ 2.5}$	4	0.15	6.78	0.79
$PM_{2.5\ -\ 10}$	4	0.68	15.25	0.58

3.3 Comparing Models

Five of the six models considered and investigated were compared to determine the best-performing model under the different circumstances and assumptions employed. Model 4 was not included in this analysis as its performance was very poor indeed and thus was not relevant. Figure 3.14 presents a summary of results of the MAPE, averaged over all days were adequate data were available from the JC campaign. The plot includes values of the corresponding RMSE displayed in white over each bar. In all models, the lowest MAPE values were registered for PM_1 confirming that all models can execute better predictions at finer fractions. The only exception was for Model 6 when the suggested AER range was used. In this case, Model 6 performed better for the $PM_{2.5\ -\ 10}$ fraction.

The models assuming steady-state conditions i.e. Model 1 and Model 2 performed much better than the models employing a non-linear solution to the MBE at non-steady-state conditions. This suggests that when considering long sampling periods steady-state conditions can indeed be assumed. Such an approach would not only simplify the calculations but also produce better estimates of the indoor particulate concentration from outdoor PM data.

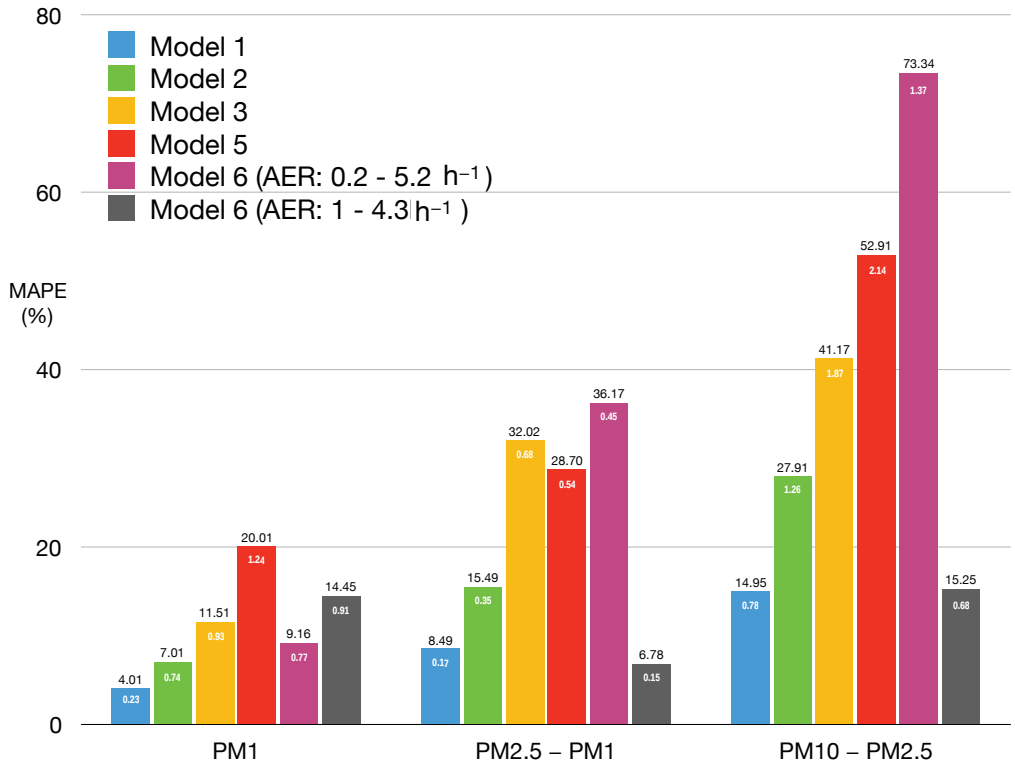

Figure 3.14: A bar graph showing the MAPE (%) and RMSE (μg m^{-3}) of different PM infiltration models at different size fraction using 17-hour averaged data.

Model 3 employed a recursive method to obtain a non-linear solution of the MBE and evaluate estimates for P and k which were later used in the same formula to estimate the indoor concentration using outdoor concentration data and an initial value of the indoor concentration. This model produced reasonable estimates of the infiltration parameters and the time series plots clearly show that the model was able to produce appreciable estimates of the indoor PM concentration. Model 4 employed a similar approach but the non-linear solution involved an integral solution of the MBE with exponential terms. This model was not able to generate reliable estimates of P and k and time series analysis confirmed the inaccurate behaviour of the modelled indoor concentration.

Model 5 employed multiple linear regression to determine the parameters β_1 and β_2

to estimate the F_{INF}. Predictions from this model were found to be less accurate at PM_1 but were appreciable for the other fractions compared to the other models.

Model 6 employed a non-linear solution of the MBE and 17-hour averaged data were used to estimate the infiltration parameters A and η. Model 6 produced appreciable predictions with MAPE of 9% for the PM_1 fraction when considering data points with corresponding AER ranging from 0.2 h^{-1} to 5.2 h^{-1}. However, the performance declined significantly for $PM_{1\text{ - }2.5}$ and $PM_{2.5\text{ - }10}$. Model 6 has limitation at low ventilation rates due to deposition losses and also at high ventilation rates as resuspension of indoor particulates becomes significant. Estimates of A and η, determined from data with corresponding AER within the suggested range (i.e. 1 h^{-1} - 4.3 h^{-1}), gave better results for the $PM_{1\text{ - }2.5}$ and $PM_{2.5\text{ - }10}$ but not for PM_1 fractions.

3.4 Black carbon surrogate

Some specific chemical species can be used as surrogates of PM. Black carbon (BC) has been previously found to be a good surrogate of $PM_{2.5}$ as it is usually expected to have a size distribution similar to that of fine particulates [51]. The main advantage of BC as a surrogate of PM is that BC is mainly of outdoor origin (traffic-related) unless there are significant indoor combustion sources, and thus assures that the measured indoor concentration is of outdoor origin. In this study, both indoor and outdoor BC data were used to investigate the correlation between BC and PM concentrations.

Figure 3.15 presents four plots of PM versus BC concentrations in $\mu g\ m^{-3}$. The two plots on the top evaluate the total particulate concentration (PM_{tot}) while the plots at the bottom evaluate the fine fraction i.e. $PM_{2.5}$. For both the indoor PM_{tot} and $PM_{2.5}$ there was a positive linear correlation with a Pearson correlation coefficient

(r) of 0.60 and 0.51 for PM_{tot} and $PM_{2.5}$ respectively. For the outdoor data a slight positive correlation ($r = 0.24$) was recorded for PM_{tot} but $PM_{2.5}$ resulted in a negative correlation ($r = -0.18$).

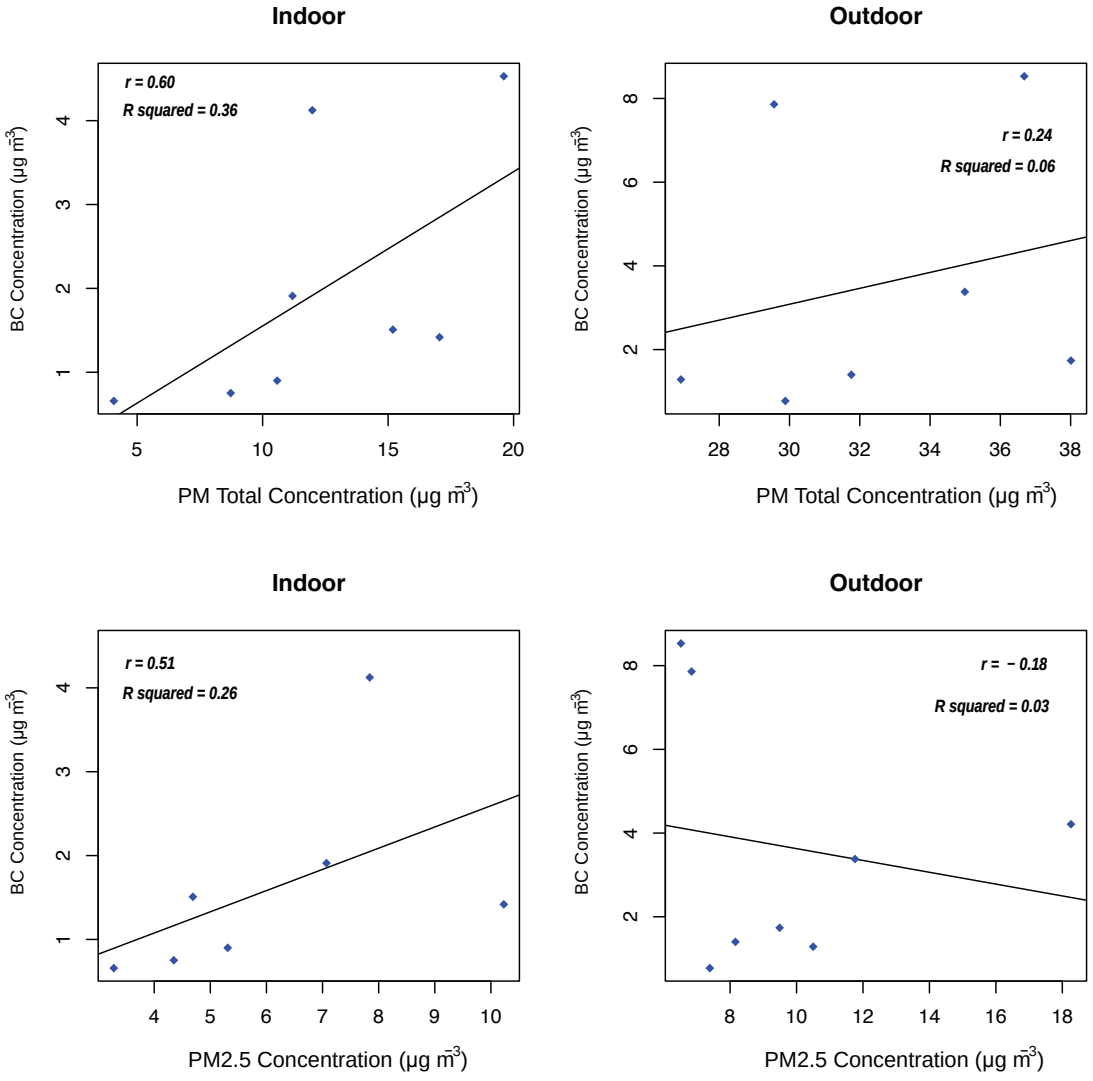

Figure 3.15: Indoor and outdoor PM_{tot} and $PM_{2.5}$ versus BC concentrations.

Figure 3.16 investigates the correlation between the F_{INF} estimates generated by PM and BC. The F_{INF} used were simply the indoor/outdoor ratios which are equivalent to P according to Model 1. The Pearson correlation coefficient was found to be 0.51 and 0.25, indicating a moderate and a weak positive correlation for PM_{tot} and

$PM_{2.5}$ respectively. It can thus be concluded that BC proved not to be a reliable surrogate for PM in this investigation. This may be attributed to several other sources contributing to atmospheric particulates such as mineral dust.

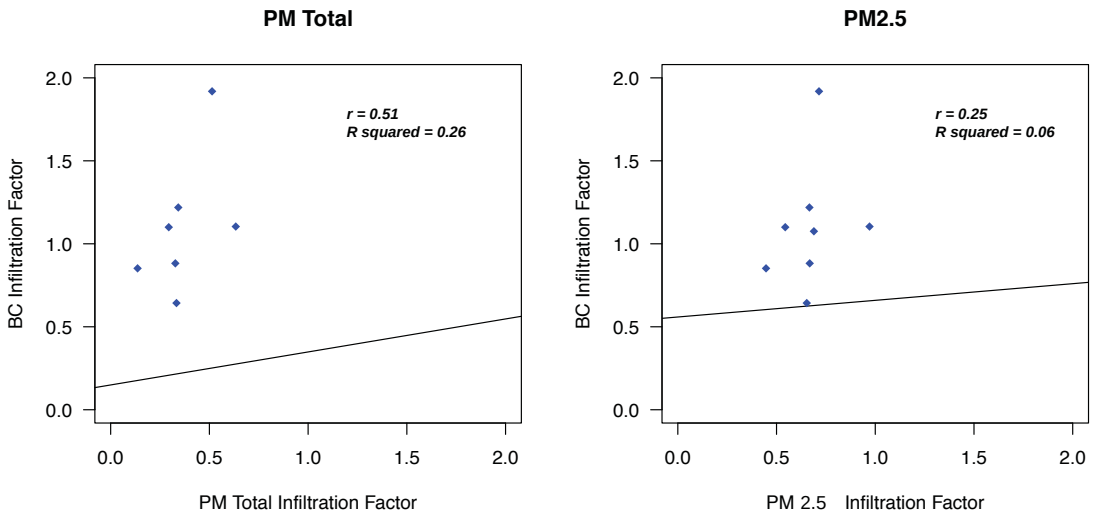

Figure 3.16: BC infiltration factors versus PM_{tot} and $PM_{2.5}$ infiltration factors.

Figure 3.17 presents indoor and outdoor time series plots of BC as well as PM_{tot} and $PM_{2.5}$ for Day 1. The plot for all days except for Day 3 (as BC data was missing) are presented in the Appendix section. The y-axis on the left hand side represents BC concentration in $\mu g\ m^{-3}$, while that on the left represents PM concentrations also in $\mu g\ m^{-3}$. The time series plots indicate that BC is behaving as expected. Since no indoor sources were present, very low concentrations of BC were detected indoors and such concentrations show that some BC do infiltrate from outdoors. However, the outdoor concentration was found to be higher and also follows PM generation. An indication that outdoors, combustion from vehicular traffic is a significant PM source.

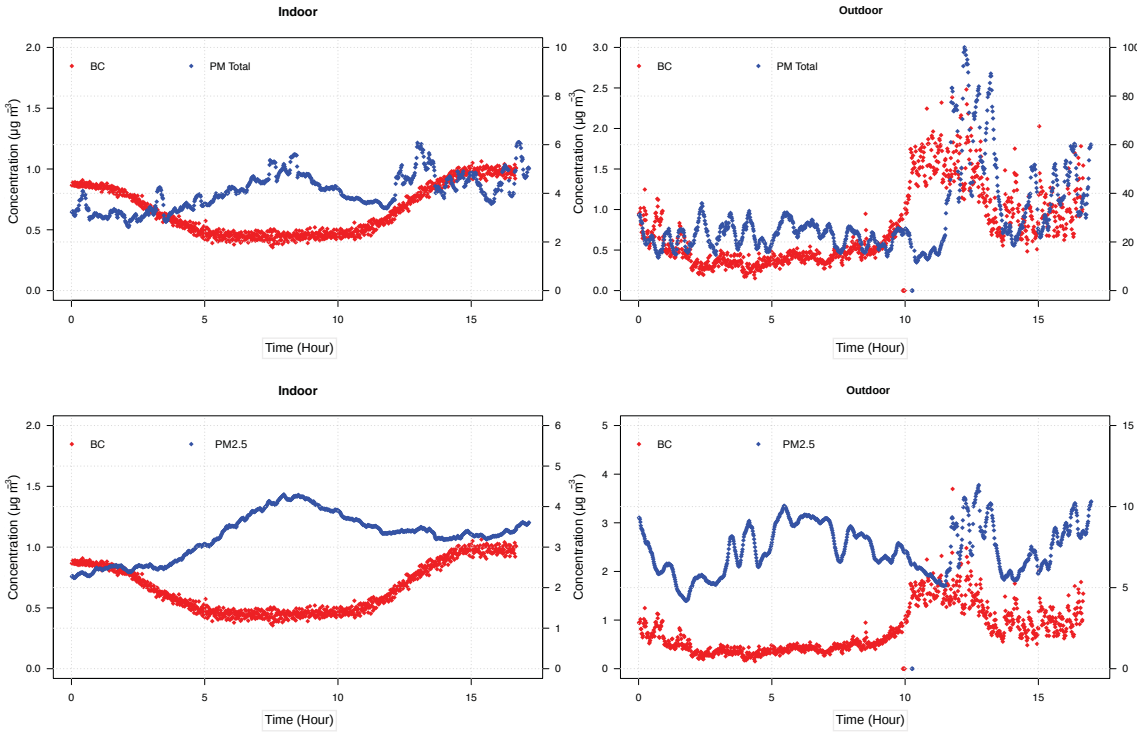

Figure 3.17: Time series plots of the indoor and outdoor PM_1 and $PM_{2.5}$ for Day 1.

3.5 Weather data and pollution roses

The wind speed and its direction not only affect the distribution and dispersion of outdoor pollutants but also the ventilation rates within buildings. Wind conditions affect the AER by determining the amount of air influx introduced into the building. In cases where no pressure differences within the building are present, the same volume of air introduced from outside must also leave the building. This has a great influence on the number of particulates that infiltrate indoors. In this section wind and pollution, roses are presented and analysed to determine the effects of atmospheric conditions on the AER and particulate infiltration.

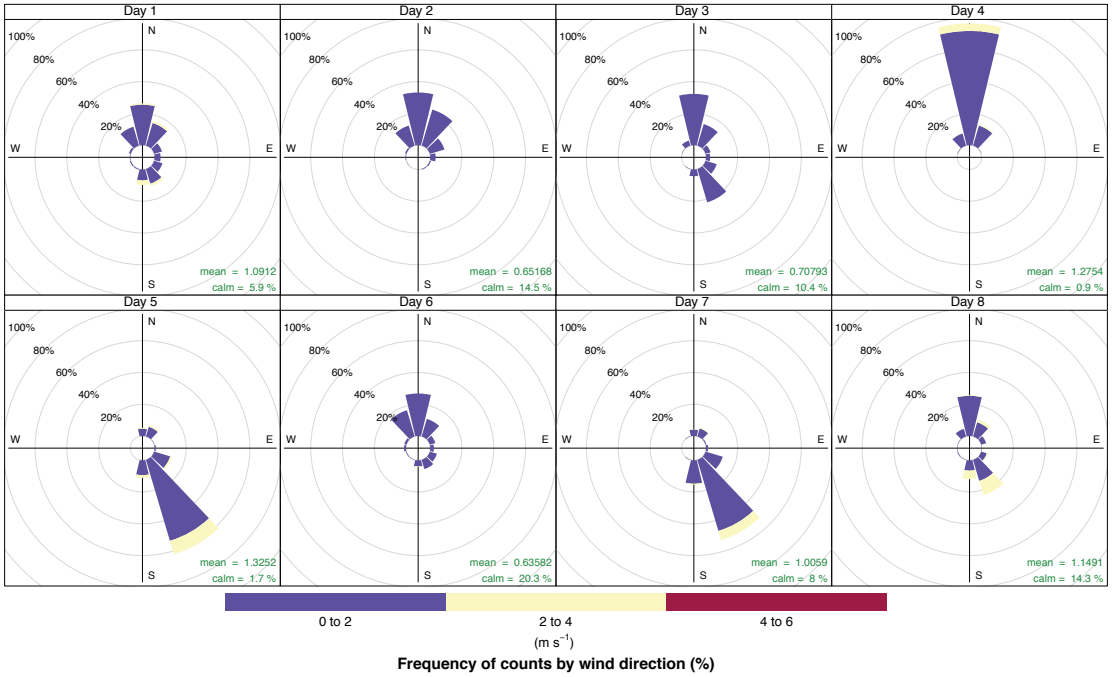

Figure 3.18: Wind rose plots for the 17-hour time frames considered over the JC campaign.

Figure 3.18 illustrates wind rose plots for each day of the campaign. The wind rose plots include the mean wind speed over the 17-hour sampling period and also presents the percentage of 'calm' i.e. when no wind speed was detected. Figure 3.19 shows the position of the MAQL within the JC campus. The map is north-oriented and thus can be used to interpret the wind rose plots in respect to the position of the MAQL during the campaign. The plots confirm that no wind was recorded from the SW to NW side of the MAQL as this part was well shielded by the 6-storey building. The wind conditions were calm over the whole campaign with a maximum mean wind speed of 1.33 m s^{-1} in Day 5.

Figure 3.19: The position of the MAQL (red star) within the JC campus. Image is north-oriented in order to interpret the wind rose plots.

The windows of the room investigated were facing SE. On Day 3, Day 5 and Day 7, the sliding windows were opened the same amount i.e. 40 cm, however, the AER for each corresponding day varied considerably. On Day 3 the wind direction was variable and the wind was facing the window (i.e. blowing from SW) for just above 20% of the sampling time. On this day the AER was estimated to be 2.69 h^{-1}. On the other hand, the wind was facing the window for around 80% and 70% of the time on Day 5 and Day 7 receptively. On these days, higher AERs were recorded. The AER was highest on Day 5 (5.16 h^{-1}) and slightly lower on Day 7 (4.11 h^{-1}). A higher AER on Day 5 may be attributed to the fact that the wind speed was slightly higher on that day.

Figure 3.20 illustrates pollution rose plots of PM_1, $PM_{1\text{ - }2.5}$ and $PM_{2.5\text{ - }10}$ for all days of the campaign. The highest ambient particulate concentration was recorded on Day 3 and Day 4. The red peak at the centre of the pollution rose of Day 3 indicates that on that particular day the source was localised, most likely coming from vehicular activities within the parking lot close by. Polar plot of Day 4, on the

other hand, suggests that the high concentration of particulates was blown in by northerly winds. This high concentration of PM is most likely coming from a very busy road network located only around 300 m further north of the JC campus.

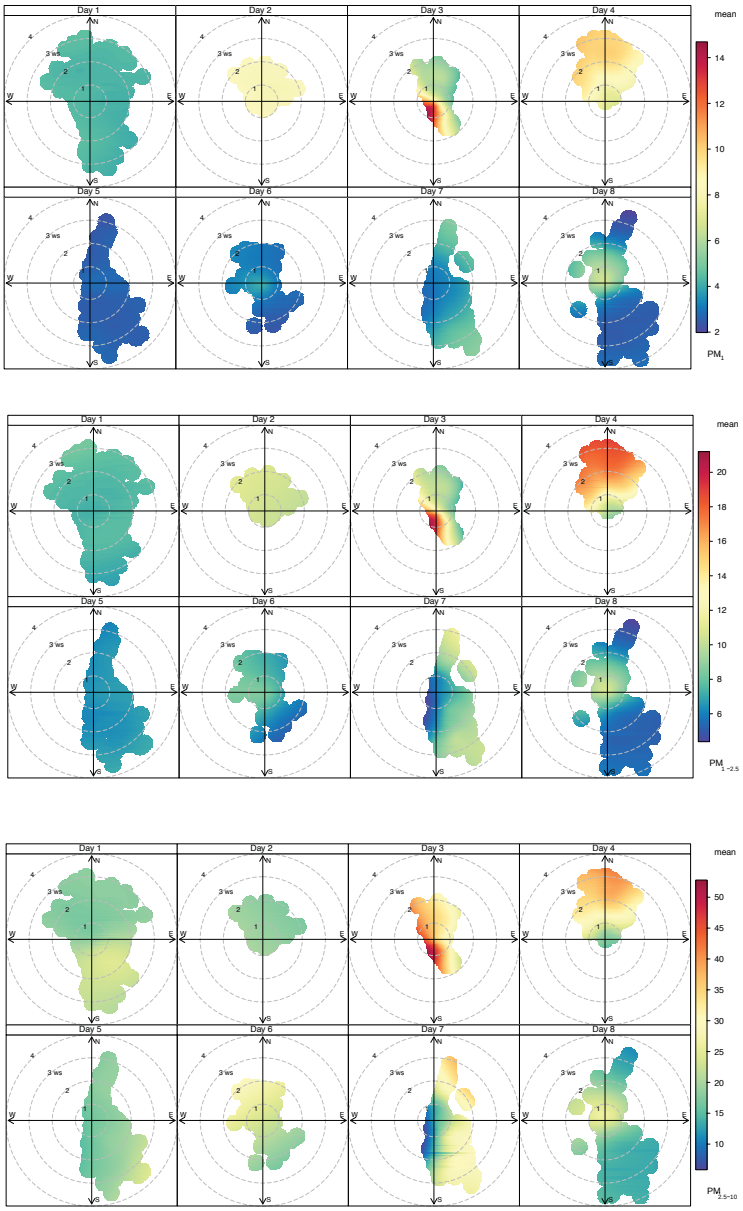

Figure 3.20: PM_1, $PM_{1\text{ - }2.5}$ and $PM_{2.5\text{ - }10}$ pollution rose plots for all days of the campaign.

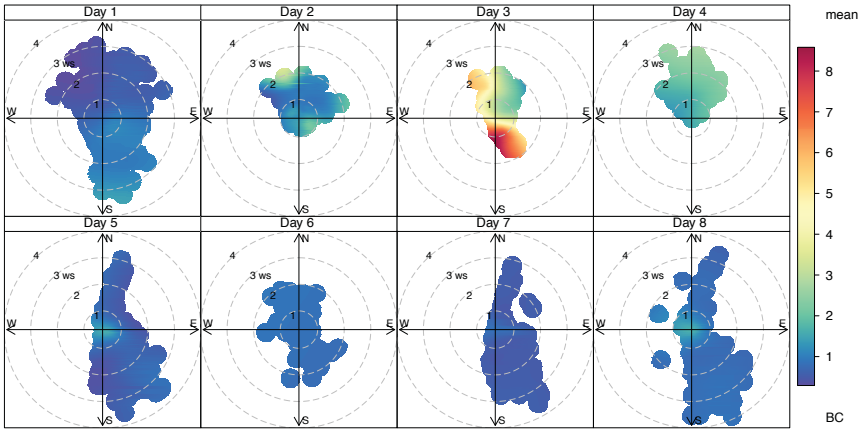

Figure 3.21: BC pollution rose plots for all days of the campaign.

Figure 3.21 presents pollution roses using BC data. The plots are very similar to the pollution roses for PM but the concentrations were found to be significantly lower for BC. The PM concentration peak recorded on Day 3 was also detected with BC data. BC is exclusively sourced from combustion, thus indicating that the high concentrations of PM on that day resulted from the vehicular activity which is the only combustion activity in the area.

BC concentrations on Day 4 however, were not that significant compared to PM concentrations. This might suggest that the PM blown from the north on that day was not exclusively sourced from traffic nearby but also other atmospheric dust.

3.6 Validation of models with an independent dataset

A separate campaign involving indoor and outdoor continuous PM measurements as well as AER estimates was carried out from June 21st till July 5th 2019 in a residential home in Birżebbuġa (BBG). Figure 3.19 illustrates a map with the location of the residential home used for investigation. The house is located in a typical residential neighbourhood where vehicular traffic is moderate. As regards to pollution sources,

the Malta Freeport is located about 1 km SE of the house under investigation. This port is very busy and includes significant pollution source both form cargo ships as well as heavy trucks used to transport shipping containers. Opposite the house, there is also a football pitch that in the satellite image used in Figure 3.22 was still a construction site.

Figure 3.22: Map illustrating the location of the residential building used for investigation in Birżebbuġa.

This area has been left intentionally blank.

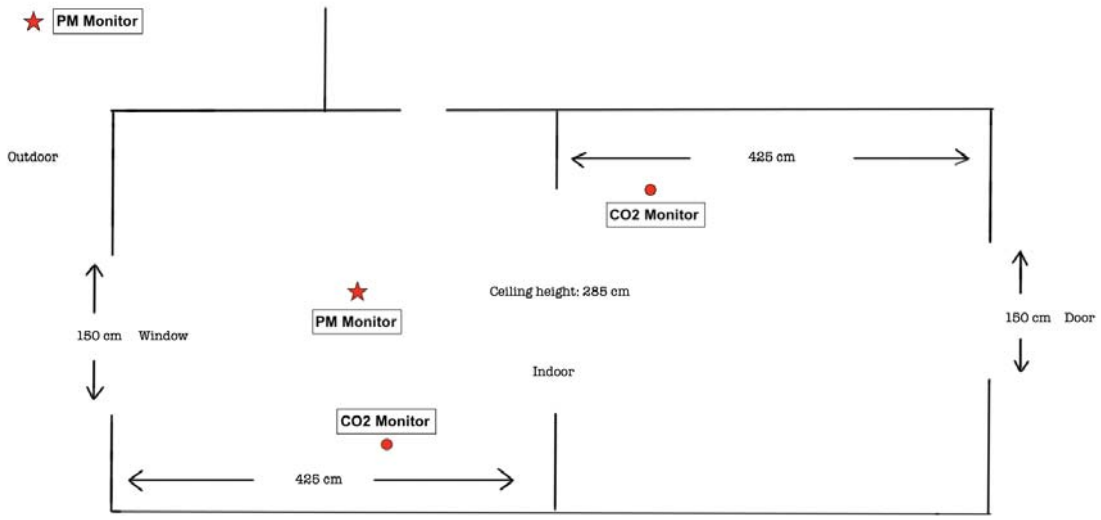

Figure 3.23: BBG indoor environment schematic.

The investigation was carried out in a sitting room that was very rarely accessed and occupied. The room was located at ground level and the windows were facing a small backyard. Figure 3.23 displays a schematic of the residential building used for investigation. Table 3.19 presents indoor and outdoor 17-hour averaged PM concentrations for different size fractions as well as AER values, and information about the state of the windows during that sampling period.

This area has been left intentionally blank.

Table 3.19: 17-hour averaged indoor and outdoor data with the corresponding AER from the BBG campaign.

Day	Window	AER (h^{-1})	Indoor PM_1 (SD) (μgm^{-3})	Outdoor PM_1 (SD) (μgm^{-3})	Indoor $PM_{1-2.5}$ (SD) (μgm^{-3})	Outdoor $PM_{1-2.5}$ (SD) (μgm^{-3})	Indoor $PM_{2.5-10}$ (SD) (μgm^{-3})	Outdoor $PM_{2.5-10}$ (SD) (μgm^{-3})
1	slightly open	0.26	4.22 (0.73)	6.31 (2.02)	1.79 (0.36)	4.98 (1.18)	3.42 (1.14)	17.53 (6.47)
2	slightly open	0.54	4.41 (0.54)	7.77 (3.12)	2.89 (0.33)	9.32 (2.75)	4.47 (1.28)	41.05 (18.73)
3	slightly open	0.44	7.63 (0.39)	10.18 (1.59)	1.96 (0.85)	5.75 (6.26)	4.33 (4.54)	24.19 (46.57)
4	closed	0.13	7.21 (1.02)	10.98 (2.14)	0.63 (0.37)	4.67 (1.57)	1.08 (0.90)	18.61 (10.45)
5	half open	1.62	9.00 (2.98)	10.24 (4.08)	2.15 (1.07)	3.29 (1.65)	7.01 (4.67)	15.57 (10.12)
6	closed	0.18	6.29 (1.17)	11.03 (1.54)	0.99 (0.77)	5.92 (1.69)	1.15 (0.96)	33.83 (12.92)
7	closed	0.13	6.52 (0.44)	13.53 (10.00)	1.64 (2.23)	4.82 (2.20)	4.47 (10.12)	23.51 (8.82)

Over the seven days of the campaign the AER varied from 0.13 h^{-1} to 1.62 h^{-1} with a mean of 0.47 ± 0.01 h^{-1}. Such AER values are considered to be typically low, and differ significantly from the mean AER recorded at JC i.e. 2.80 h^{-1}. It has been determined that throughout the campaign, the mean outdoor concentrations were 10.01 $\mu g\ m^{-3}$, 5.54 $\mu g\ m^{-3}$, and 24.83 $\mu g\ m^{-3}$ for PM_1, $PM_{1-2.5}$, and $PM_{2.5-10}$ respectively, whilst the mean indoor concentration was found to be 6.47 $\mu g\ m^{-3}$, 1.70 $\mu g\ m^{-3}$, and 3.70 for PM_1, $PM_{1-2.5}$, and $PM_{2.5-10}$ respectively.

By their derivation, certain models perform poorly at low AERs mainly because they assume no deposition losses, however, for low ventilation rates, deposition losses become effectively significant. Chao et al. state that the typical AER is not low enough for deposition losses to be significant however the BBG campaign suggests otherwise. In this section, the models were validated with this other independent dataset and the effects of low AERs on the models' performance was investigated. Since the analysis on the new dataset was essentially the same as the one carried

on the JC dataset, most of the tables and figures are presented in the Appendix section.

On the contrary to what was done for the JC campaign, where λ was calculated by increasing the indoor PM concentration by fully opening the windows and allowing the free entrance of ambient PM, this time, indoor PM decay curves were used to estimate λ. The decay curves were generated by resuspension caused by indoor activities when CO_2 was released daily to estimate the AER. As before, times series plots were considered to identify resuspension curves in the indoor concentration to evaluate λ. Day 4, Day 6 and Day 7 were considered for analysis to have three tests where the windows were completely closed and thus apply similar conditions used for the evaluation of λ in the JC campaign.

Table 3.20: Average λ from Test 1, Test 2 and Test 3 for different size fractions.

PM Size Fraction	λ (h^{-1})
PM_1	0.48
$PM_{1\text{ -}2.5}$	0.51
$PM_{2.5\text{ - }10}$	0.80

Table 3.20 shows the averaged values of λ from the three tests for different size fractions. The values are comparable with those obtained from the JC campaign for PM_1 (0.45 h^{-1}) and $PM_{1\text{ - }2.5}$ (0.50 h^{-1}) however the value differs marginally for the $PM_{2.5\text{ - }10}$ fraction (1.19 h^{-1}) even though the mean indoor $PM_{2.5\text{ - }10}$ concentrations were similar (3.70 $\mu g\ m^{-3}$ and 3.19 $\mu g\ m^{-3}$ for BBG and JC respectively). As already stated, Model 1 fails at low AERs as deposition effects become significant. Even though the BBG dataset incorporated data with low AER it was still validated against this other independent dataset with this assumption violated. This was done

to investigate the significance of this assumption. P was found to be 0.64, 0.30, and 0.13 for PM_1, $PM_{1\text{ - }2.5}$, and $PM_{2.5\text{ - }10}$ respectively. Both the RMSE and MAPE were found to be significantly higher than those calculated from the JC dataset incorporating the assumption that the model works for ventilation rates higher than the corresponding λ. The MAPE from the BBG analysis was found to be 27%, 20% and 18% higher than the one from JC for PM_1, $PM_{1\text{ - }2.5}$, and $PM_{2.5\text{ - }10}$ respectively. This reassures the significance of the assumption employed by the model and that its violation has significant effect on the performance of the model.

Model 2 was also revalidated against the BBG dataset. Once again both the RMSE and MAPE were found to be significantly higher than those obtained from the JC dataset indicating that the model performed much better at higher AERs. The MAPE from the BBG analysis was found to be 58%, 58% and 37% higher than the one from JC for PM_1, $PM_{1\text{ - }2.5}$, and $PM_{2.5\text{ - }10}$ respectively.

When Model 3 was applied, k was found to be negligible in all fractions only for Day 2 and Day 5 where the AER was 0.54 h^{-1} and 1.62 h^{-1} respectively. In all other cases (with lower corresponding AERs) the estimates of k were found to be significant. A non-zero value of k was expected as for such low AERs, deposition losses become significant. The average MAPE using this method was found to be 6%, 17% and 27% for PM_1, $PM_{1\text{ - }2.5}$, and $PM_{2.5\text{ - }10}$ respectively. These values are 58%, 52% and 66% lower than those obtained from the JC analysis for PM_1, $PM_{1\text{ - }2.5}$, and $PM_{2.5\text{ - }10}$ respectively. This suggests the Model 3 works better at typically lower AER.

Even though Model 4 proved to be unreliable when validated against JC data, it was also validated again against the new dataset from BBG. Surprisingly, it was found that this time around the model worked much better and reasonable estimates of the infiltration parameters were produced. The mean MAPE was found to be 22%, 41%, 58% for PM_1, $PM_{1\text{ - }2.5}$, and $PM_{2.5\text{ - }10}$ respectively. This implies that Model 4 can be applied in situations where the AERs are typically low.

Model 5, employing multilinear regression of the dynamic solution of the MBE was only revalidated against minute data ($\Delta t = \frac{1}{60}$) as it was readily available and from the previous analysis, it was concluded that minute and hourly data gave the same estimates of β_1 and β_2. The mean MAPE over the full campaign was found to be 87%, 139%, and 149% for PM_1, $PM_{1\text{ - }2.5}$, and $PM_{2.5\text{ - }10}$ respectively. These values are very poor indeed and once again are all higher than those estimated using the JC dataset. It can be thus concluded that Model 5 produced unreliable infiltration estimates, especially for low AER as it was the case when using the JC dataset.

Finally, Model 6 was validated against the BBG dataset even though the AER attributed do not fall within the range suggested by authors. The model performs only appreciably well for PM_1 but was inadequate for the other size fractions, such result was expected.

Chapter 4

Conclusion

4.1 Conclusions and limitations

This study examines different methodologies used to estimate the indoor PM concentration of outdoor origin. Six mathematical models that describe the behaviour of PM indoors were investigated with the aim of finding out which model was able to correctly predict the fraction of outdoor PM that infiltrates indoors. It was immediately clear the estimation of infiltration parameters remains an open scientific challenge. The main issue lies in the estimation of the the infiltration factor (F_{INF}) or the parameters that define it: the AER (a), penetration efficiency (P), and deposition rate (k).

The steady-state approach is a simple and widely used method to determine PM infiltration parameters. In this study two models assuming steady-state conditions (Model 1 and Model 2) were evaluated against the data from the JC and BBG campaign. Model 1 worked remarkably well when using parameters estimated from the JC dataset. In case of the BBG analysis the model performed poorly but this was expected as the BBG dataset included AERs that are lower than the corresponding λ for the respective fractions - making deposition substantial. The derivation of Model

1 strictly assumes that deposition losses has to be assumed negligible. This makes Model 1 an effective modelling tool for typically high ventilation rates however in cases where the AER is typically low (as it was the case in Birżebbuġa), such model becomes impractical.

The main disadvantage associated with this approach assuming steady-sate conditions is that all parameters are assumed constant over the time frame considered - which must be several hours long. In reality this is rarely the case as both the infiltration parameters and the outdoor concentration are subject to significant daily variations and also shorter-term variations. Nevertheless, if there is no sudden increases in the ambient PM concentrations, as it was the case for the JC campaign, the models can be notably accurate. In fact this study concluded that for 17-hour averaged data, Model 1 and Model 2 out-performed all other models considered. It was also concluded that infiltration estimates using Model 1 were actually better then those produced by Model 2 even though the latter model incorporates experimental values of the AER. Model 1 however assumes ventilation rates that are higher than the total particulate loss rate (λ) that in this study was calculated experimentally and found to be 0.45 h^{-1}, 0.50 h^{-1}, and 1.19 h^{-1} for PM_1, $PM_{1\text{ - }2.5}$, and $PM_{2.5\text{ - }10}$ respectively. This means that under relatively stable conditions and ventilation rates higher than λ, Model 1 was able to produce reliable estimates of F_{INF}. The mean AER when the windows were completely closed was found to be 0.21 ± 0.01 h^{-1} however this value increased significantly when windows (sliding) were opened as little as 20 cm. This indicates that Model 1 would be more appropriate to estimate infiltration parameters in the warm months of the year where window are typically left ajar.

This study also revealed that models that assume steady-state conditions do better than models using minute data and employ a dynamic solution of the MBE. However, such models give a more complete picture of how particles behave and move into and out of the building. Model 3 estimated P and k through a non-linear solution of the

MBE. The indoor concentration was then predicted using the established parameters through a recursive method approach. This method produced appreciable minute-concentration estimates that were sensitive to sudden fluctuations in the ambient PM concentration. Model 3 was the only model that performed significantly better when validated using BBG data suggesting that the model was able to produce better estimates of p and k when the AER is typically lower.

Another important conclusion of this study that was rarely considered in previous investigations is the fact that all models considered were found to perform significantly better for finer particulates except for Model 6 under the limited AER range. From a health point of view, exposure of PM_1 is much more concerning than exposure to coarser particulates suggesting that such models can be a reliable modelling tool to predict the exposure of PM_1 of ambient origin.

In this study, BC was found not to be a reliable surrogate of PM. Weather data analysis also confirmed that the outdoor PM detected was mostly generated from places nearby and not locally. It was also confirmed that the AER is a highly variable parameter and the wind dynamics influence this value significantly both with regards to wind speed and its direction.

4.1.1 Future Work

This study investigated different approaches to estimate the infiltration of ambient particulates in buildings. Future sampling campaigns would be needed to give better statistical significance of the typical infiltration parameters for buildings in Malta as the two campaigns considered in this study showed significant variations. It would also be helpful to investigate long-term trends of the infiltration parameters as these are subject to change seasonally and from place to place.

This study focused on the outdoor fraction of particulates that makes its way indoor

through the building envelope, however it is well established that indoor sources have a major impact on the indoor air quality in general. The models investigated in this study can be validated once again without assuming negligible indoor sources. This however, would require specialised experimental protocols involving experiment chambers to estimate the generation rate of several typical indoor sources.

Work is still needed to understand different chemical and biological PM mechanism that would ultimately influence the real exposure and consequent health effects of indoor PM. Nevertheless, the models presented in this study help to enlighten some aspects of the complex dynamics involved in the study of indoor PM of outdoor origin.

References

[1] Diapouli, E., Chaloulakou, A., Mihalopoulos, N. and Spyrellis, N. (2008). Indoor and outdoor pm mass and number concentrations at schools in the athens area, *Environmental monitoring and assessment*, **136(1-3)**, 13–20.

[2] Seguel, J. M., Merrill, R., Seguel, D. and Campagna, A. C. (2017). Indoor air quality, *American Journal of Lifestyle Medicine*, **11(4)**, 284–295.

[3] Abdul-Wahab, S. A., En, S. C. F., Elkamel, A., Ahmadi, L. and Yetilmezsoy, K. (2015). A review of standards and guidelines set by international bodies for the parameters of indoor air quality, *Atmospheric Pollution Research*, **6(5)**, 751–767.

[4] Künzli, N., Kaiser, R., Medina, S., Studnicka, M., Chanel, O., Filliger, P., Herry, M., Horak Jr, F., Puybonnieux-Texier, V., Quénel, P. et al. (2000). Public-health impact of outdoor and traffic-related air pollution: a european assessment, *The Lancet*, **356(9232)**, 795–801.

[5] Liang, J. (2013). *Chemical modeling for air resources: fundamentals, applications, and corroborative analysis*, Academic Press.

[6] Organization, W. H. et al. (2003). Health aspects of air pollution with particulate matter, ozone and nitrogen dioxide: report on a who working group, bonn, germany 13-15 january 2003.

[7] Tiwari, S., Pandithurai, G., Attri, S., Srivastava, A., Soni, V., Bisht, D., Kumar, V. A. and Srivastava, M. K. (2015). Aerosol optical properties and their relationship with meteorological parameters during wintertime in delhi, india, *Atmospheric Research*, **153**, 465–479.

[8] Introduction to visibility issues.

[9] for Standardization (CEN), E. C. (1993). Din en 481, workplace atmospheres–size fraction definitions for measurement of airborne particles.

[10] of Governmental Industrial Hygienists, A. C. (1995). Threshold limit values for chemical substances and physical agents and biological exposure indices, American Conference of Governmental Industrial Hygienists.

[11] Rai, P. K. and Chutia, B. M. (2014). Biomagnetic monitoring of atmospheric particulate pollution through roadside tree leaves in aizawl city, mizoram and their temporal and spatial variations, *International Research Journal of Environmental Sciences*, **3(8)**, 46–53.

[12] (2018), Health matters: air pollution.
URL `https://www.gov.uk/government/publications/health-matters-air-pollution/health-matters-air-pollution`

[13] (2006), Comeap: cardiovascular disease and air pollution.
URL `https://www.gov.uk/government/publications/comeap-cardiovascular-disease-and-air-pollution`

[14] (2015), Particulate air pollution: health effects of exposure.
URL `https://www.gov.uk/government/publications/particulate-air-pollution-health-effects-of-exposure`

[15] Agency, E. E. (2013). Indoor air quality.

[16] Diapouli, E., Chaloulakou, A. and Koutrakis, P. (2013). Estimating the concentration of indoor particles of outdoor origin: A review, *Journal of the Air & Waste Management Association*, **63(10)**, 1113–1129.

[17] Allen, R., Larson, T., Sheppard, L., Wallace, L. and Liu, L.-J. S. (2003). Use of real-time light scattering data to estimate the contribution of infiltrated and indoor-generated particles to indoor air, *Environmental science & technology*, **37(16)**, 3484–3492.

[18] Tung, T. C., Chao, C. Y. and Burnett, J. (1999). A methodology to investigate the particulate penetration coefficient through building shell, *Atmospheric Environment*, **33(6)**, 881–893.

[19] Thatcher, T. L., Lunden, M. M., Revzan, K. L., Sextro, R. G. and Brown, N. J. (2003). A concentration rebound method for measuring particle penetration and deposition in the indoor environment, *Aerosol Science & Technology*, **37(11)**, 847–864.

[20] Dockery, D. W. and Spengler, J. D. (1981). Indoor-outdoor relationships of respirable sulfates and particles, *Atmospheric Environment (1967)*, **15(3)**, 335–343.

[21] Lunden, M. M., Thatcher, T. L., Hering, S. V. and Brown, N. J. (2003). Use of time-and chemically resolved particulate data to characterize the infiltration of outdoor pm2. 5 into a residence in the san joaquin valley, *Environmental science & technology*, **37(20)**, 4724–4732.

[22] Koutrakis, P., Briggs, S. L. and Leaderer, B. P. (1992). Source apportionment of indoor aerosols in suffolk and onondaga counties, new york, *Environmental Science & Technology*, **26(3)**, 521–527.

[23] JENKINS, P. (1996). Personal exposure to airborne particles and metals: results from the particle team study in riverside, california, *Journal of Exposure Anahsis and Environmental Epidemiolog*, **6(1)**, 57.

[24] Abt, E., Suh, H. H., Catalano, P. and Koutrakis, P. (2000). Relative contribution of outdoor and indoor particle sources to indoor concentrations, *Environmental science & technology*, **34(17)**, 3579–3587.

[25] Ott, W., Wallace, L. and Mage, D. (2000). Predicting particulate (pm10) personal exposure distributions using a random component superposition statistical model, *Journal of the Air & Waste Management Association*, **50(8)**, 1390–1406.

[26] Long, C. M., Suh, H. H., Catalano, P. J. and Koutrakis, P. (2001). Using time- and size-resolved particulate data to quantify indoor penetration and deposition behavior, *Environmental Science & Technology*, **35(10)**, 2089–2099.

[27] Zhu, Y., Hinds, W. C., Krudysz, M., Kuhn, T., Froines, J. and Sioutas, C. (2005). Penetration of freeway ultrafine particles into indoor environments, *Journal of Aerosol Science*, **36(3)**, 303–322.

[28] MacNeill, M., Wallace, L., Kearney, J., Allen, R., Van Ryswyk, K., Judek, S., Xu, X. and Wheeler, A. (2012). Factors influencing variability in the infiltration of pm2. 5 mass and its components, *Atmospheric Environment*, **61**, 518–532.

[29] Kopperud, R. J., Ferro, A. R. and Hildemann, L. M. (2004). Outdoor versus indoor contributions to indoor particulate matter (pm) determined by mass balance methods, *Journal of the Air & Waste Management Association*, **54(9)**, 1188–1196.

[30] Switzer, P. and Ott, W. (1992). Derivation of an indoor air averaging time model from the mass balance equation for the case of independent source inputs and fixed air exchange rates, *Journal of Exposure Analysis and Environmental Epidemiology*, **2(Suppl 2)**, 113–135.

[31] Chao, C. Y. and Tung, T. C. (2001). An empirical model for outdoor contaminant transmission into residential buildings and experimental verification, *Atmospheric Environment*, **35(9)**, 1585–1596.

[32] Chao, C. Y., Wan, M. and Cheng, E. C. (2003). Penetration coefficient and deposition rate as a function of particle size in non-smoking naturally ventilated residences, *Atmospheric Environment*, **37(30)**, 4233–4241.

[33] Wilson, W. E., Mage, D. T. and Grant, L. D. (2000). Estimating separately personal exposure to ambient and nonambient particulate matter for epidemiology and risk assessment: why and how, *Journal of the Air & Waste Management Association*, **50(7)**, 1167–1183.

[34] Ebelt, S. T., Wilson, W. E. and Brauer, M. (2005). Exposure to ambient and nonambient components of particulate matter: a comparison of health effects, *Epidemiology*, 396–405.

[35] Lai, A. C. (2002). Particle deposition indoors: a review, *Indoor air*, **12(4)**, 211–214.

[36] Jamriska, M. and Morawska, L. (2003). Quantitative assessment of the effect of surface deposition and coagulation on the dynamics of submicrometer particles indoors, *Aerosol Science & Technology*, **37(5)**, 425–436.

[37] Chang, K.-N., Chen, Y.-K., Huang, S.-H., Chen, C.-W., Lai, C.-Y. and Chen, C.-C. (2012). Penetration of charged particles through metallic tubes, *Journal of Aerosol Science*, **48**, 10–17.

[38] Nazaroff, W. W. (2004). Indoor particle dynamics, *Indoor air*, **14**, 175–183.

[39] Wallace, L. (1996). Indoor particles: a review, *Journal of the Air & Waste Management Association*, **46(2)**, 98–126.

[40] Liu, D.-L. and Nazaroff, W. W. (2003). Particle penetration through building cracks, *Aerosol Science & Technology*, **37(7)**, 565–573.

[41] Amaral, S., de Carvalho, J., Costa, M. and Pinheiro, C. (2015). An overview of particulate matter measurement instruments, *Atmosphere*, **6(9)**, 1327–1345.

[42] Mettler Toledo. *Emissions Testing Gravimetric Determination of Particulate Matter*.

[43] Agency, E. P. (2017). Method 201adetermination of pm10 and pm2.5 emissions from stationary sources (constant sampling rate procedure).

[44] Giechaskiel, B., Maricq, M., Ntziachristos, L., Dardiotis, C., Wang, X., Axmann, H., Bergmann, A. and Schindler, W. (2014). Review of motor vehicle particulate emissions sampling and measurement: From smoke and filter mass to particle number, *Journal of Aerosol Science*, **67**, 48–86.

[45] Thomas, J. W. (1955). The diffusion battery method for aerosol particle size determination, *Journal of Colloid Science*, **10(3)**, 246–255.

[46] Centre for Atmospheric Science, O. R. M. U., Simon Building, Differential mobility particle sizer (dmps).
URL `http://www.cas.manchester.ac.uk/restools/instruments/aerosol/differential/`

[47] PALAS. *Fidas 200 / Fidas 200 S Continuous ambient air quality monitoring system for PM1, PM2.5 according to EN 14907* and PM10 according to EN 12341*.*

[48] Extech Instruments. *CO2/Humidity/Temperature Datalogger Model SD800.*

[49] Aglan, H. A. (2003). Predictive model for co 2 generation and decay in building envelopes, *Journal of applied physics*, **93(2)**, 1287–1290.

[50] Hicklin, W., Farrugia, P. S. and Sinagra, E. (2018). Investigations of vocs in and around buildings close to service stations, *Atmospheric Environment*, **172**, 93–101.

[51] Ebelt, S. T., Wilson, W. E. and Brauer, M. (2005). Exposure to ambient and nonambient components of particulate matter: a comparison of health effects, *Epidemiology*, 396–405.

Appendix

Junior College Campaign

The following plots present the outdoor concentration (LHS y-axis) and the indoor measured and modelled concentration (RHS y-axis) for the eight days studied at the JC. The modelled concentration are derived when **Model 3** was applied.

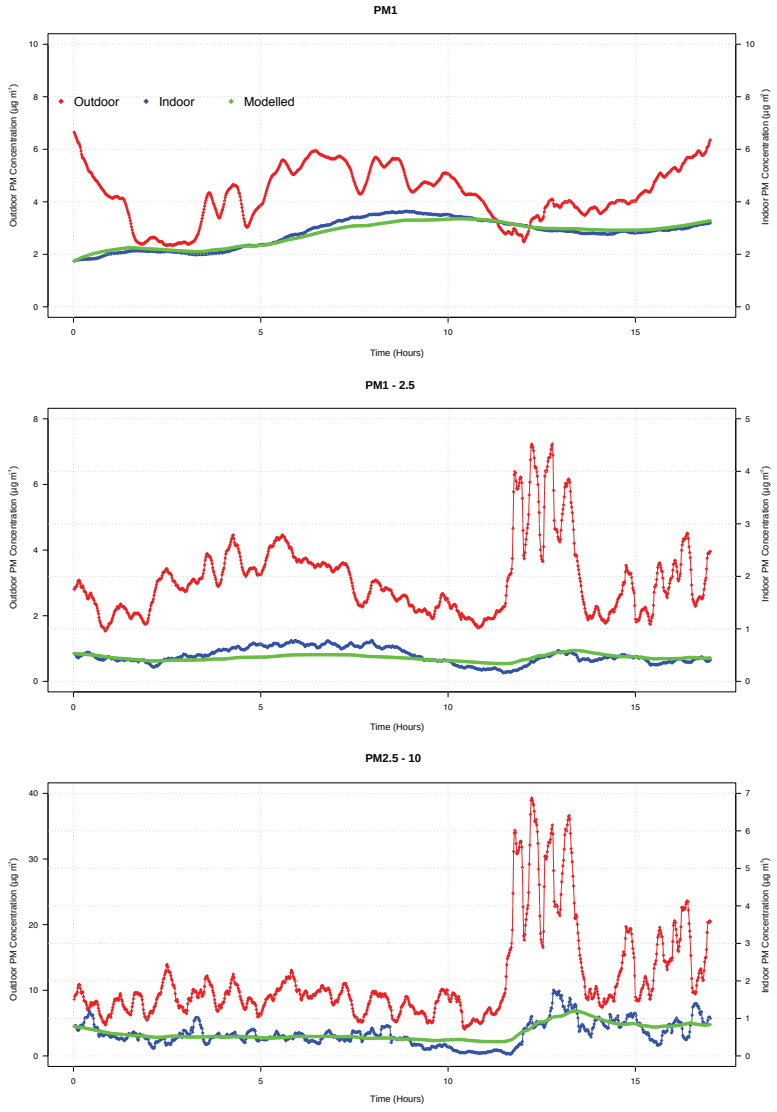

Figure 1: PM time series plots for Day 1 of the JC campaign.

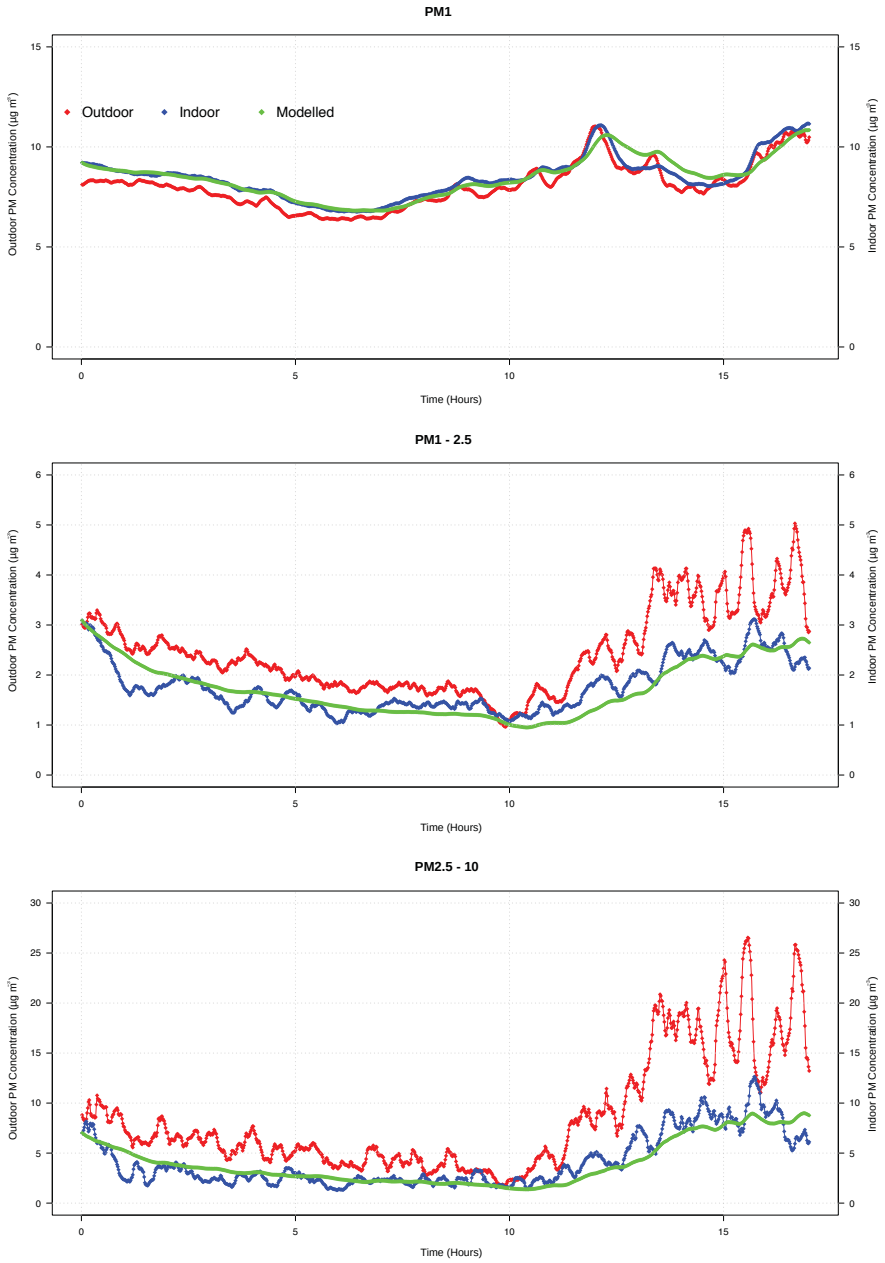

Figure 2: PM time series plots for Day 2 of the JC campaign.

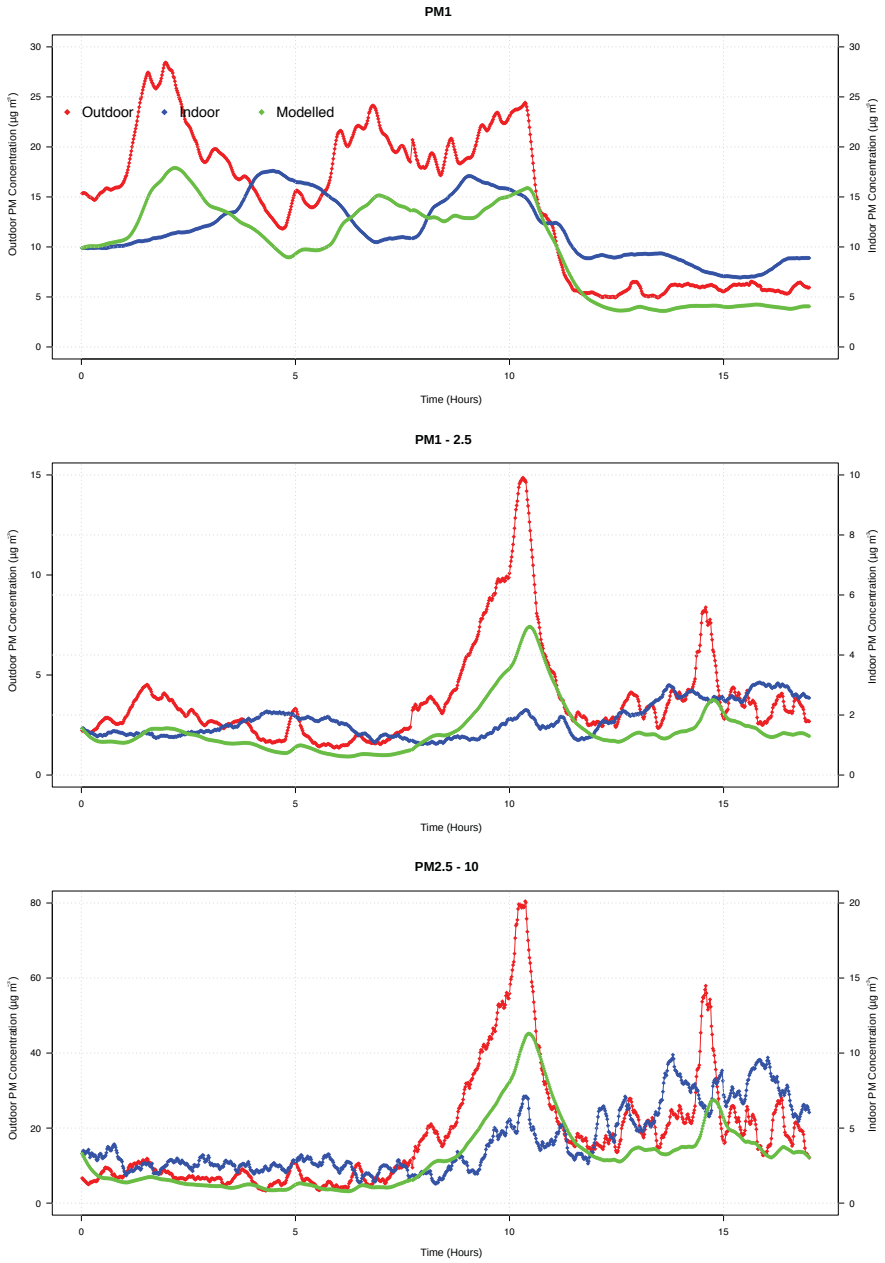

Figure 3: PM time series plots for Day 3 of the JC campaign.

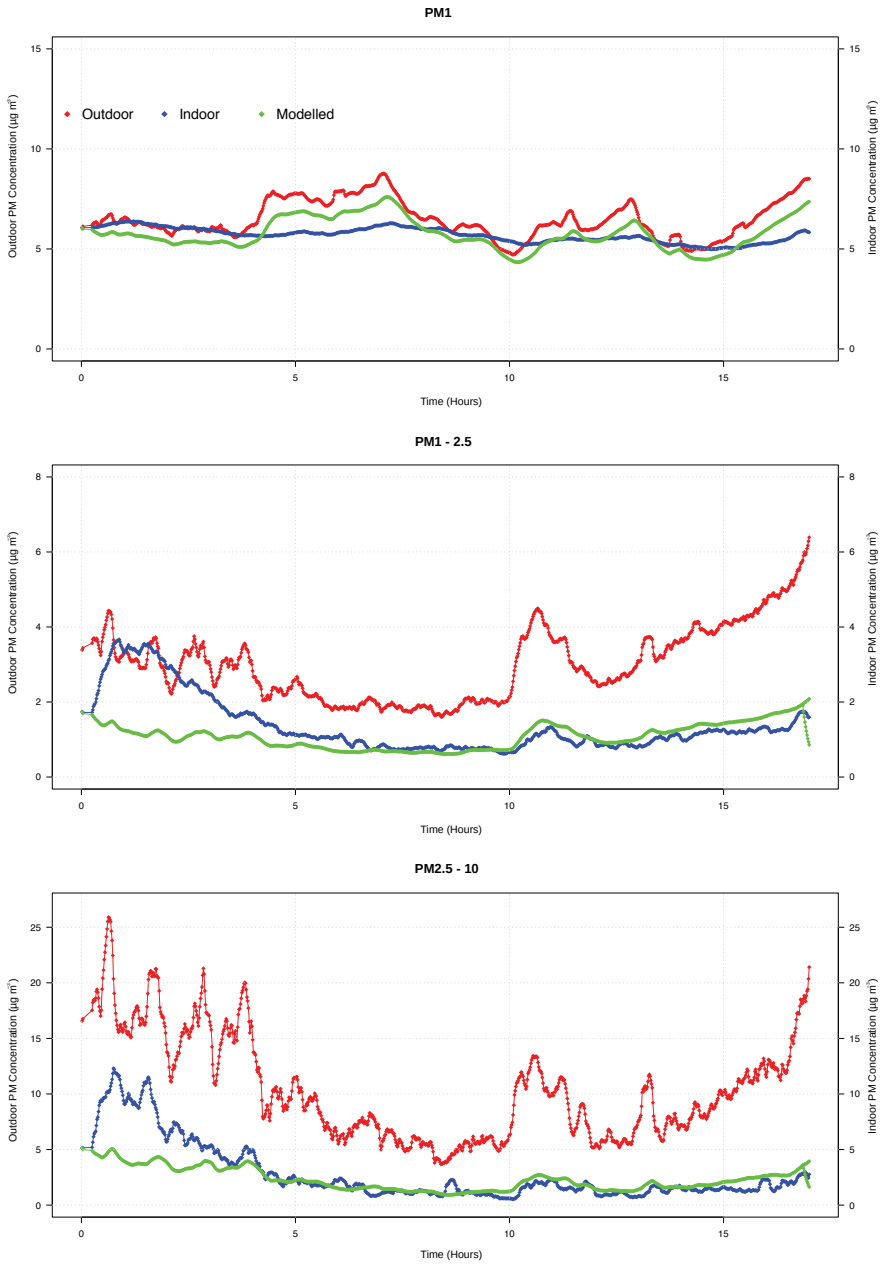

Figure 4: PM time series plots for Day 4 of the JC campaign.

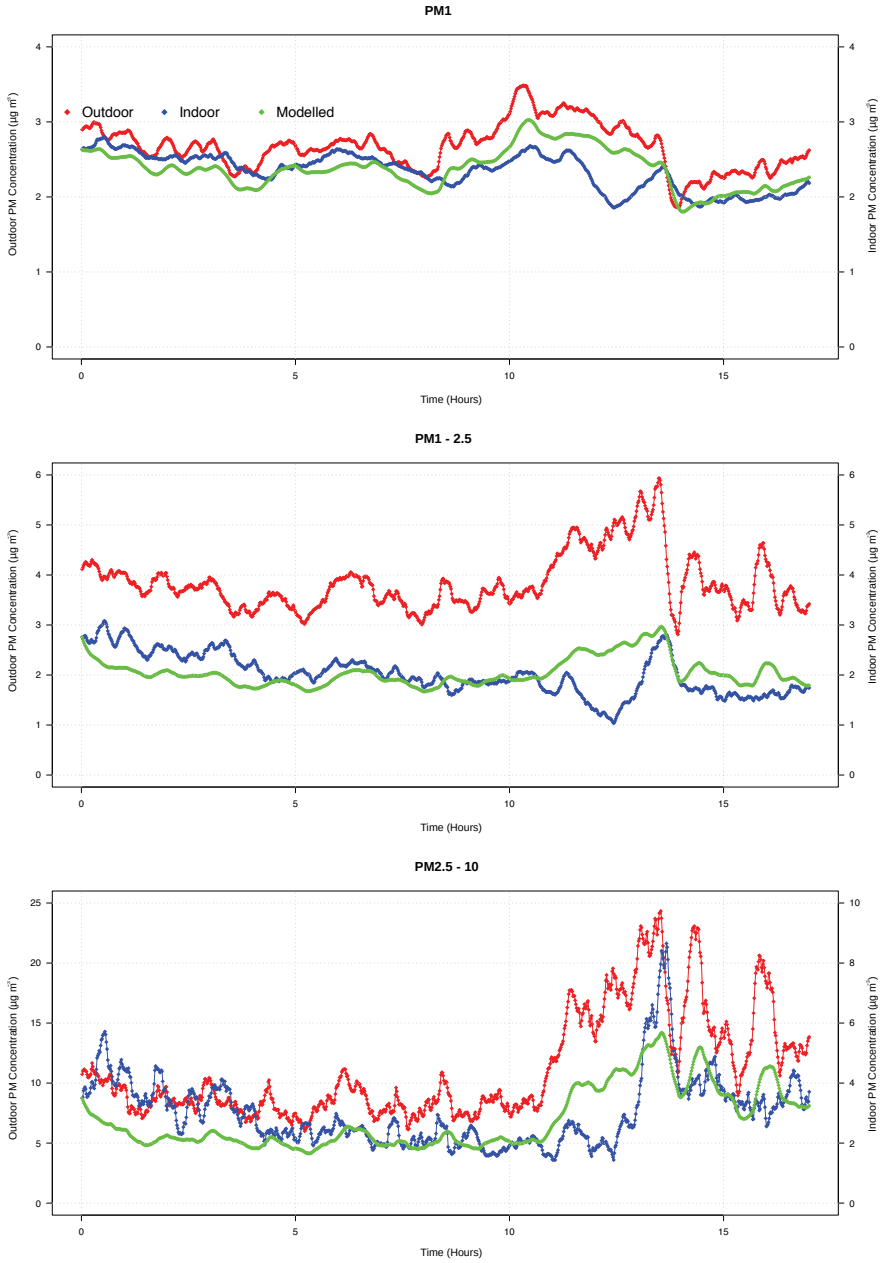

Figure 5: PM time series plots for Day 5 of the JC campaign.

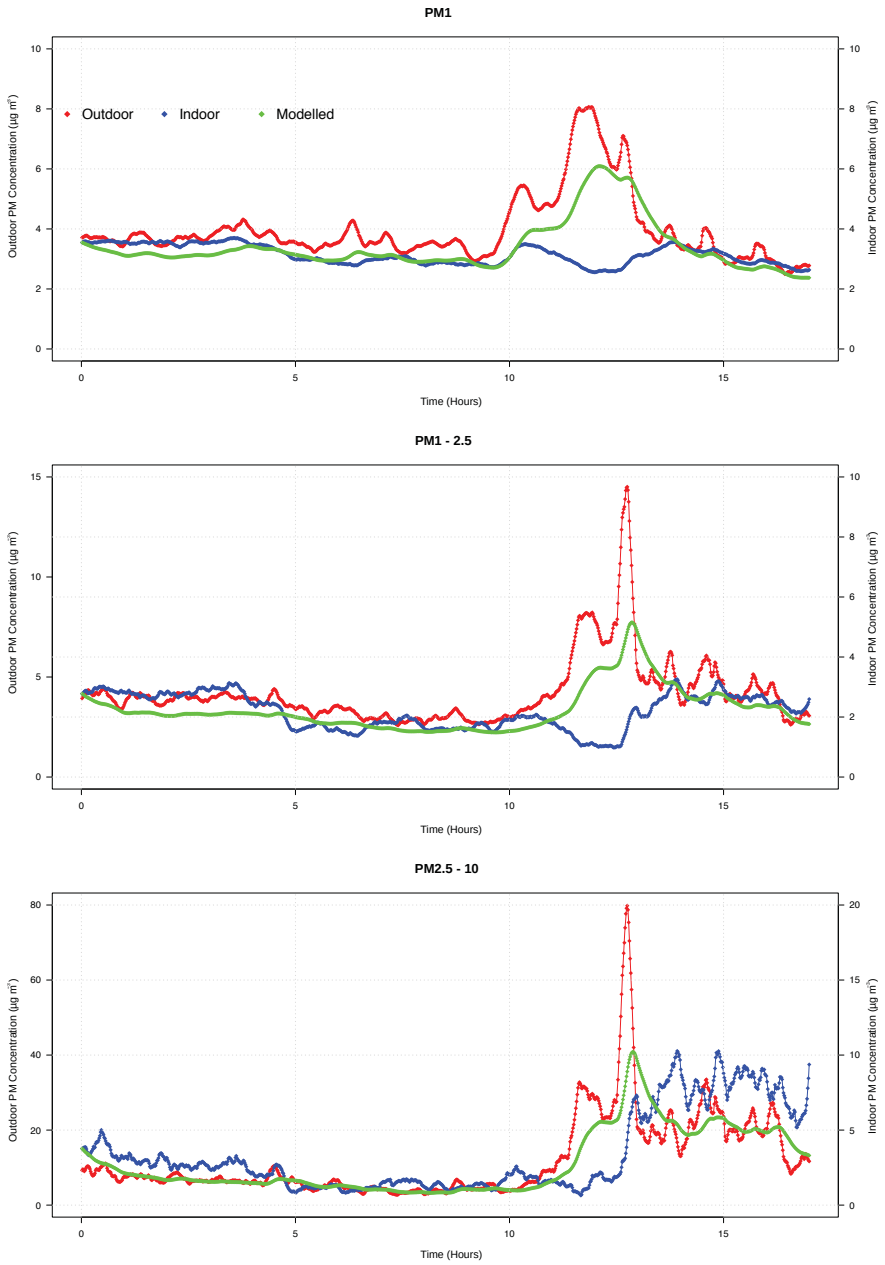

Figure 6: PM time series plots for Day 6 of the JC campaign.

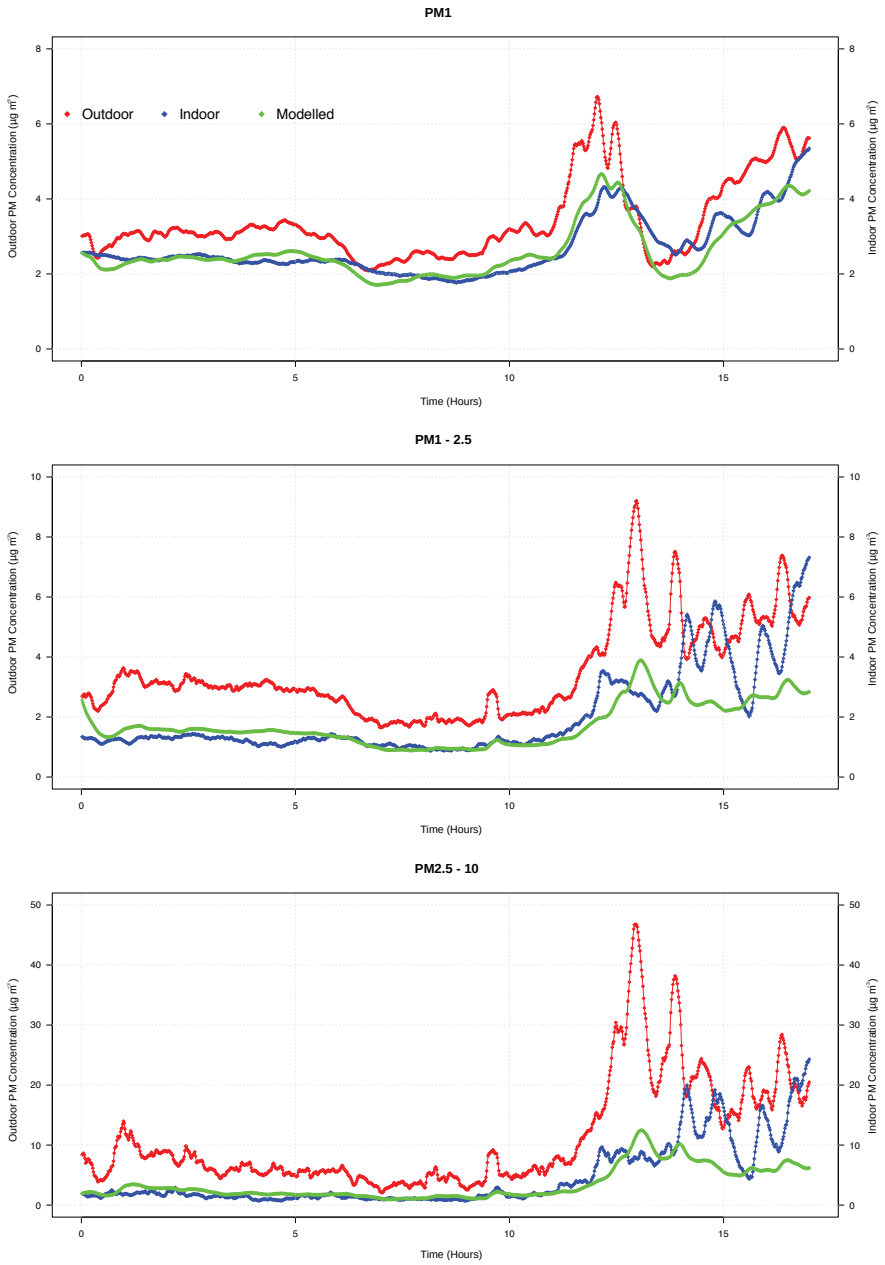

Figure 7: PM time series plots for Day 7 of the JC campaign.

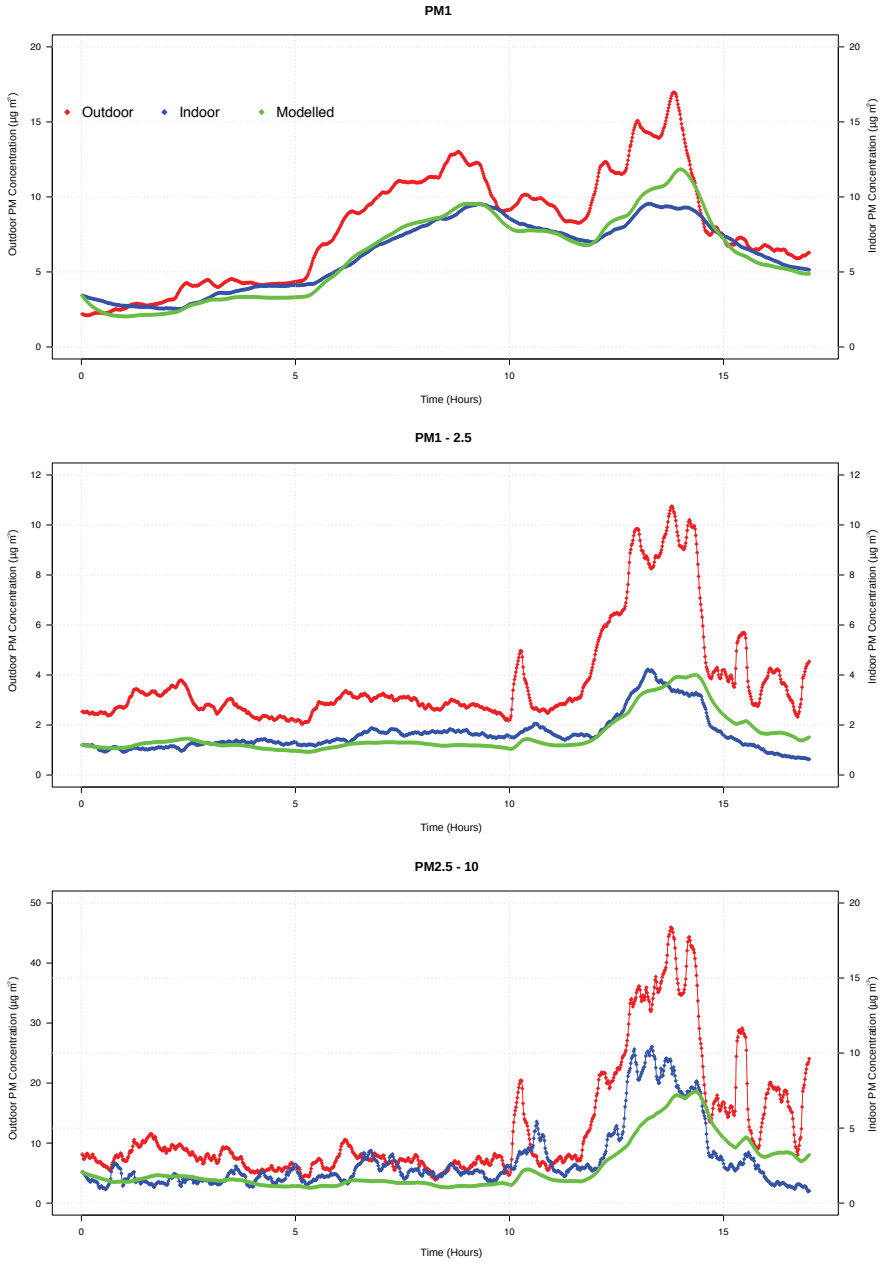

Figure 8: PM time series plots for Day 8 of the JC campaign.

The following plots present the outdoor concentration (LHS y-axis) and the indoor measured and modelled concentration (RHS y-axis) for the eight days studied at the JC. The modelled concentration are derived when **Model 4** was applied.

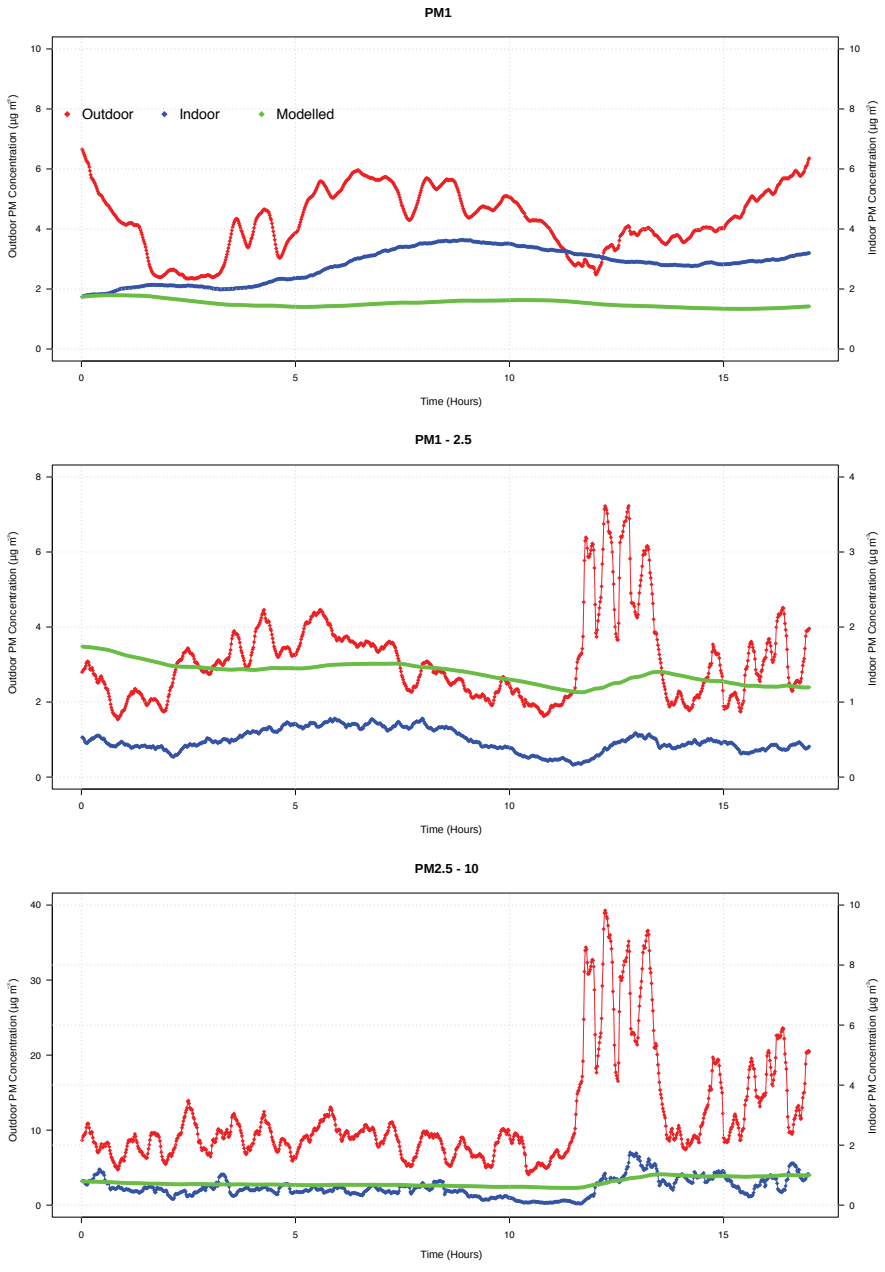

Figure 9: PM time series plots for Day 1 of the JC campaign.

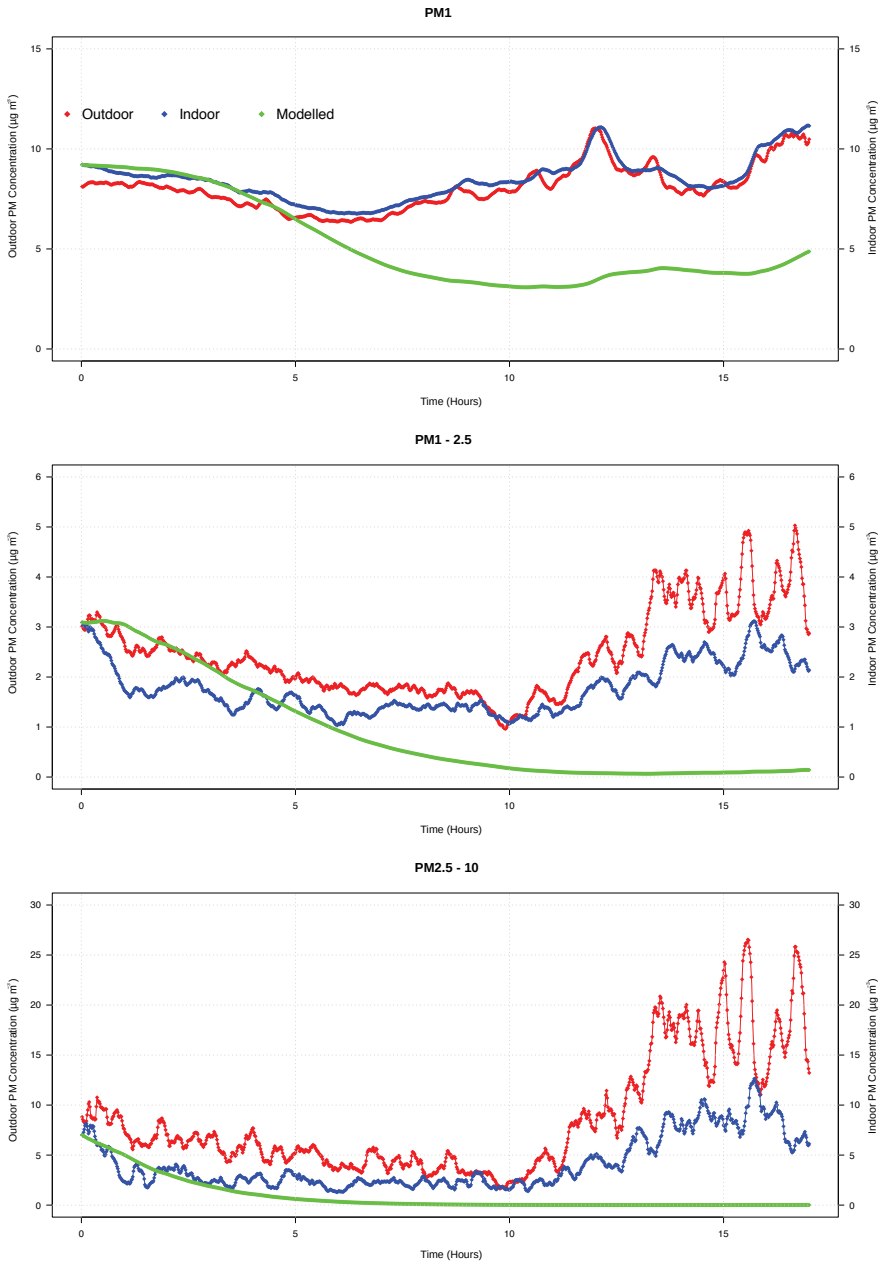

Figure 10: PM time series plots for Day 2 of the JC campaign.

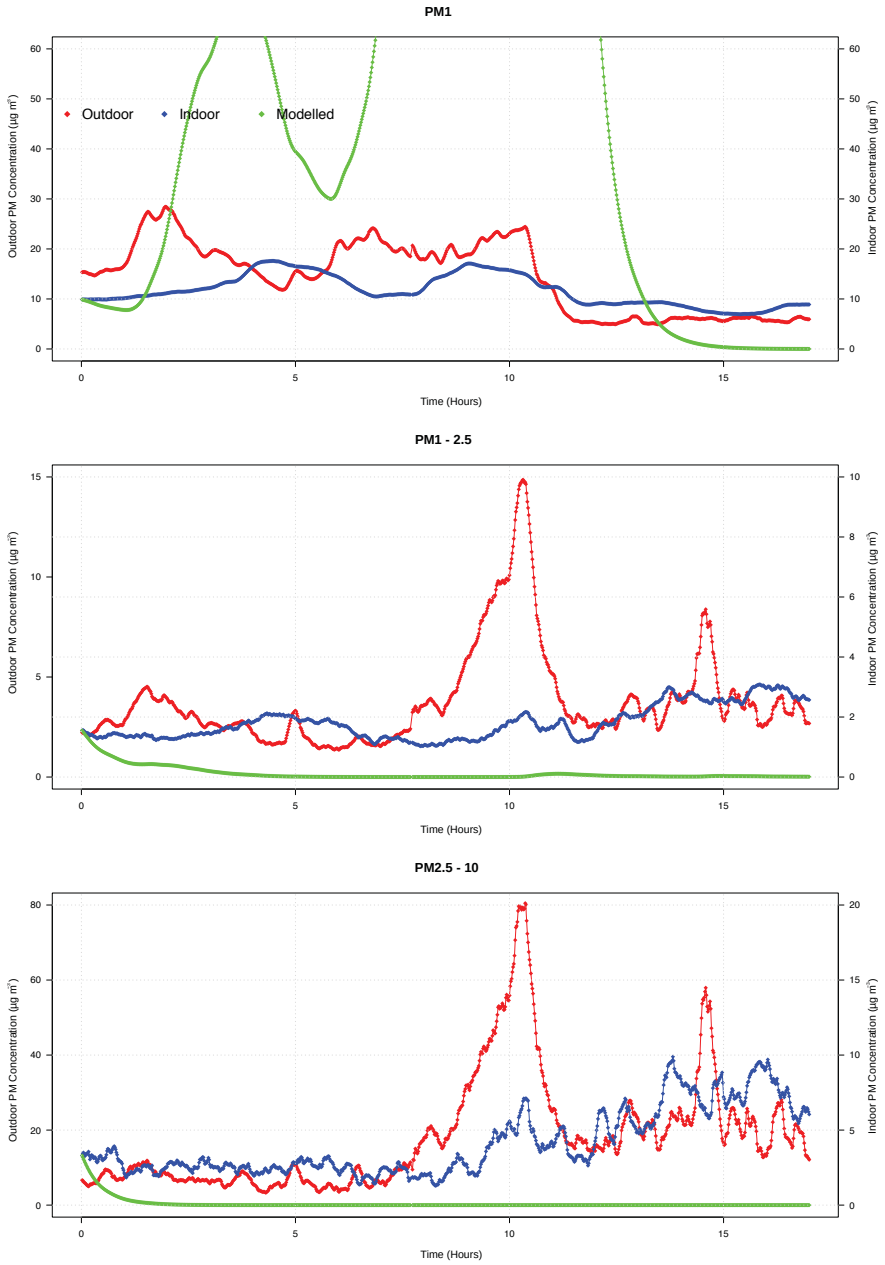

Figure 11: PM time series plots for Day 3 of the JC campaign.

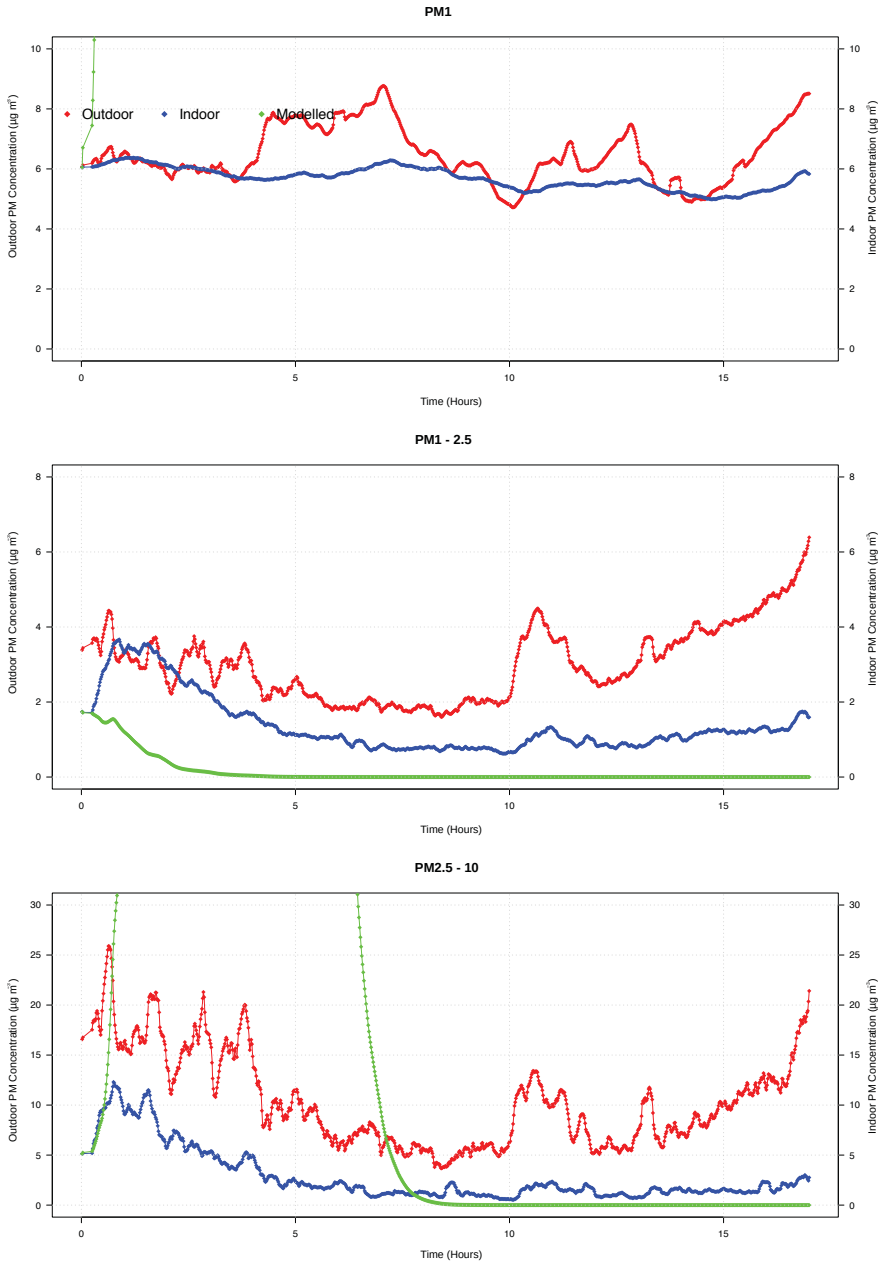

Figure 12: PM time series plots for Day 4 of the JC campaign.

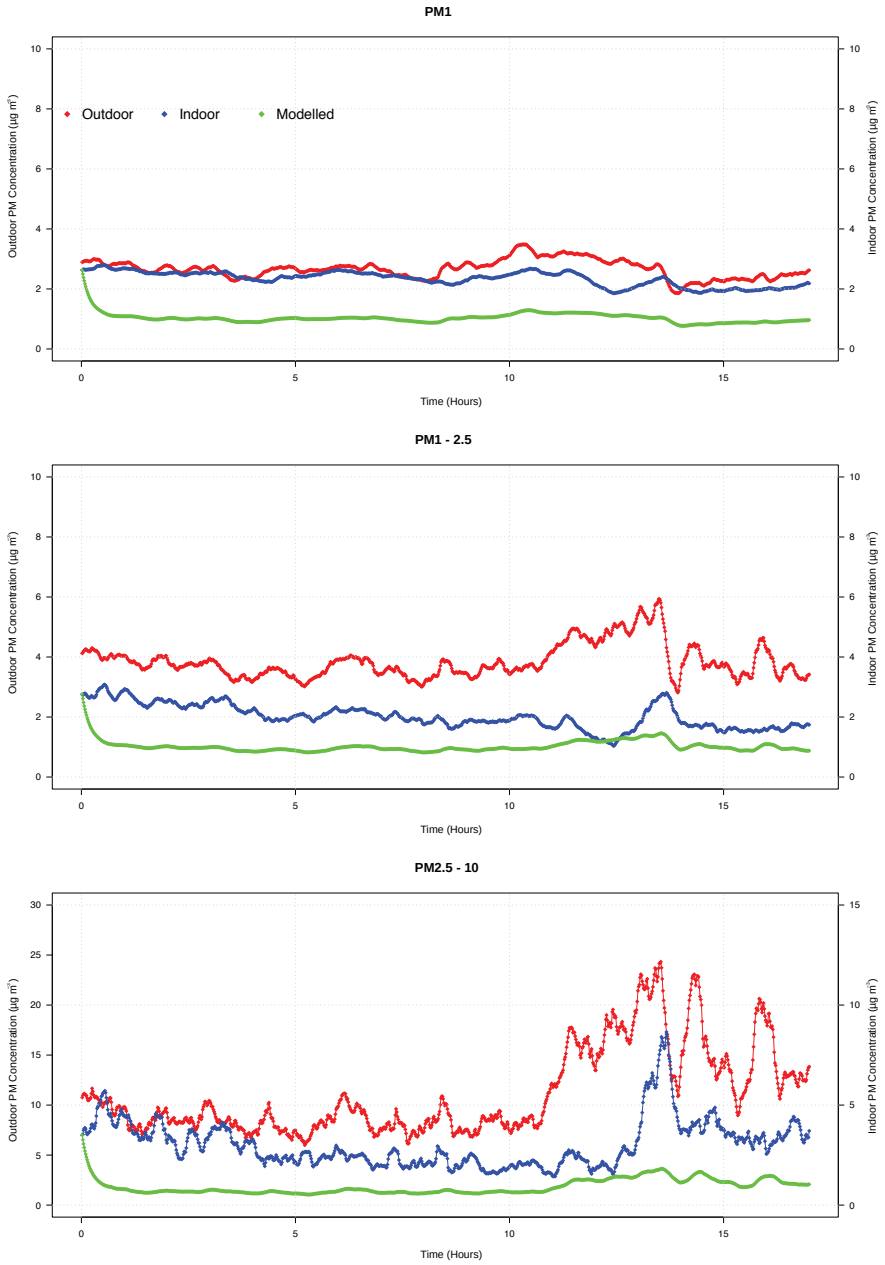

Figure 13: PM time series plots for Day 5 of the JC campaign.

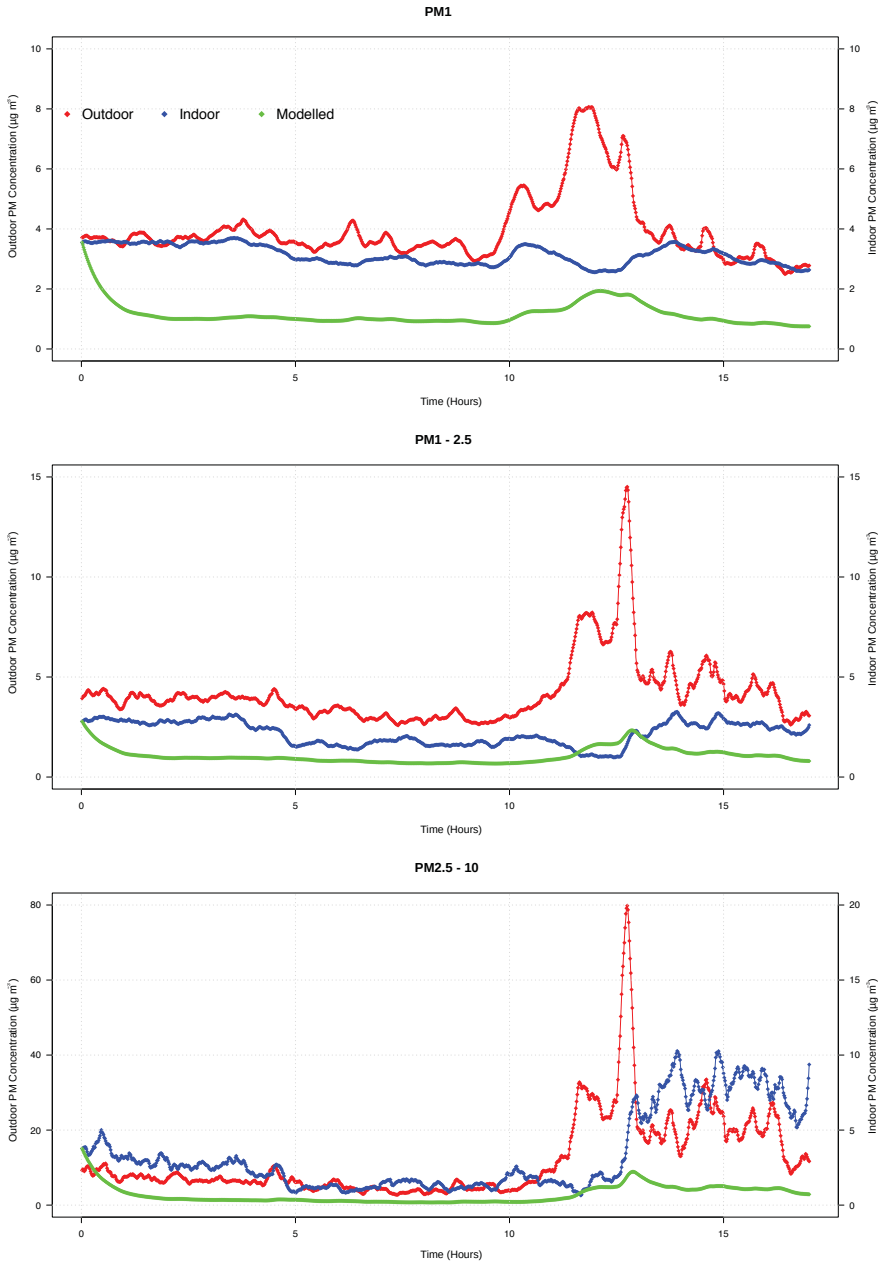

Figure 14: PM time series plots for Day 6 of the JC campaign.

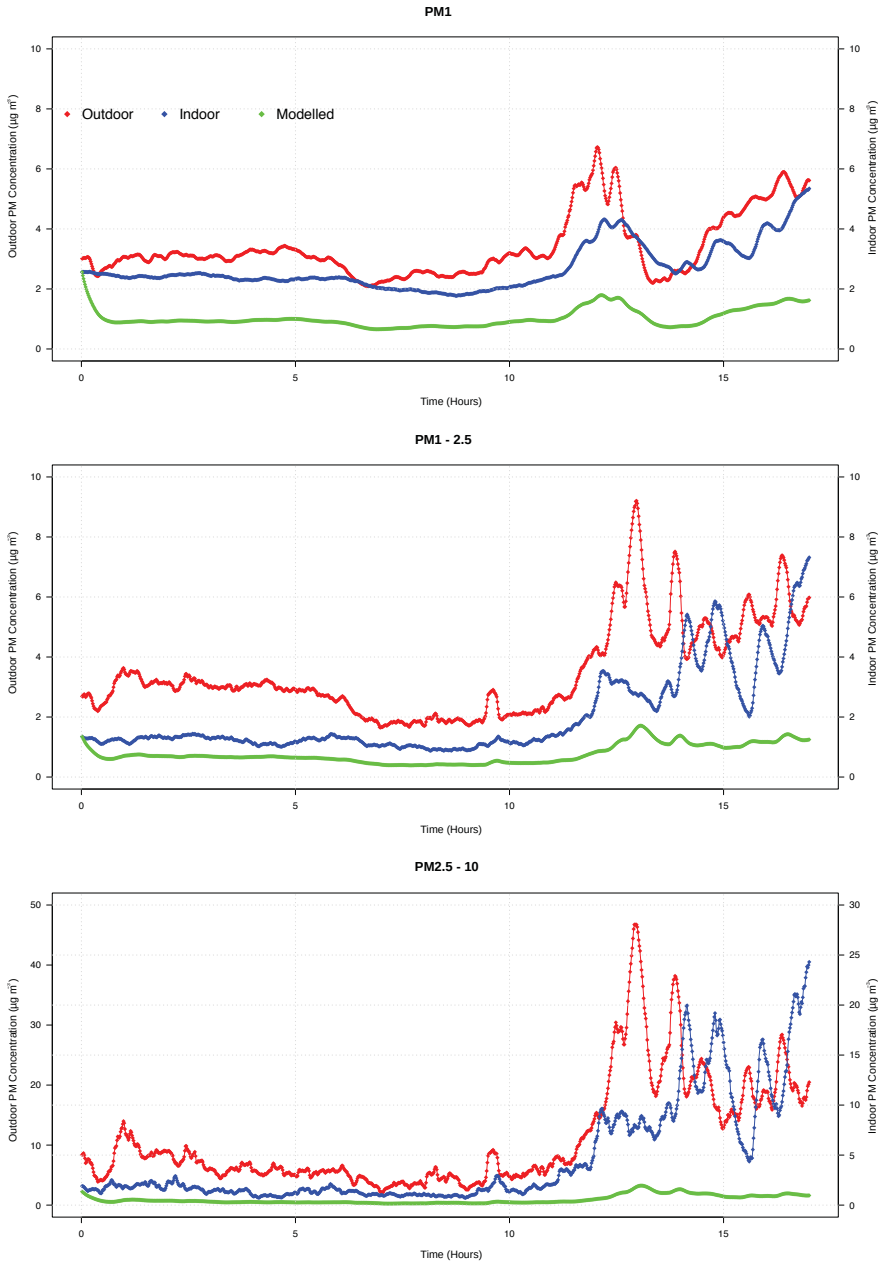

Figure 15: PM time series plots for Day 7 of the JC campaign.

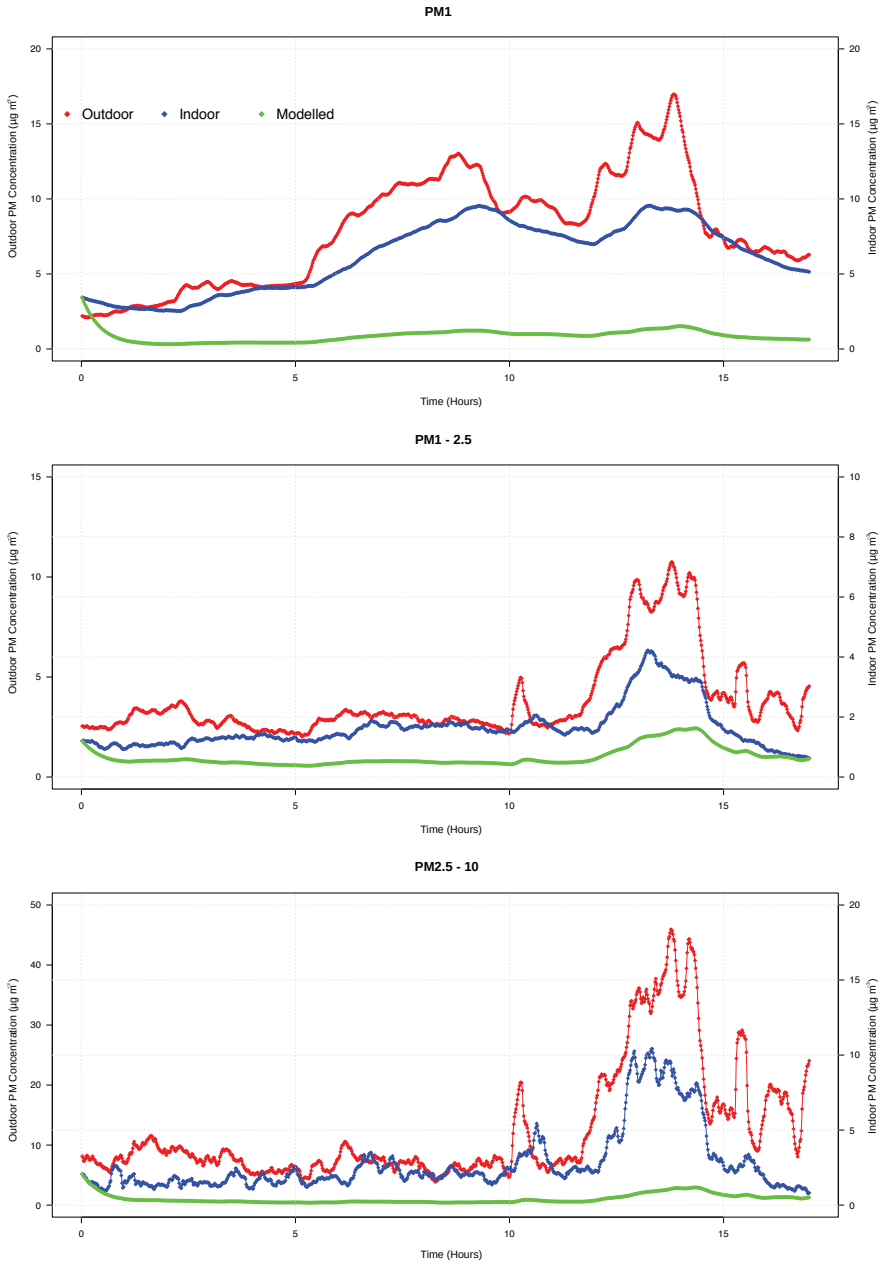

Figure 16: PM time series plots for Day 8 of the JC campaign.

The following plots present time series of the BC concentration (LHS y-axis) and PM concentration (RHS y-axis) both for indoor and outdoor scenarios.

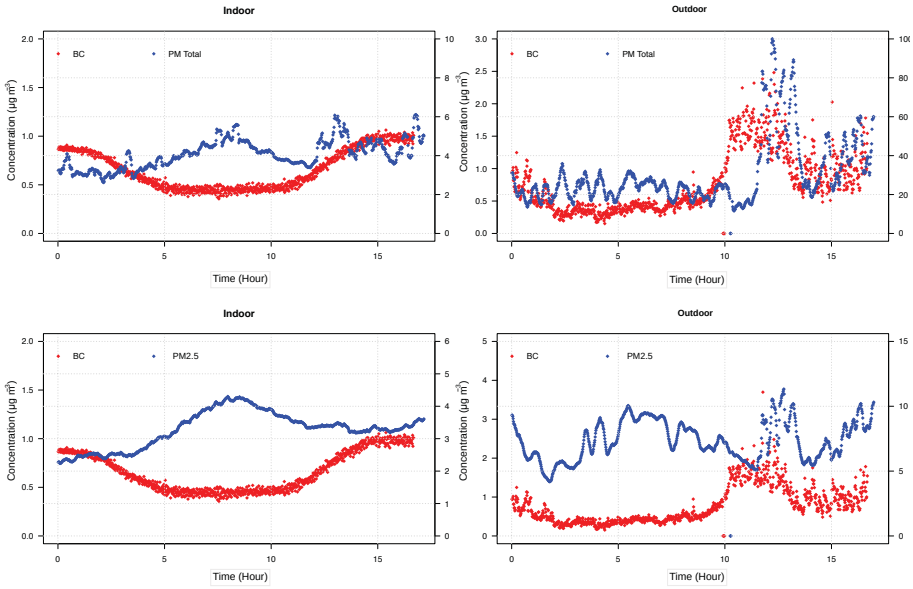

Figure 17: BC time series plots for Day 1 of the JC campaign.

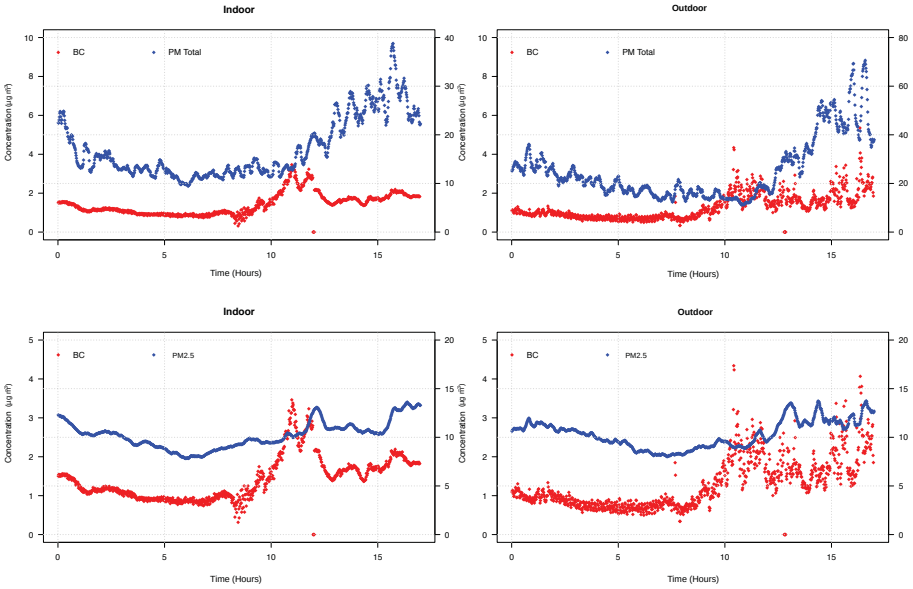

Figure 18: BC time series plots for Day 2 of the JC campaign.

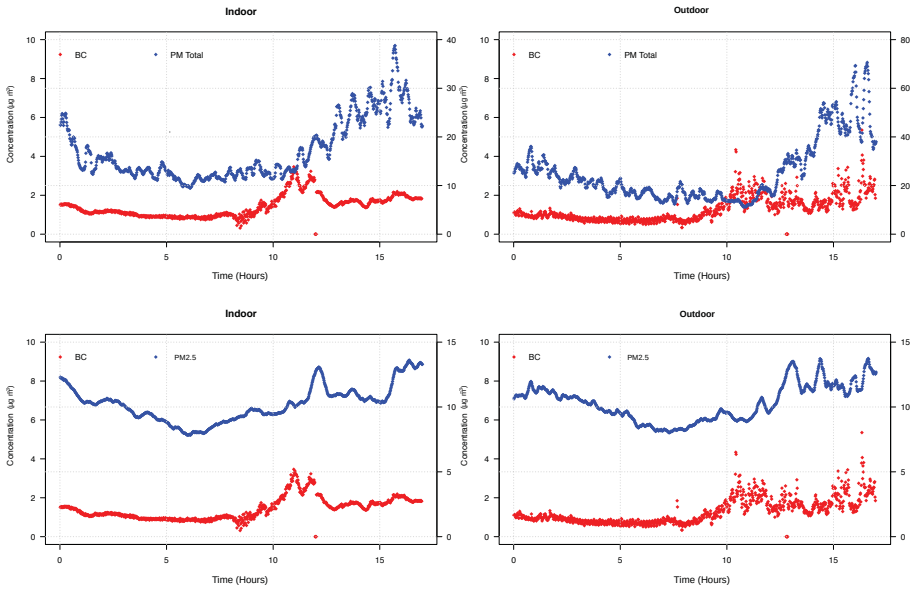

Figure 19: BC time series plots for Day 4 of the JC campaign.

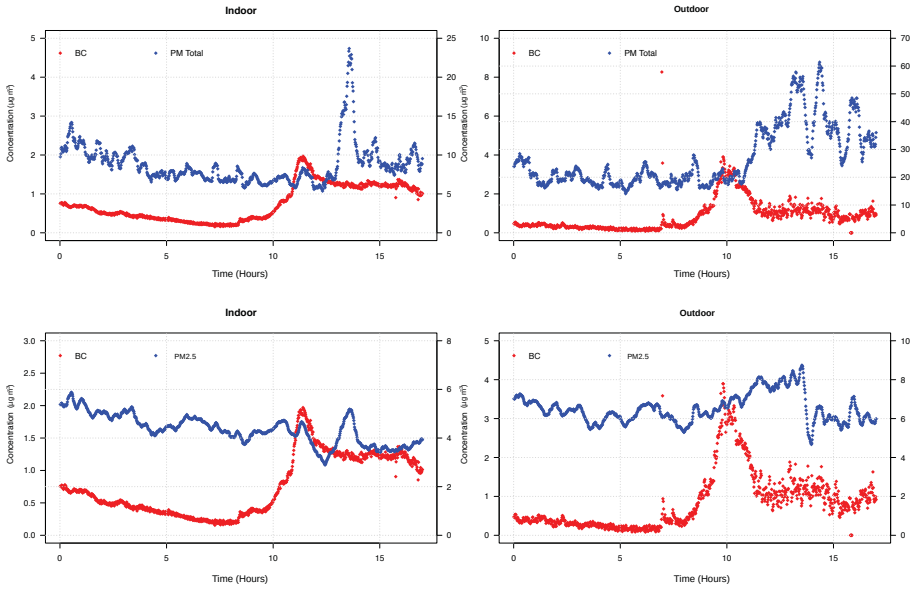

Figure 20: BC time series plots for Day 5 of the JC campaign.

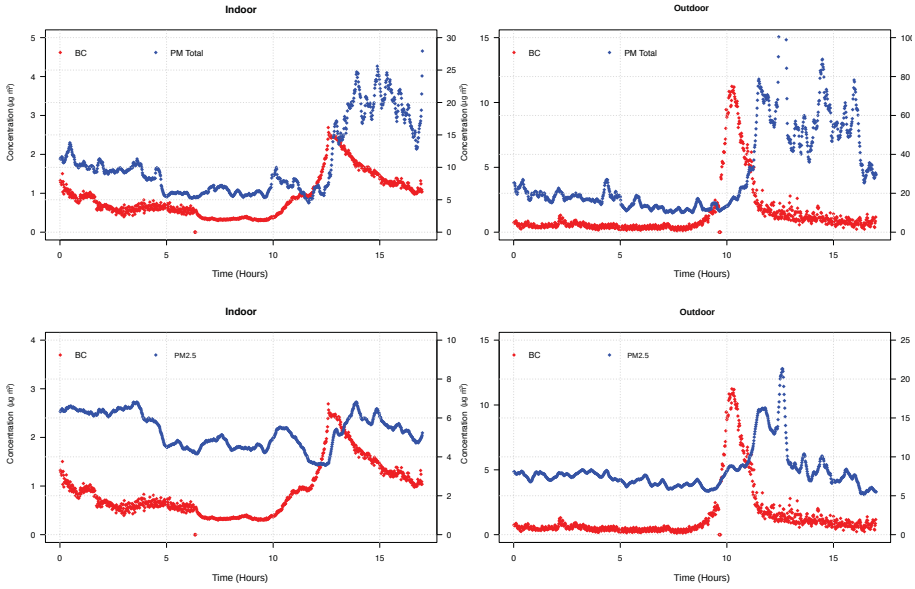

Figure 21: BC time series plots for Day 6 of the JC campaign.

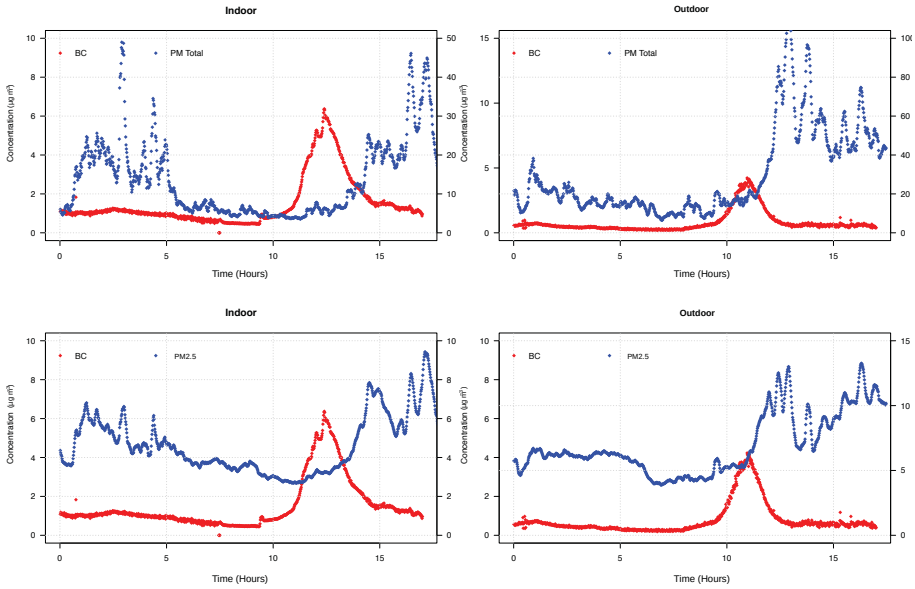

Figure 22: BC time series plots for Day 7 of the JC campaign.

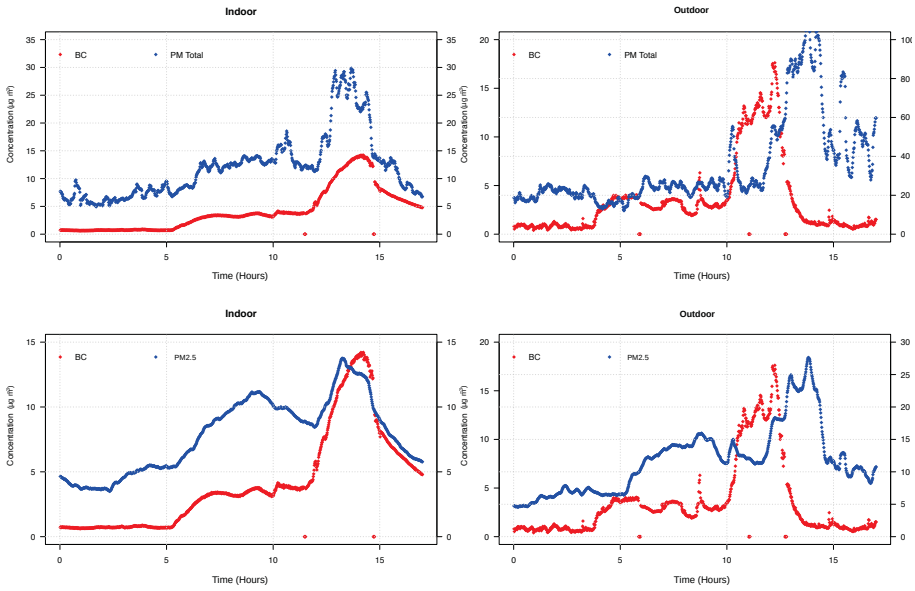

Figure 23: BC time series plots for Day 8 of the JC campaign.

This area has been left intentionally blank.

Birżebbuġa Campaign

Table 1 illustrates the experimental values determined to estimate λ at different size fractions on three different events. Table 2 shows the averaged values of λ from the three tests carried out.

Table 1: Determination of λ through decay curves of indoor PM concentration.

Fraction	C_{int} (μgm^{-3})	C_{SS} (μgm^{-3})	λ (SD) (h^{-1})	R^2
Test 1				
PM_1	8.83	7.18	0.87 (0.003)	0.99
$PM_{1\text{ - }2.5}$	14.77	0.65	0.42 (0.003)	0.97
$PM_{2.5\text{ - }10}$	64.02	1.47	0.71 (0.006)	0.97
Test 2				
PM_1	15.59	4.45	0.14 (0.0005)	0.99
$PM_{1\text{ - }2.5}$	52.77	1.22	0.56 (0.002)	0.99
$PM_{2.5\text{ - }10}$	220.04	2.66	0.86 (0.004)	0.99
Test 3				
PM_1	6.28	5.26	0.42 (0.004)	0.99
$PM_{1\text{ - }2.5}$	19.32	0.79	0.55 (0.002)	0.99
$PM_{2.5\text{ - }10}$	105.08	1.54	0.83 (0.005)	0.98

Table 2: Average λ from Test 1, Test 2 and Test 3 for different size fractions.

PM Size Fraction	λ (h^{-1})
PM_1	0.48
$PM_{1\text{ -}2.5}$	0.51
$PM_{2.5\text{ - }10}$	0.80

The following tables and plots presents the regression and error analysis when **Model 1** was applied.

Table 3: Regression analysis when Model 1 was applied.

Dockery BBG	N	Gradient (SD)	R^2
PM_1	7	0.64 (0.05)	0.96
$PM_{1\text{ - }2.5}$	7	0.30 (0.04)	0.89
$PM_{2.5\text{ - }10}$	7	0.13 (0.04)	0.65

Table 4: Statistical evaluation when Model 1 was Applied.

Model 1	N	RMSE (μgm^{-3})	MAPE (%)	R^2
PM_1	7	1.35	15.21	0.36
$PM_{1\ -\ 2.5}$	7	0.63	42.78	0.25
$PM_{2.5\ -\ 10}$	7	2.47	84.19	0.04

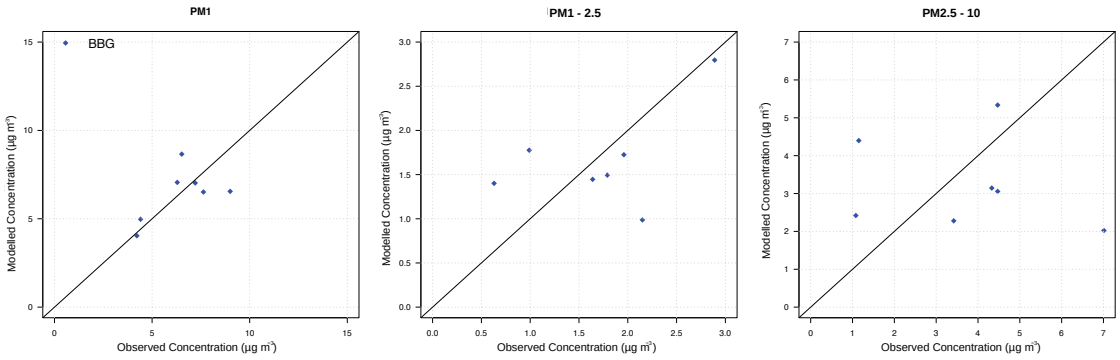

Figure 24: Comparison of modelled and observed values for different size fractions, when Model 1 was applied.

The following tables and plots presents the regression and error analysis when **Model 2** was applied.

Table 5: Regression analysis when Model 2 was applied.

Model 2	N	Gradient (SD)	y-intercept (SD)	R^2	P	k (h^{-1})
PM_1	7	0.07 (0.04)	1.28 (0.18)	0.42	0.78	0.05
$PM_{1\ -\ 2.5}$	7	0.50 (0.24)	1.73 (1.19)	0.46	0.58	0.29
$PM_{2.5\ -\ 10}$	7	1.55 (1.35)	4.04 (6.89)	0.21	0.25	0.38

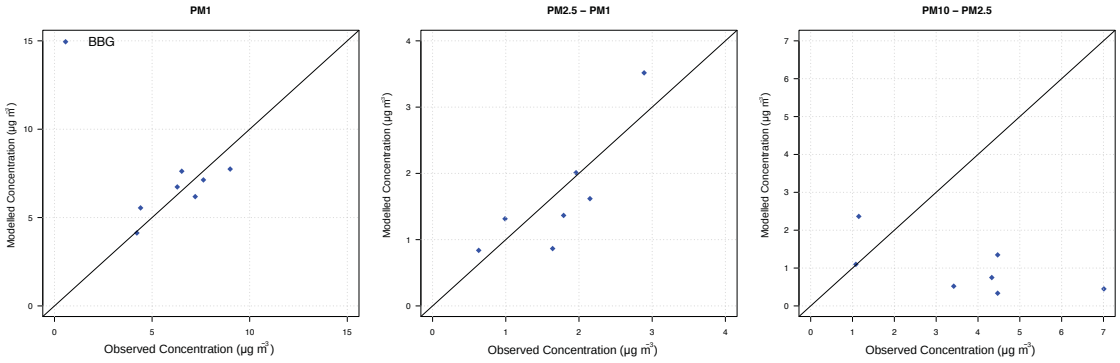

Figure 25: Comparison of modelled and observed values for different size fractions, when Model 2 was applied.

Table 6: Statistical evaluation when Model 2 was applied using the analytical estimation of k.

Model 2	N	RMSE (μgm^{-3})	MAPE (%)	R^2
PM_1	7	0.89	12.37	0.69
$PM_{1\ -\ 2.5}$	7	0.48	26.55	0.69
$PM_{2.5\ -\ 10}$	7	3.64	75.81	0.43

The following tables and plots presents the regression and error analysis when **Model 3** was applied.

Table 7: Estimated values of P and k, at different size fractions of PM.

		PM_1		$PM_{1\ -\ 2.5}$		$PM_{2.5\ -\ 10}$	
Day	AER	P	k	P	k	P	k
1	0.26	0.68	0.01	0.33	0.01	0.21	0.01
2	0.54	0.52	0	0.23	0	0.09	0
3	0.44	0.76	0	0.42	0.14	0.35	0.47
4	0.13	0.54	0	0.07	0.07	0.03	0.14
5	1.62	0.82	0	0.58	0	0.33	0
6	0.18	0.42	0	0.05	0.05	0.01	0.09
7	0.13	0.44	0	0.41	0.40	0.16	0.77

Table 8: Statistical analysis when Model 3 was applied.

		RMSE (μgm^{-3})			MAPE (%)		
Day	AER	PM_1	$PM_{1 - 2.5}$	$PM_{2.5 - 10}$	PM_1	$PM_{1 - 2.5}$	$PM_{2.5 - 10}$
1	0.26	0.24	0.35	0.94	3.81	11.71	18.58
2	0.54	0.55	0.34	1.35	10.54	12.14	21.74
3	0.44	0.23	0.36	1.92	2.57	7.97	16.88
4	0.13	0.23	0.17	0.58	2.29	13.94	26.94
5	1.62	2.68	0.74	3.95	14.91	18.84	34.05
6	0.18	0.35	0.16	0.24	4.85	15.59	18.07
7	0.13	0.45	2.52	10.90	5.16	35.85	53.50

This area has been left intentionally blank.

The following plots present the outdoor concentration (LHS y-axis) and the indoor measured and modelled concentration (RHS y-axis) for the seven days studied at BBG. The modelled concentration are derived when **Model 3** was applied.

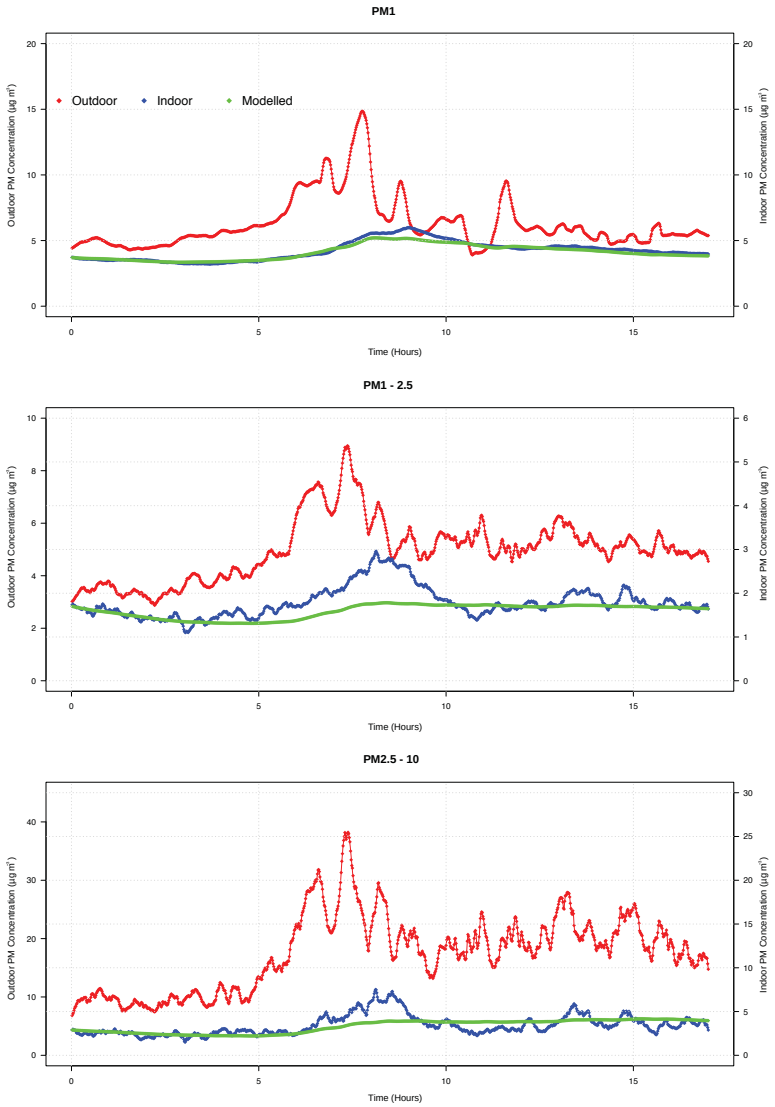

Figure 26: PM time series plots for Day 1 of the BBG campaign.

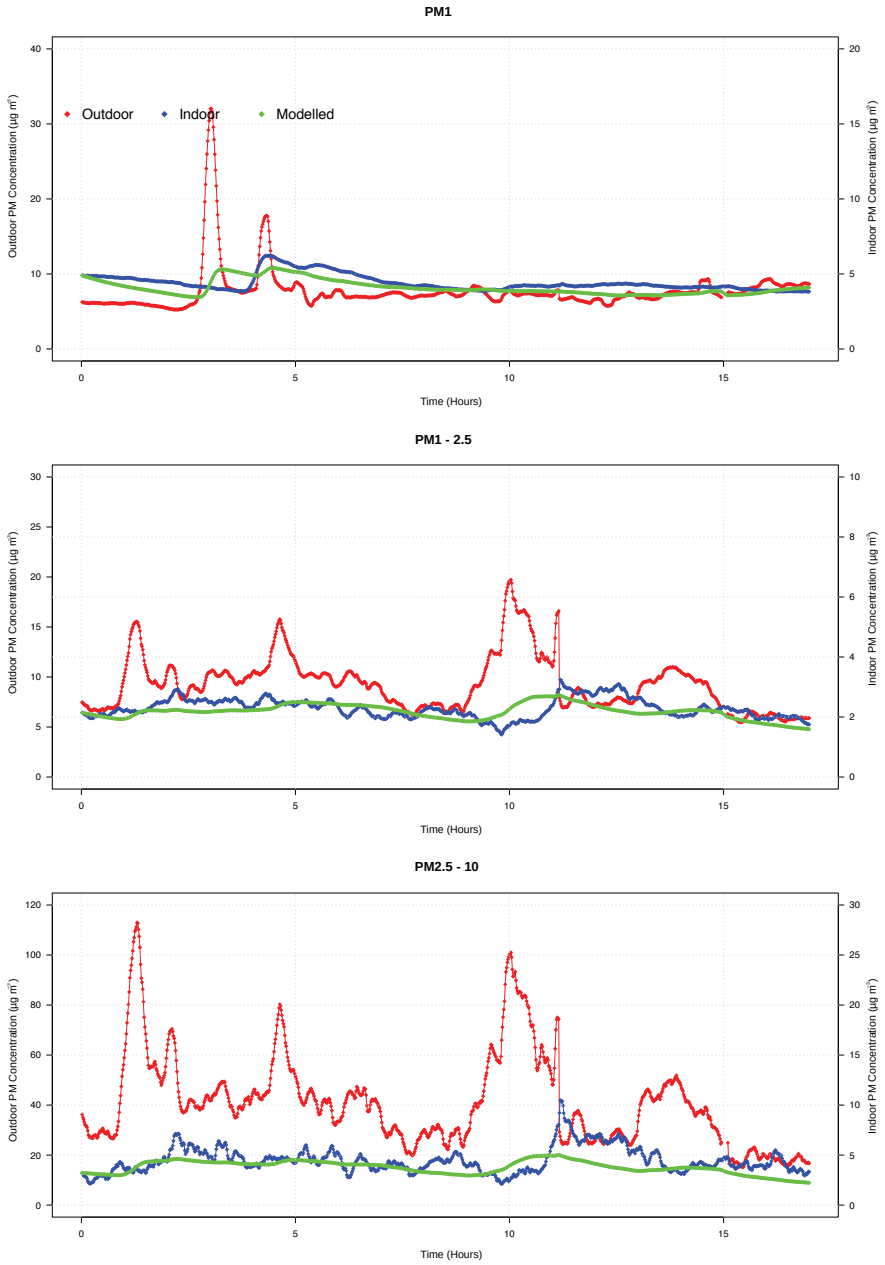

Figure 27: PM time series plots for Day 2 of the BBG campaign.

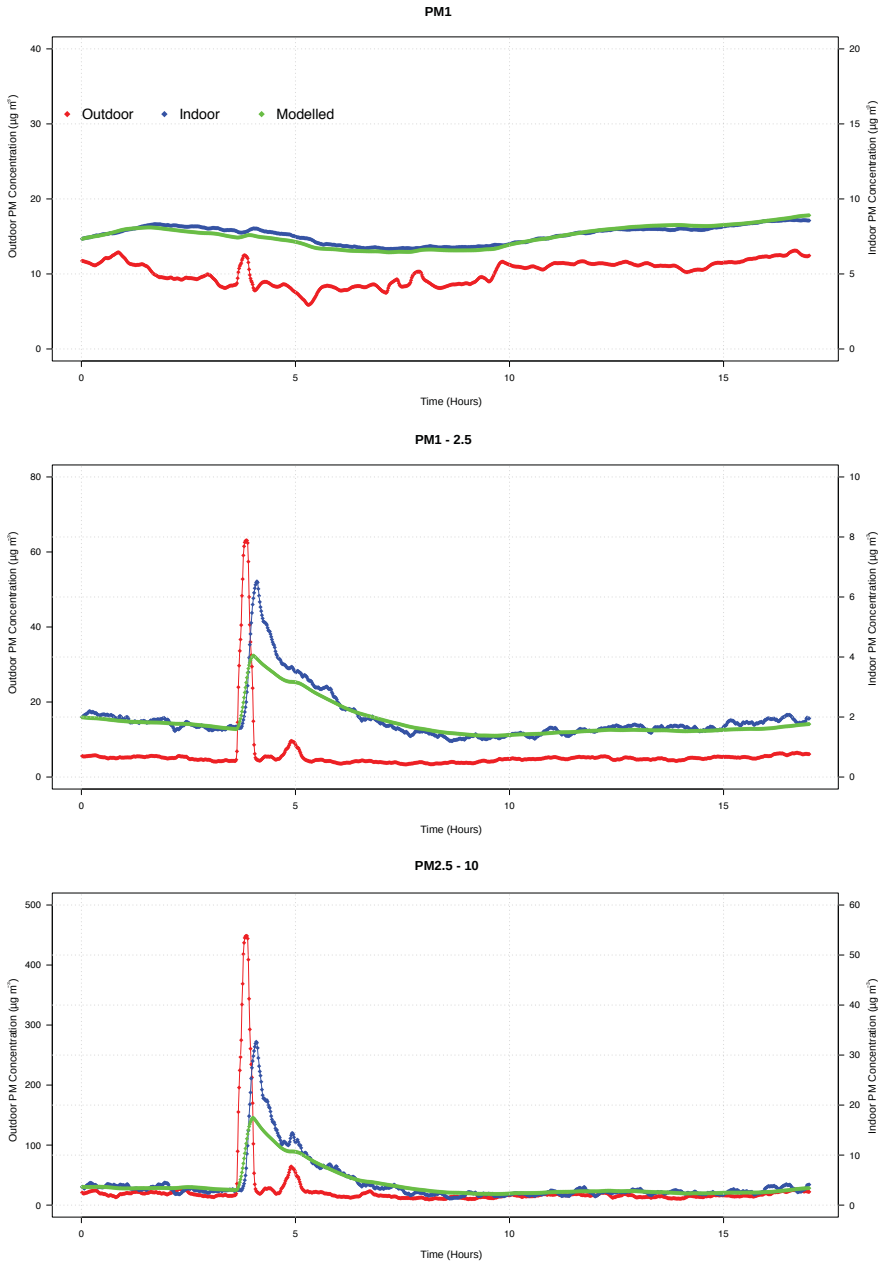

Figure 28: PM time series plots for Day 3 of the BBG campaign.

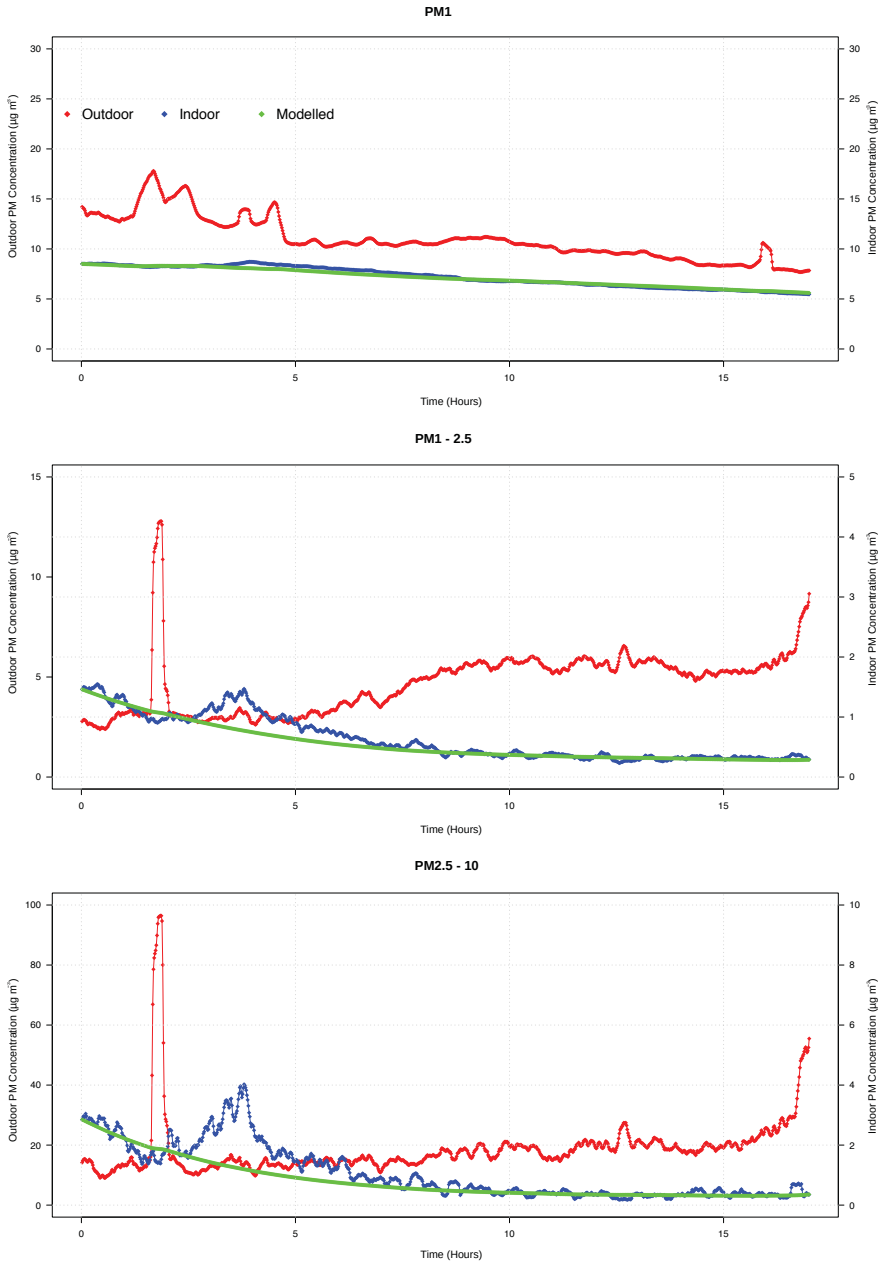

Figure 29: PM time series plots for Day 4 of the BBG campaign.

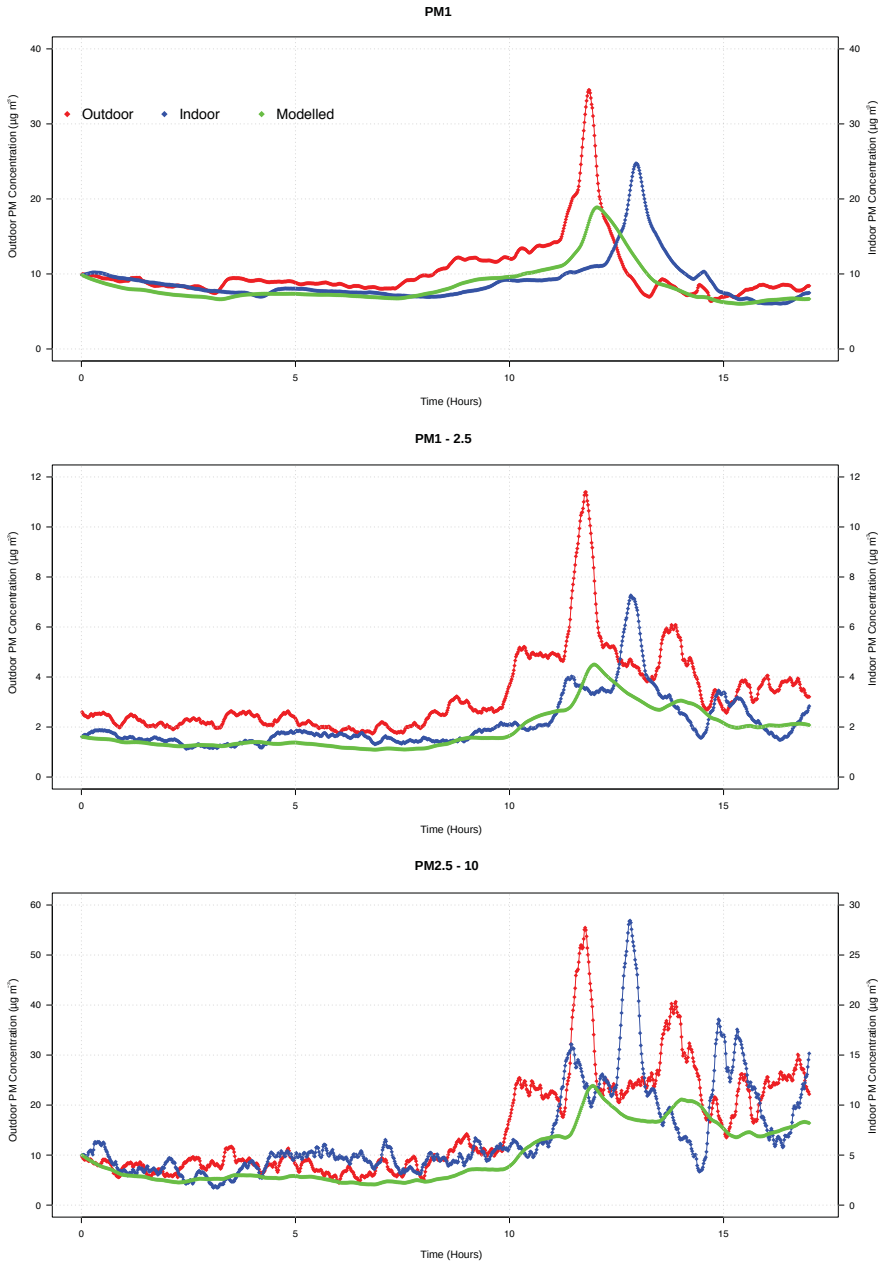

Figure 30: PM time series plots for Day 5 of the BBG campaign.

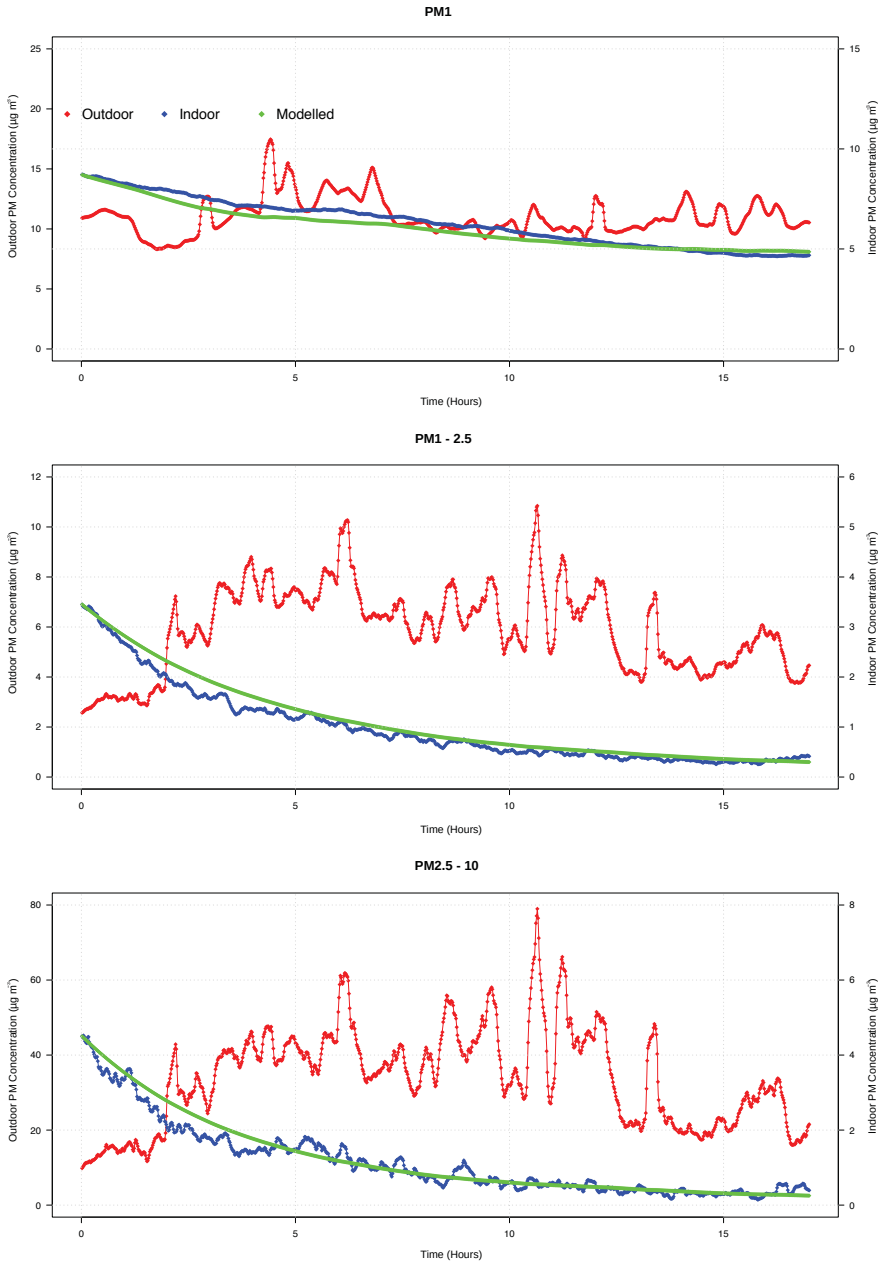

Figure 31: PM time series plots for Day 6 of the BBG campaign.

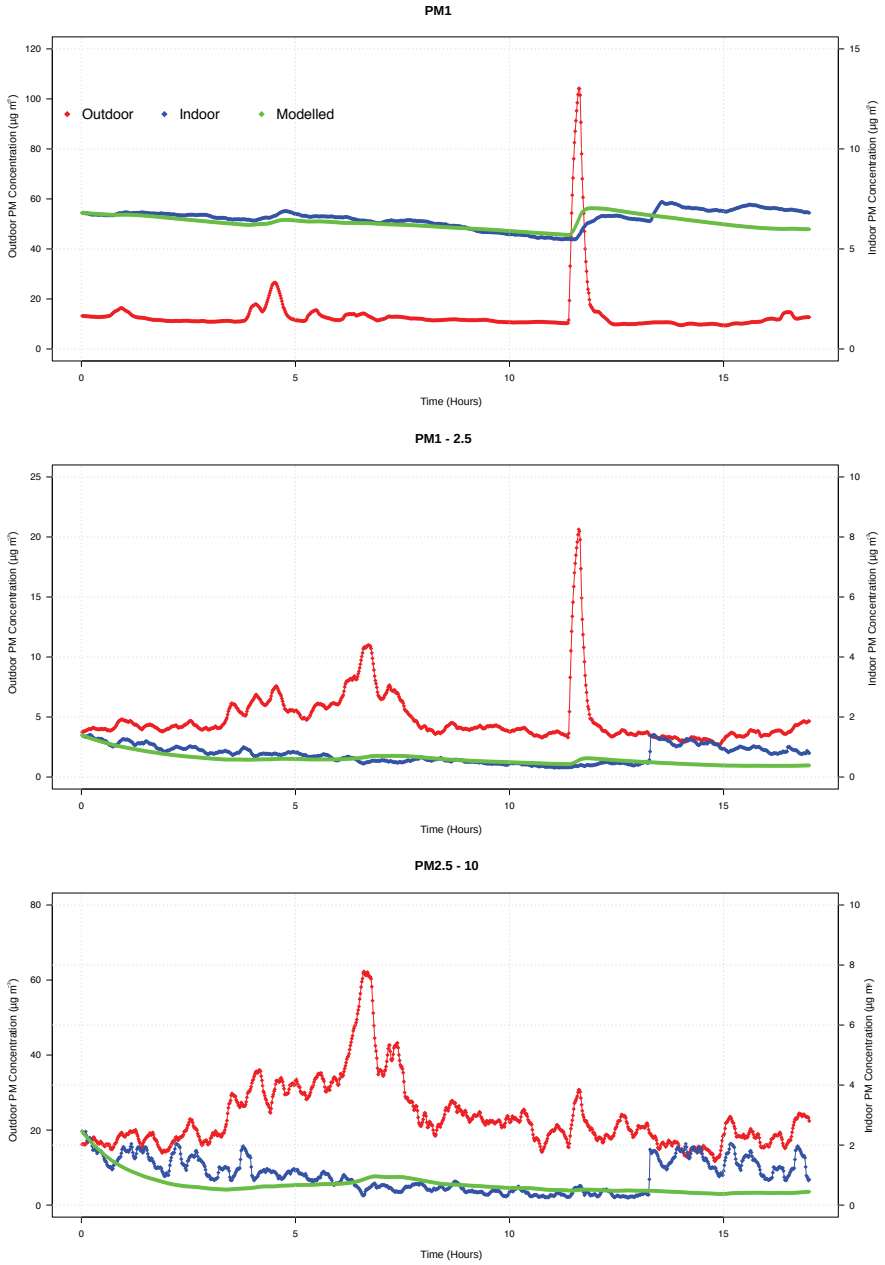

Figure 32: PM time series plots for Day 7 of the BBG campaign.

The following tables and plots presents the regression and error analysis when **Model 4** was applied

Table 9: Values of P and k, at different size fractions of PM.

		PM_1		$PM_{1\text{ - }2.5}$		$PM_{2.5\text{ - }10}$	
Day	AER	P	k	P	k	P	k
1	0.26	0.15	0	0.31	0.19	0.08	0.19
2	0.54	0.12	0	0.10	0	0.02	0
3	0.44	0.10	0	0.28	0.33	0.06	0.51
4	0.13	0.07	0	0.25	0.14	0.02	0.16
5	1.62	0.02	0.16	0.22	0	0.03	0
6	0.18	0.07	0	0.07	0.08	0.01	0.09
7	0.13	0.07	0	1.31	0.93	0.53	1.84

Table 10: Statistical evaluation when Model 4 was applied.

		RMSE (μgm^{-3})			MAPE (%)		
Day	AER	PM_1	$PM_{1\text{ - }2.5}$	$PM_{2.5\text{ - }10}$	PM_1	$PM_{1\text{ - }2.5}$	$PM_{2.5\text{ - }10}$
1	0.26	1.05	0.95	2.76	20.63	44.92	64.93
2	0.54	0.93	0.55	2.72	17.65	19.65	49.65
3	0.44	1.18	1.33	3.48	12.58	49.96	58.63
4	0.13	0.19	0.15	0.64	2.18	16.47	48.57
5	1.62	9.17	2.33	8.32	95.92	92.55	94.45
6	0.18	0.13	0.14	0.34	1.66	14.67	21.35
7	0.13	0.39	0.48	0.87	4.26	49.72	66.66

This area has been left intentionally blank.

The following plots present the outdoor concentration (LHS y-axis) and the indoor measured and modelled concentration (RHS y-axis) for the eight days studied at the JC. The modelled concentration are derived when **Model 4** was applied.

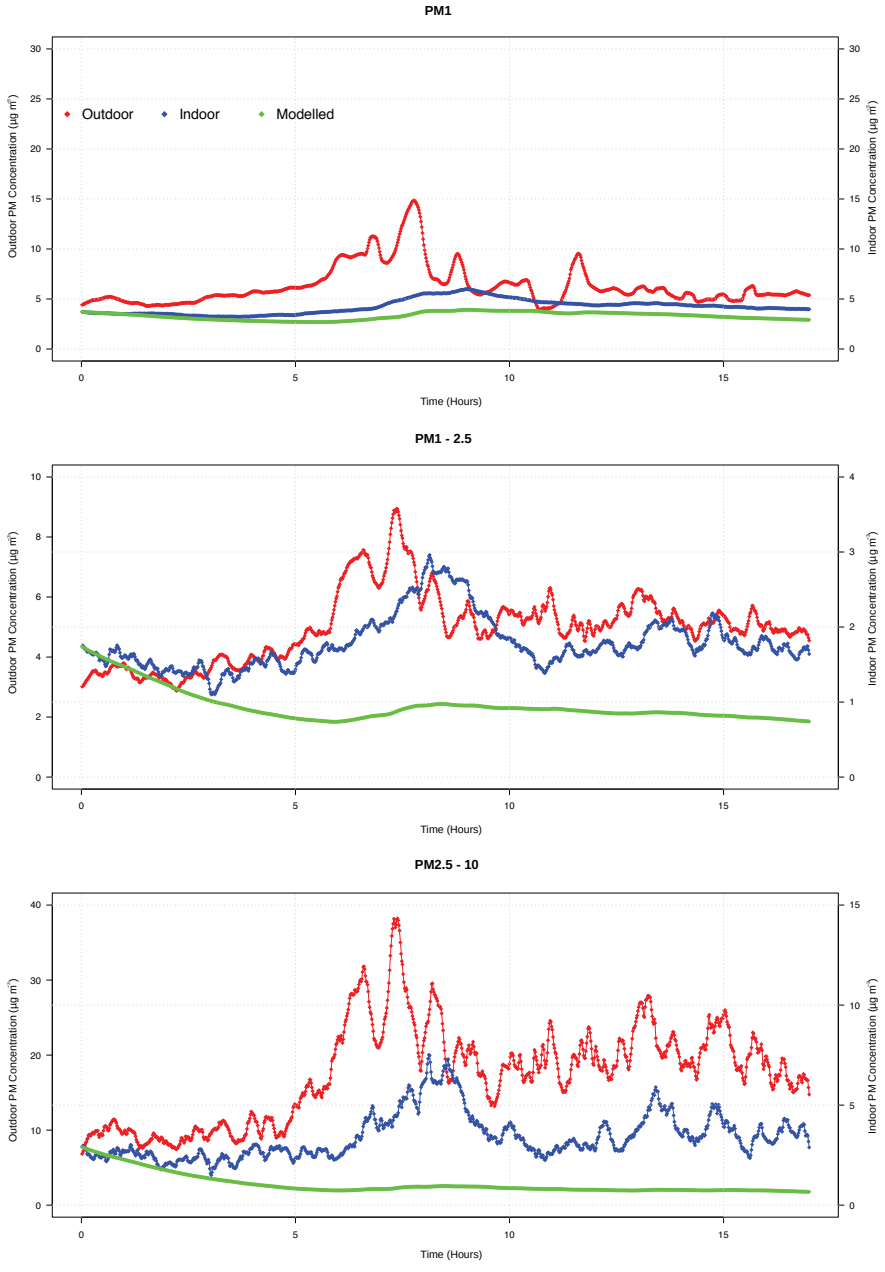

Figure 33: PM time series plots for Day 1 of the BBG campaign.

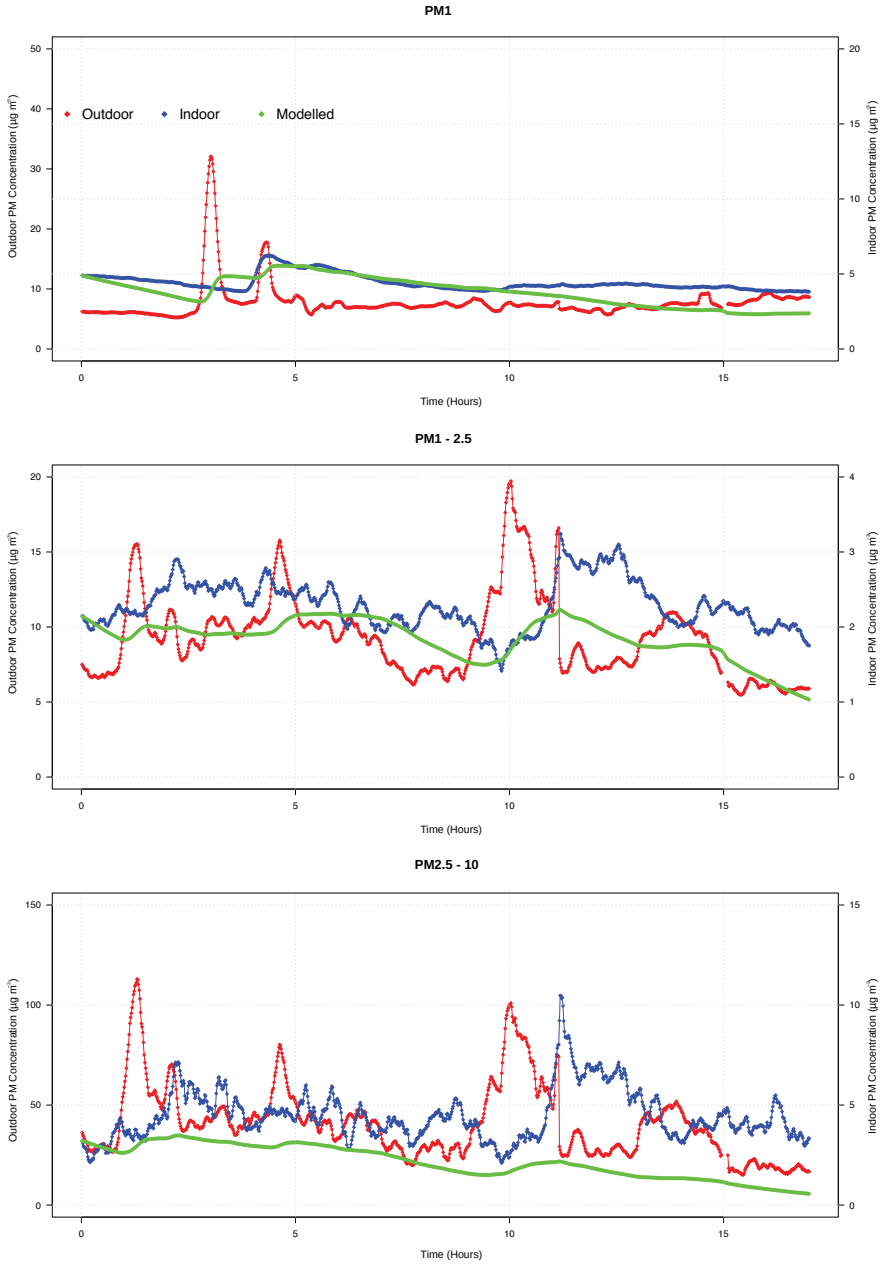

Figure 34: PM time series plots for Day 2 of the BBG campaign.

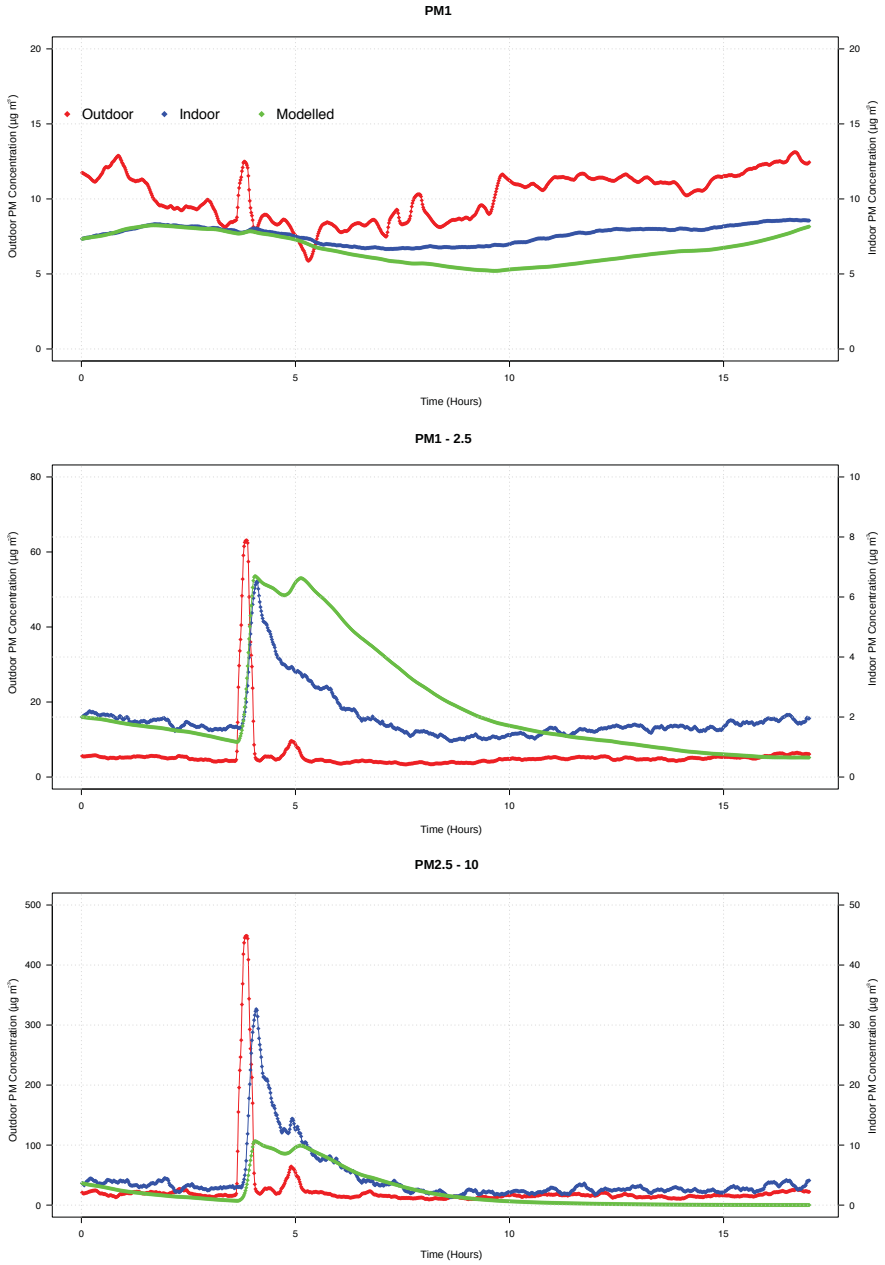

Figure 35: PM time series plots for Day 3 of the BBG campaign.

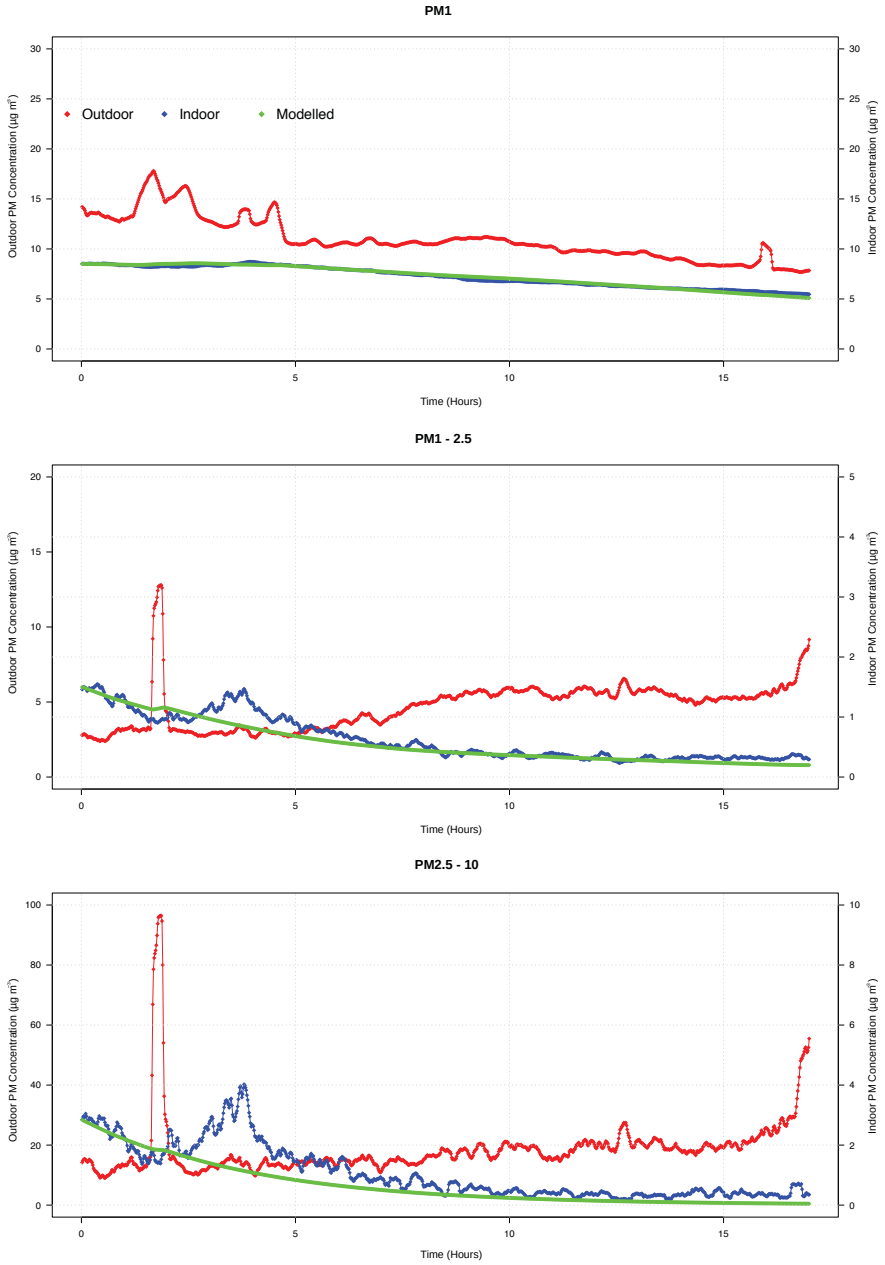

Figure 36: PM time series plots for Day 4 of the BBG campaign

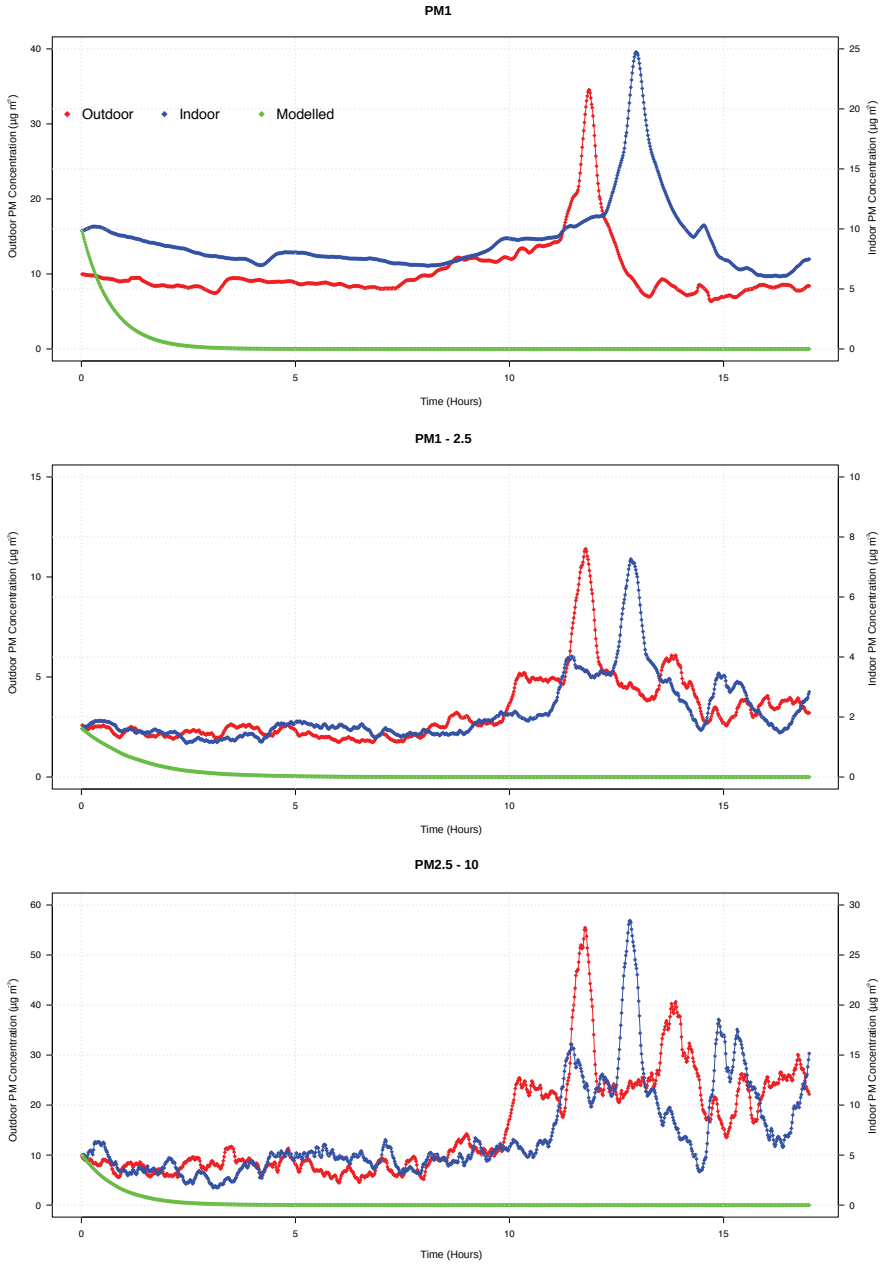

Figure 37: PM time series plots for Day 5 of the BBG campaign.

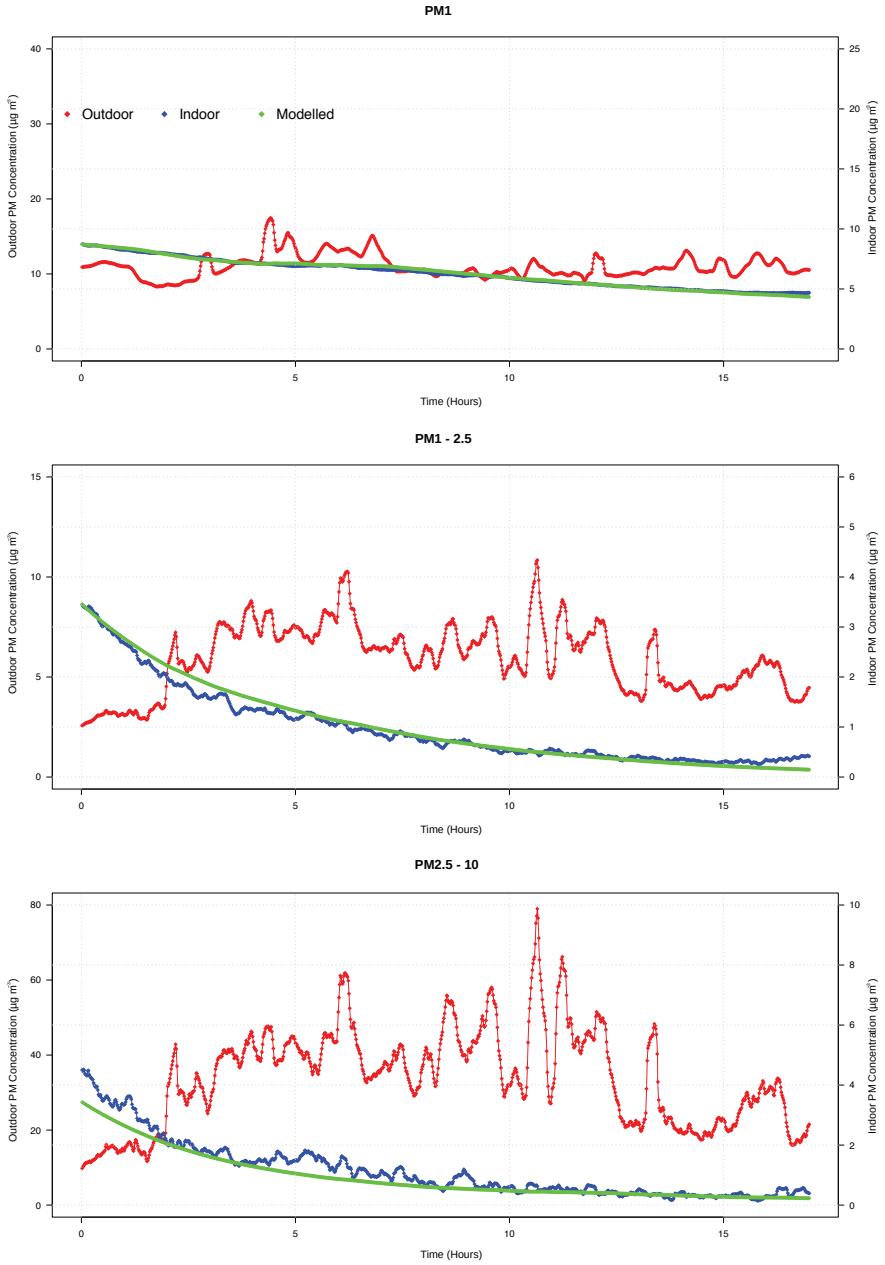

Figure 38: PM time series plots for Day 6 of the BBG campaign.

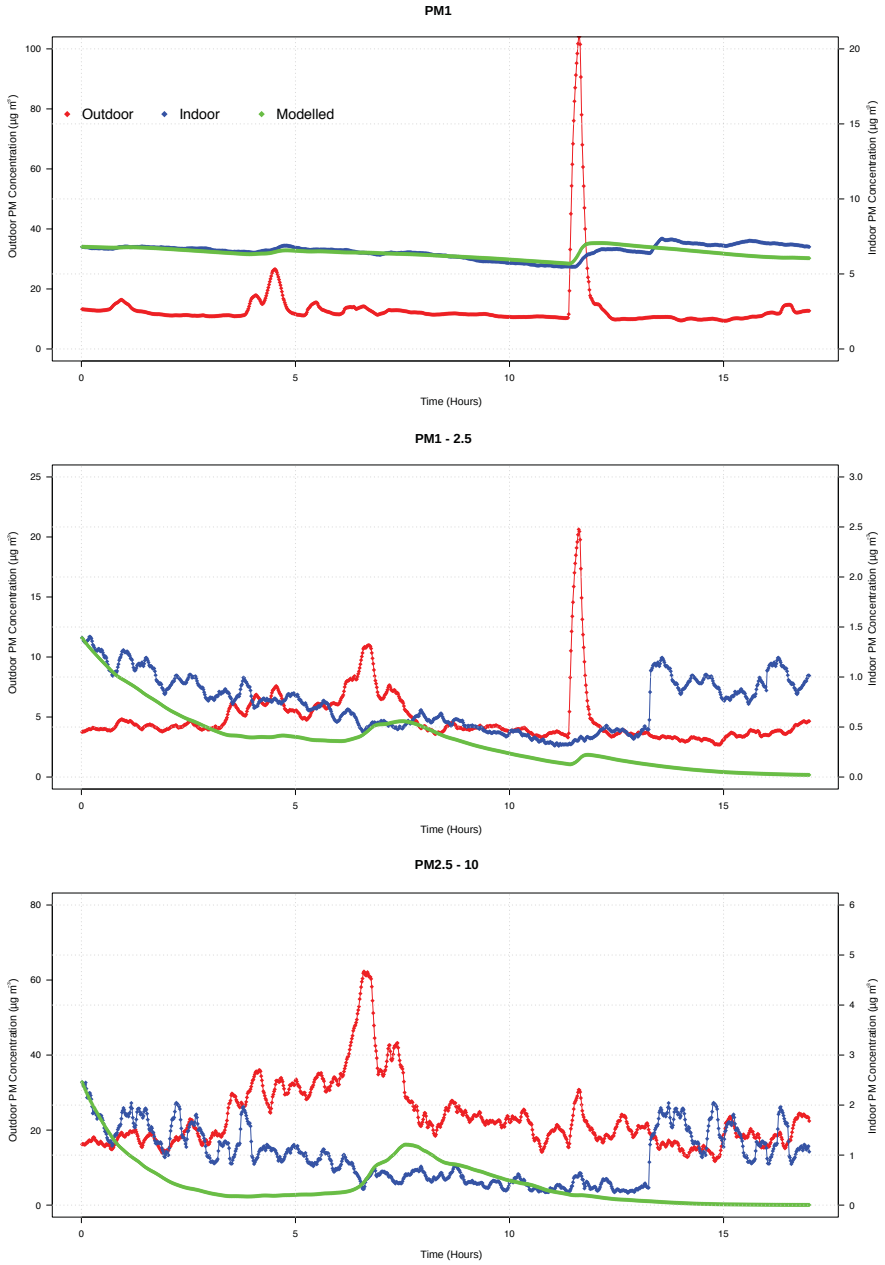

Figure 39: PM time series plots for Day 7 of the BBG campaign.

Evaluation of **Model 5**.

Table 11: Regression analysis when Model 5 was applied.

		F_{INF}		
Day	AER	PM_1	$PM_{1\text{ - }2.5}$	$PM_{2.5\text{ - }10}$
1	0.26	1	0.44	0.18
2	0.54	1.25	1	0.10
3	0.44	0.80	0.83	0.36
4	0.13	1	0.09	0.00003
5	1.62	2.5	-	-
6	0.18	0.08	-	0.006
7	0.13	-	-	0.18

Table 12: Statistical evaluation when Model 5 was applied.

		RMSE (μgm^{-3})			MAPE (%)		
Day	AER	PM_1	$PM_{1\text{ - }2.5}$	$PM_{2.5\text{ - }10}$	PM_1	$PM_{1\text{ - }2.5}$	$PM_{2.5\text{ - }10}$
1	0.26	2.81	0.58	1.02	51.72	26.11	23.20
2	0.54	6.58	7.55	2.52	123.05	317.32	44.99
3	0.44	1.17	5.84	16.80	13.10	156.32	143.78
4	0.13	4.03	0.52	1.40	51.86	56.33	99.89
5	1.62	19.50	-	-	196.78	-	-
6	0.18	5.53	-	1.36	85.50	-	68.93
7	0.13	-	-	10.70	-	-	510.20

Evaluation of **Model 6**.

Table 13: Regression analysis when Model 6 was applied using the full dataset.

Model 2	N	Gradient (SD)	y-intercept (SD)	R^2	η	A (h^{-1})
PM_1	7	−0.81 (0.19)	−0.76 (0.13)	0.78	0.81	0.47
$PM_{1\text{ - }2.5}$	7	−0.53 (0.09)	−0.19 (0.06)	0.87	0.53	0.83
$PM_{2.5\text{ - }10}$	7	0.32 (0.07)	−0.05 (0.05)	0.81	0.32	0.95

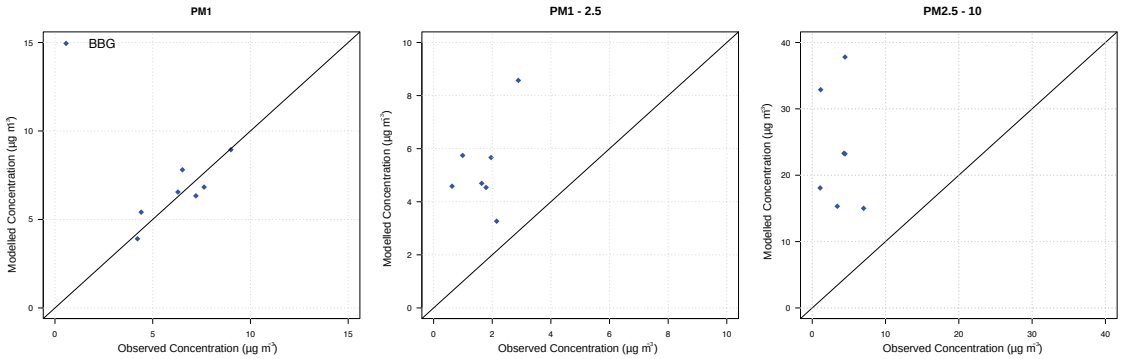

Figure 40: Comparison of modelled and observed values for different size fractions, when Model 6 was applied.

Table 14: Statistical evaluation when Model 6 was applied using the full dataset.

Model 2	N	RMSE (μgm^{-3})	MAPE (%)	R^2
PM_1	7	0.78	11.04	0.77
$PM_{1\ -\ 2.5}$	7	3.82	269.37	0.23
$PM_{2.5\ -\ 10}$	7	21.80	914.23	0.05